miRNA profiling for diagnosis of chronic pain in polyneuropathy

Antonio Pellegrino

Univ.-Diss.

for the achievement of an academic degree as
"doctor rerum naturalium" (Dr. rer. nat.)
in the discipline "Biochemistry"

submitted to
Faculty of Science
Institute for Biochemistry and Biology
University of Potsdam

Place and Date of the disputation:
Potsdam-Golm, 06.03.2023

Main Supervisor: PD Dr. Harald Seitz
Fraunhofer Institute for Cell Therapy and Immunology
Branch Bioanalytics and Bioprocesses (IZI-BB)
Biomarker Validation and Assay Development
Am Mühlenberg 13
14476 Potsdam-Golm
Second supervisor: Prof. Dr. Zoran Nikoloski
University of Potsdam
Institute of Biochemistry and Biology
house 29, room 1.15
Karl-Liebknecht-Str. 24-25,
14476 Potsdam-Golm

Published online on the
Publication Server of the University of Potsdam:
https://doi.org/10.25932/publishup-58385
https://nbn-resolving.org/urn:nbn:de:kobv:517-opus4-583858

Affirmation in lieu of an oath

I hereby affirm that the dissertation entitled: “miRNA profiling for diagnosis of chronic pain in polyneuropathy” is my own work, written independently and without assistance other than the resources cited.

I have indicated the bodies of work, including tables and illustrations, which originate from earlier work of other authors. In each case I have quoted the origin thereof.

This dissertation has not been submitted, in either identical or similar form, to any other examination authority or university, and has not yet been published.

I did not invent nor falsify the data presented in this dissertation. The data have been acquired by myself or were made available for this analysis from reliable sources as indicated. I am obliged to give the main supervisor access to all original data until the examination procedure is completed.

Kriftel,11 October 2022

_____

Acknowledgments

I would like to take this opportunity to thank all the people who supported me in the process of working on and writing this dissertation:

First of all, I would like to thank Harald Seitz, who is not only the main supervisor, but in whose working group 'Biomarker Validation and Assay Development' I was able to work on and write this dissertation for the last 4 years with his support. Thanks to the whole group for the always good working atmosphere, the fun during the work and the countless excursions. Thanks to Sandra Mükusch for her help and guidance, some experiments of this thesis are based on her preliminary work. Special thanks go to Denise Danne, it was wonderful to work and laugh with you as well as to follow your development through the years. Thanks also to Juliane Grimm and Dorothea Hallier, it was a pleasure to share a lab with you. Further thanks go to Lena-Lotte Windler, who was also able to achieve awesome results under my guidance, it was wonderful to work with you and a pleasure to follow your development during your thesis and beyond.

I would also like to thank my colleagues at the Fraunhofer Institute for Cell Therapy and Immunology, Department of Bioanalytics and Bioprocesses (IZI-BB) in Potsdam Golm. Especially, Eva Ehrentreich-Förster for hosting me in her department. Thanks also to Martina Obry, Erik Hahn, Anika Andersson and Dirk Michel. Further, I would like to thank Zoran Nikoloski for the university secondary supervision as well as Christoph Weigel for his always open ear and being the third reviewer.

Thanks for all the collaborations and contributions especially by University Hospital Schleswig-Holstein Kiel (Philipp Hüllemann and Sophie-Charlotte Farbig), Marien Hospital Herne (Nina Babel and Toralf Roch), MicroDiscovery (Arif Malik and Chris Bauer), Charité (Christoph Stein and Viola Seitz) and the University of Kassel (Friedrich Wilhelm Herberg).

Special thanks go to my friends and family as well as a huge thank you to Timo Ramm and his wife Franziska Ramm. Thank you both for your always open ears, the motivation and the awesome fun we had during and especially after work! Without you both this work would have been difficult to achieve.

Thanks to my girlfriend, Lena Pylypiw, and her dog, Mo, for all the loving support in the moments of doubt. I am looking forward to a relaxed but exciting future with you. Without you both this work would have been difficult to achieve.

Last but not least I would like to thank my mother and my grandparents. You were the ones who supported me through the years and ensured the foundation, with persistent perseverance, for all this. Thank you!

Table of content

List of figures

List of tables

Abbreviations

3’-UTR	3’-Untranslated Region
AGO	Argonaute protein
AKAP79	A-Kinase Anchoring Protein 79
AKAPs	A Kinase Anchoring proteins
AKT	Protein Kinase B
AMPA	α-Amino-3-hydroxy-5-Methyl-4-isoxazolepropionic Acid
APS	Ammonium Persulfate
ARMS	Ankyrin-Rich Membrane Spanning protein
ATP	Adenosine Triphosphate
AVPR1A	Arginine Vasopressin Receptor 1A
BCA	Bicinchoninic Acid assay
BDNF	Brain-derived Neurotrophic Factor
BPKDi	2′-(cyclohexylamino)-6-(1-piperazinyl)-[2,4′-bipyridine]-4-carboxamide
CaMK	Ca2+/calmodulin-dependent protein Kinase
CaMKII	Calcium/calmodulin-dependent protein kinase II
cAMP	cyclic Adenosine Monophosphate
CCL2	Cysteine-Cysteine chemokine Ligand 2
CCR4-NOT	Carbon Catabolite Repression - Negative On TATA-less
cDNA	complementary DNA
c-Fos	Fos proto-oncogene
CGRP	Calcitonin Gene-Related Peptide
COX-2	Prostaglandin-endoperoxide synthase 2
CREB	cAMP Response Element-Binding protein
CXCL1	C-X-C motif Ligand 1
DAAM1	Dishevelled Associated Activator of Morphogenesis 1
DCP1	mRNA-Decapping enzyme 1
DCP2	mRNA-Decapping enzyme 2
DN	Diabetic Neuropathy
DNA	Deoxyribonucleic Acid
Dpn I	Type IIM restriction enzyme Dpn I
DRG	Dorsal Root Ganglia
DSP	Distal Symmetric Polyneuropathy
EC_{50}	Half maximal effective concentration
EDC	1-Ethyl-3-(3-dimethylaminopropyl)carbodiimide

EDC4	Enhancer of mRNA-Decapping protein 4
EDTA	Ethylenediaminetetraacetic Acid
eIF4E	eukaryotic translation Initiation Factor 4E
FDA	U.S. Food and Drug Administration
FMNL3	Formin Like 3
GABA	Gamma-Aminobutyric Acid
GPCR	G Protein-Coupled Receptor
GW182	Trinucleotide Repeat Containing Adaptor 6A
HEK293	Human Embryonic Kidney 293
IASP	International Association for the Study of Pain
IGSF11	Immunoglobulin Superfamily member 11
IL-1β	Interleukin 1 beta
IMBX	3-Isobutyl-1-methylxanthin
KIDINS220	Kinase D Interacting Substrate 220 kDa
KIM	Kinesin-Interacting motif
LRRC27	Leucine Rich Repeat Containing 27
m^7G	7-Methylguanosine
MAP2K	Mitogen-Activated Protein Kinase Kinase
MAPK	Mitogen-Activated Protein Kinase
MFI	Mean Fluorescence Intensity
miR	micro Ribonucleic Acid
miRNA	micro Ribonucleic Acid
mRNA	messenger Ribonucleic Acid
MYH10	Myosin Heavy chain 10
MYT1L	Myelin Transcription factor 1
NGF	Nerve Growth Factor
NHS	N-Hydroxysuccinimide
NK1-R	Neurokinin 1 Receptor
NMDA	N-methyl-D-aspartate
NO	Nitric Oxide
NOS	Nitric Oxide Synthase
NT	Neurotrophin
PAN2	Poly(A) specific ribonuclease subunit PAN2
PAN3	Poly(A) specific ribonuclease subunit PAN3
PBS	Phosphate-Buffered Saline
PBST	Phosphate-Buffered Saline with Tween 20 Detergent

PDZ	PSD-95/Disc large/Zonula occludens-1
PE	Phycoerythrin
PGE_2	Prostaglandin E_2
PI3K	Phosphoinositid-3-Kinase
PKA	Protein Kinase A
PKC	Protein Kinase C
PKD	Protein Kinase D
PNP	Polyneuropathies
pre-miRNA	precursor miRNA
pre-RISC	precursor RNA-induced silencing complex
pri-miRNA	primary miRNA
qPCR	quantitative real-time Polymerase Chain Reaction
QST	Quantitative Sensory Testing
RIPA	Radioimmunoprecipitation Assay buffer
RISC	RNA-induced silencing complex
RNA	Ribonucleic Acid
SDS-PAGE	Sodium Dodecyl Sulfate–Polyacrylamide Gel Electrophoresis
SETD5	SET Domain containing 5
shRNA	short hairpin RNA
STXBP5	Syntaxin Binding Protein 5
SYT4	Synaptotagmin 4
TEMED	Tetramethylethylendiamin
TNF-α	Tumor Necrosis Factor α
TRBP	TAR RNA-binding protein
Trk	Tropomyosin-related kinase
TrkB-R	Tropomyosin receptor kinase B
TRPA	Transient Receptor Potential cation channel subfamily A
TRPM	Transient Receptor Potential cation channel subfamily M
TRPV1	Transient Receptor Potential Vanilloid type 1
TTC21B	Tetratricopeptide repeat domain 21B
USP6NL	USP6 N-terminal Like
VEGF	Vascular Endothelial Growth Factor
XRN1	5′-3′ exoribonuclease 1
YFP	Yellow Fluorescent Protein

1. Introduction

The translation of an extracellular signal into an intracellular response, is a fundamental biochemical process for every organism to react to its environment and is called signal transduction. While signal transduction in single cell organisms is based on adapting their behavior to the food supply or the presence of toxic substances, thus responding directly to environmental stimuli, multicellular organisms receive numerous extracellular and intracellular signals [1, 2]. Stimuli such as heat or pain that trigger signal transduction, lead to a cell-specific response, due to characteristic cell-specific effector proteins [3]. Whereas stimuli trigger cell-specific responses, the mechanism of signal transduction can be generalized as a molecular circuit. First, the release of a primary messenger occurs as a result of an electrical, chemical, physical, or mechanical stimulus. Primary messengers are, for instance, cytokines, hormones or growth factors and are called ligands. They specifically bind to different transmembrane or intracellular target proteins, which act as receptors [4, 5]. As a result of the ligand´s interaction with the extracellular domain of transmembrane proteins like the transient receptor potential vanilloid type 1 (TRPV1) channel, a change in the tertiary or quaternary structure of the receptor occurs, subsequently triggering a structural change in the intracellular domain [6]. In the next step, translation and amplification of the extracellular signal occurs through a change in concentration of small intracellular molecules, the second messengers. Second messengers like calcium ions (Ca^{2+}) or cyclic adenosine monophosphate (cAMP) amplify the signal and can often diffuse unimpeded into other cellular compartments, acting on processes throughout the cell and leading to regulation of cellular activities [7]. Due to the generation of second messengers, activating a variety of effector proteins as a final step in signal transduction, these effector proteins form the center of the communication system. In this context, an important role is played by protein kinases including protein kinase A (PKA), these protein kinases can activate or inactivate signal proteins via phosphorylation. At the end of each signal transduction there is either a change in enzyme activity or gene expression, including micro ribonucleic acid (miRNA) expression, resulting in a physiological response [8]. The entire mechanism of signal transduction is feedback controlled. Once the response to the signal is complete, it is terminated, for example, by dephosphorylation of the effector protein by protein phosphatases [9]. Thus, resulting in the termination of the corresponding physiological response, for example, pain.

1.1 Pain

Pain has a crucial importance for the organism. It protects against injury and draws attention to damage that has already occurred. For example, acute pain, which occurs when an extremity is injured, causes a protective posture, facilitating the injury or inflammation to heal. However, a complete lack of nociception, ability to feel pain, leads to recurrent injury and even self-mutilation [10]. Pain is defined by the International Association for the Study of Pain (IASP) as an "unpleasant sensory and emotional experience associated with actual or potential tissue damage" [11]. Treatment of the underlying medical condition is crucial to may resolve the pain. However, pain may persist despite successful management of the condition that initially caused it, resulting in chronic pain. Chronic pain is defined by the IASP as "pain that persists or recurs for longer than three months" [12]. In chronic pain conditions, such as neuropathic pain, the primary warning function is no longer present since these pain states can persist permanently even without a triggering stimulus. Such pain often becomes the sole or predominant clinical problem in some patients and warrants specific diagnostic evaluation, therapy as well as rehabilitation. Chronic pain is a frequent condition, affecting an estimated 20 % of people worldwide [13]. Studies showed that peripheral and central sensitization mechanisms play a relevant role in the manifestation of localized and widespread chronic pain. Thus, almost any patient suffering from chronic pain will show impairments in the central nervous system [14]. However, duration, localization and origin as well as the underlying pathophysiology are used to classify acute and chronic pain. Etiologically, nociceptor pain (pain that arises from actual/threatened damage to non-neural tissue and is due to the activation of nociceptors), neuropathic pain (pain caused by a lesion/disease of the somatosensory nervous system) and nociplastic pain (pain that arises from altered nociception despite no clear evidence of actual/threatened tissue damage or evidence for disease/lesion of the somatosensory system causing the pain) can be distinguished from each other [15]. The sensation of pain starts with the activation of pain receptors. Different stimuli can excite the polymodal, high-threshold and bipolar pain receptors, the nociceptors. These free nerve endings of the primary afferent neurons convert mechanical, chemical, or thermal pain stimuli into an electrical signal in the form of action potentials [16]. Stimulated Aδ- and C-fibers, whose somata are localized in the dorsal root ganglia (DRG), synaptically transmit these peripheral pain stimuli to nociceptive spinal cord neurons in the laminae of the dorsal horn. In addition, nociceptors differ in terms of conduction velocity, which depends on the diameter and extent of myelination [17]. The unmyelinated peptidergic and non-peptidergic C-fibers have a small diameter and conduct at a speed of 0.5-2 m/s, whereas the thinly myelinated Aδ-fibers have an intermediate diameter and conduct pain stimuli at a speed of 5-30 m/s [18]. These nociceptors have to

be distinguished from myelinated Aα- and Aβ-fibers, which are excited by physiological, low-threshold, non-noxious touch and are responsible for proprioception [19]. In the dorsal horn, excitatory neurotransmitter (glutamate) and neuropeptides (BDNF, CGRP, substance P) mediate the synaptic pain signal to a second spinal cord neuron. In particular, glutamate activates postsynaptic α-amino-3-hydroxy-5-methyl-4-isoxazolepropionic acid (AMPA) and N-methyl-D-aspartate (NMDA) receptors of projection neurons [20]. These ascend laterally as the spinothalamic tract into the thalamus and into various brain regions [21]. In the primary and secondary somatosensory cortex, a conscious perception of pain is generated, to which an affective component is attributed by the integration of the limbic system (Figure 1.1.1: Pain perception). Pathways descending from the brainstem and interneurons may additionally modulate pain processing in terms of an endogenous antinociceptive system [22].

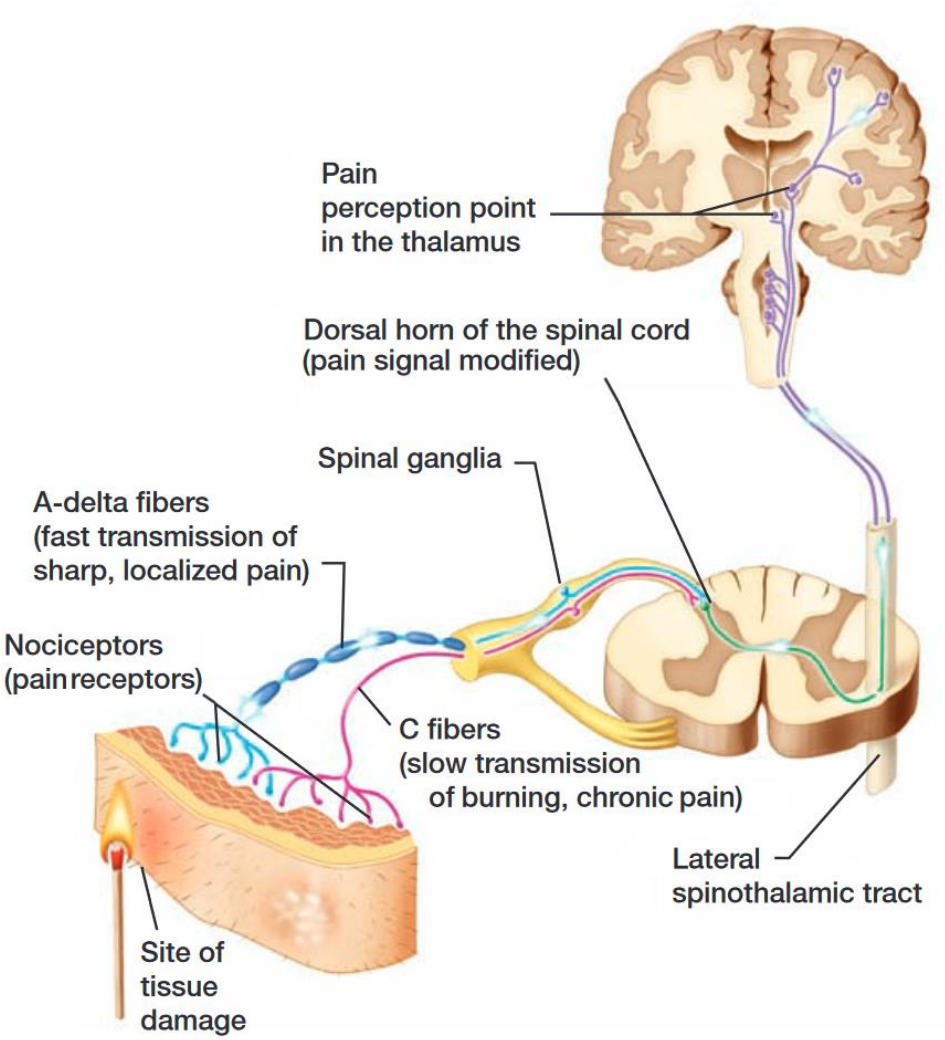

Figure 1.1.1: Pain perception
Pain perception starts at the site of tissue damage where nociceptors are activated and mediate the pain signal via Aδ-fibers/C-fibers to the dorsal horn of the spinal cord. In the dorsal horn the pain signal ascends laterally as the spinothalamic tract into various brain regions where a conscious perception of pain is generated [23].

Neurotransmitters, neuropeptides and other mediators not only alter the synaptic transmission of nociceptive stimuli in the spinal cord, but also regulate mechanisms of peripheral and central sensitization, that play a relevant role in the manifestation of chronic pain. In chronic pain, sensitization of the nociceptive system can occur in the damaged/inflamed tissue (peripheral sensitization) as well as in the spinal cord/brain (central sensitization) [14]. Long term, such changes lead to an increase in pain, which in the case of nociceptor pain can take the form of hyperalgesia (increased pain from a stimulus that normally provokes pain) and allodynia (pain due to a stimulus that does not normally provoke pain), or in the case of neuropathic pain additionally take the form of ectopic discharges (ongoing spontaneous electrical nerve impulses) [24]. In peripheral sensitization, pro-inflammatory mediators are produced and released from nociceptors/immune cells, including macrophages, mast cells, neutrophils and platelets, as a result of tissue damage (Figure 1.1.2: Peripheral sensitization). These include neuropeptides (bradykinin, CGRP, substance P), histamine, serotonin, eicosanoids and their related lipids (prostaglandins, thromboxanes, leukotrienes), endocannabinoids, cytokines (TNF-α, IL-1β), and chemokines (CXCL1, CCL2). The pro-inflammatory mediator secreting immune cells are either already present in the tissue or infiltrate from the blood plasma into the injured tissue. The release of adenosine triphosphate (ATP) and protons from the damaged tissue activates receptors like TRPV1. This leads to calcium influx into the nociceptor, causing its depolarization and generating an action potential [17, 25].

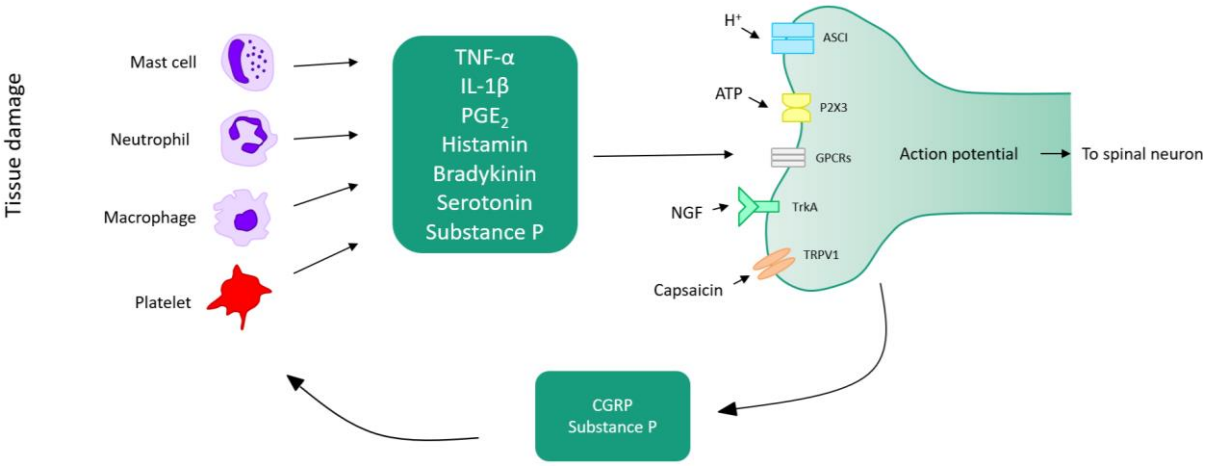

Figure 1.1.2: Peripheral sensitization
In peripheral sensitization, pro-inflammatory mediators are produced and released from nociceptors/immune cells creating a self-maintaining pain circuit [26].

Ion channels such as TRP channels are crucial for the conversion of painful stimuli into electrical signals [27]. In addition, the stimulated nociceptor releases pro-inflammatory mediators into the surrounding tissue activating the present immune cells even more [17].

Thus, contributing to peripheral sensitization and creating a self-maintaining pain circuit. As a result of sensitization of inflammatory-stimulated nociceptors, for example, by phosphorylation of TRP channels, the excitation threshold of the membrane is decreased, and action potentials are consequently generated more rapidly [28]. In addition, silent nociceptors are recruited, increasing the painful input to the spinal cord [29]. The mentioned sensitization mechanisms are manifested in increased pain sensitivity to nociceptive (hyperalgesia) and non-nociceptive (allodynia) stimuli. Due to the ongoing irritation of peripheral nociceptors, a secondary hyperalgesia can occur when the inflammation spreads to the surrounding tissue [30]. In neuropathic pain, ectopic action potential formation/discharge of injured or dysfunctional nerve fibers may occur in the course of peripheral sensitization [24]. Vasodilation and plasma extravasation accompany inflammation, generating the symptoms of dolor (pain), rubor (redness), calor (warmth), and tumor (swelling), which additionally cause impaired function of the affected tissue [17]. In the spinal cord and brain, central sensitization results in increased neuronal activity and modifications of pain- and inflammation-related genes and proteins that enhance mechanisms of nociception in the central nervous system (Figure 1.1.3: Central sensitization). Processes of primary and secondary hyperalgesia increase the receptive field of the spinal cord neurons and increase their sensitivity [31]. During the early phase of central sensitization, peripheral pain stimuli in the dorsal horn of the spinal cord are synaptically transmitted to projection neurons via the release of glutamate, which activates various receptors like AMPA receptors at the post synapse, causing depolarization.

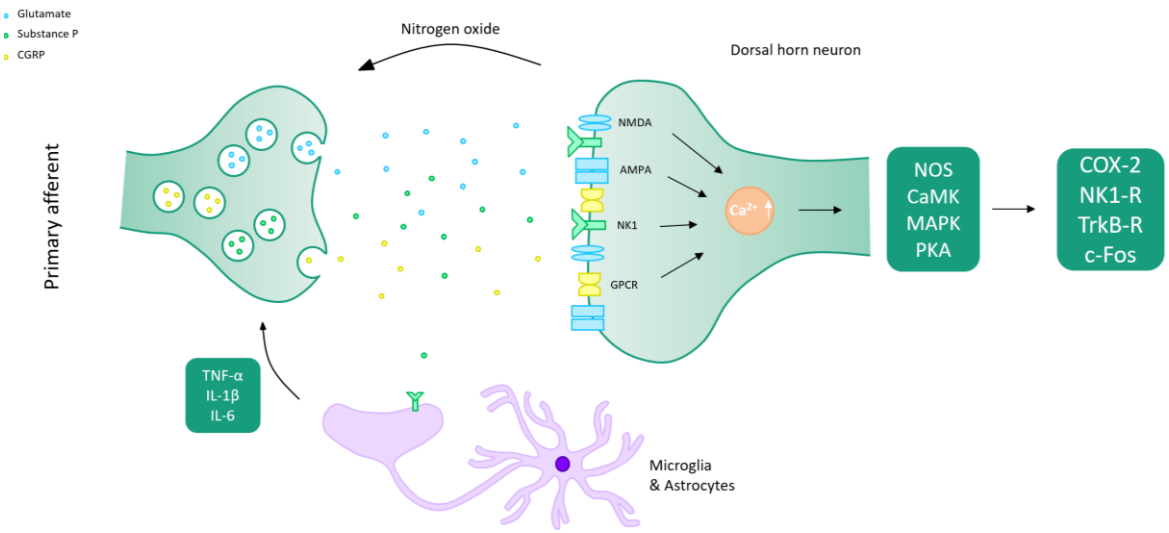

Figure 1.1.3: Central sensitization
In the central nervous system, central sensitization results in increased neuronal activity and modifications of pain- and inflammation-related genes and proteins that enhance mechanisms of nociception. In addition, microglia can regulate gene expression in spinal neurons and glial cells via the release of pro-inflammatory cytokines [26].

With sustained stimulation and stronger, noxious stimuli, additional NMDA receptors are activated at the pre-depolarized membrane. In this case, the activation of AMPA receptors releases NMDA-bound magnesium ions resulting in abolishment of the NMDA receptor blockade [17, 32]. As a result, cations enter the neuron through the nonspecific NMDA receptor and positively affect the membrane potential. In addition, glutamate binds to metabotropic glutamate receptors, activating G protein-coupled receptor (GPCR) signaling cascades and thus contributing to the development of neuroplastic adaptations. Excitatory neuropeptides (CGRP, substance P) enhance glutamate activity, whereas inhibitory transmitters (GABA, glycine) and aminergic transmitters (serotonin) modulate the synaptic transmission. The early phase of central sensitization is primarily regulated by post-translational modifications of existing ion channels and receptors. In the late phase of central sensitization, increased postsynaptic calcium influx through NMDA receptors leads to the activation of numerous protein kinases (PKA, PKC, CaMK, MAPK, NOS), which stimulate the expression of pro-inflammatory genes (COX-2, NK1-R, TrkB-R, c-Fos) or regulate the release of inflammatory mediators (NO, PGE_2, TNF-α, bradykinin, NGF, IL-1β) via intracellular signaling cascades, manifesting in chronic pain [17, 25, 31]. However, in addition to the mentioned excitatory sensitization mechanisms, loss of inhibitory interneurons and interaction of neurons with glial cells can also lead to increased pain sensation. Microglia can regulate gene expression in spinal neurons and glial cells via the release of pro-inflammatory cytokines. Thus, modulating pain transmission in the dorsal horn of the spinal cord [33–35]. Additionally, significant evidence exists that pain and inflammatory responses are regulated via miRNAs.

1.2 miRNA

Micro ribonucleic acids (miRNAs) belong to the class of small non-coding ribonucleic acids (RNAs) with a length of 17-25 nucleotides [36]. The main role of miRNAs is the regulation of protein levels by modulating their respective messenger ribonucleic acid (mRNA) target via degradation [37, 38]. In 1993, miRNAs were discovered for the first time in *Caenorhabditis elegans* and described as “mediators of temporal pattern formation” [39, 40]. Today it is known, that up to 1 % of the human genome encodes for miRNA genes [41]. These genes are transcribed in the nucleus, where the biogenesis of miRNAs begins (Figure 1.2.1: miRNA biogenesis).

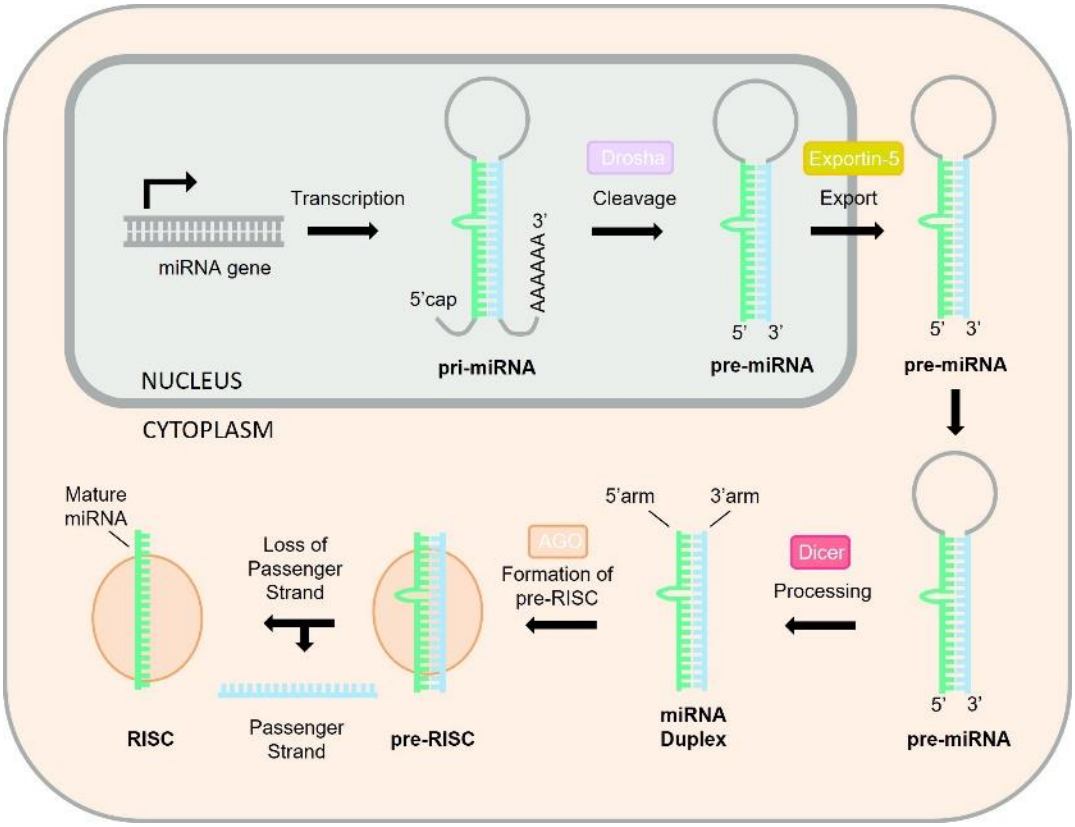

Figure 1.2.1: miRNA biogenesis
miRNA is transcribed and cleaved in the nucleus before it is exported into the cytoplasm. In the cytoplasm the miRNA is processed and forms the RISC with AGO, exerting the main mechanisms [42].

The primary miRNA (pri-miRNA) is transcribed via RNA polymerase II/III and forms, due to its complementary sequence, a hairpin-like structure with a loop at the end [43]. This pri-miRNA, which consists of hundreds of nucleotides, still resides in the nucleus and is recognized by a RNase III enzyme called Drosha. Drosha cleaves the pri-miRNA into a new, about 70 nucleotides long, hairpin-like structure, the precursor miRNA (pre-miRNA) [44]. Then, the pre-miRNA is then transported from the nucleus into the cytoplasm via Exportin-5, where it is processed again by another RNase III enzyme called Dicer [45]. Processing via Dicer results in a short miRNA duplex without loop at the end. This miRNA duplex is directly used by the argonaute protein (AGO), as Dicer and AGO form a complex mediated by the TAR RNA-binding protein (TRBP), to form the precursor RNA-induced silencing complex (pre-RISC) [46]. One of the miRNA strands, known as the passenger strand, will leave the pre-RISC for degradation [47]. The miRNA strand that stayed in the pre-RISC is known as the guide strand and has most likely the less stable 5' end or a uracil at the beginning [48]. The complex of guide strand and pre-RISC forms the RNA-induced silencing complex (RISC). This RISC, containing the mature miRNA, exerts the main mechanisms in the human body, gene regulation by mediating degradation of the

complementary mRNA and modulation of transcription and translation via canonical and non-canonical actions [49–51]. A canonical action, in terms of the RISC mechanism, is the completely complementary binding to the target mRNA´s 3'-untranslated region (3'-UTR) via the miRNA seed sequence. The seed sequence of a miRNA is nucleotide 2 to 7 of the 5' end and upon binding, translational repression and ultimately degradation is initiated [52]. This process is called the miRNA mediated 5' to 3' mRNA decay pathway (Figure 1.2.2: miRNA mediated mRNA decay pathway) [53, 54]. In this pathway, mRNAs are first deadenylated, then decapped and finally degraded by the cytoplasmic 5' to 3' exonuclease 1 (XRN1) [55, 56]. The mRNA´s 3' poly(A) tail deadenylation is mediated by the interaction of AGO and the trinucleotide repeat containing adaptor 6A (GW182), which recruits a deadenylase complex including the polyA specific ribonuclease subunit 2 and 3 (PAN2–PAN3) and the carbon catabolite repression - negative on TATA-less complex (CCR4–NOT) [57]. Meanwhile, miRNA induced translational repression is caused by AGO binding to the mRNA´s 5' m^7G-cap, leading to competition of the AGO complex and the eukaryotic translation initiation factor 4E (eIF4E) for association with the target´s mRNA cap structure and thus preventing effective translation initiation [58]. In addition, decapping factors including the mRNA-decapping enzyme 2 and 1 (DCP2, DCP1) and the enhancer of mRNA-decapping protein 4 (EDC4) are recruited by the AGO machinery, forming a decapping complex and facilitating the mRNAs decay via XRN1 [59].

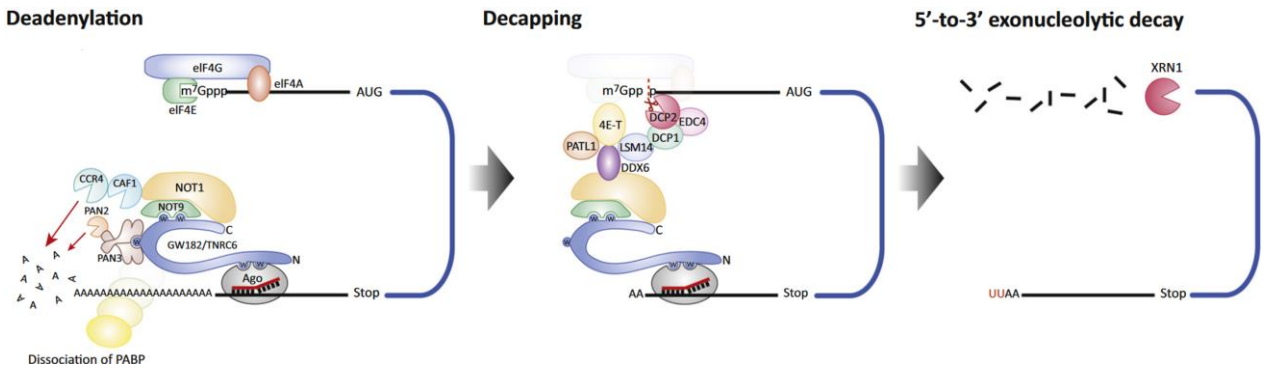

Figure 1.2.2: miRNA mediated mRNA decay pathway
In the 5' to 3' mRNA decay pathway which is induced by the complementary binding RISC complex, mRNAs are first deadenylated, then decapped and finally degraded via multiple protein complexes [54].

In some cases, mRNA degradation due to cleavage can be the result of the conserved endonuclease activity of AGO2, requiring extensive base-pairing between miRNAs and their mRNA targets [60]. On the other hand, a non-canonical action, in terms of the RISC mechanism, is the miRNAs partial binding to the target mRNA. About 60 % of all RISC/mRNA interactions are non-canonical interactions in humans, leading to a tremendous number of potential target mRNAs for a single miRNA. At the same time, a

single mRNA might contain multiple miRNA binding sites, leading to an even more tremendous number of regulated biological processes by this mechanism [61]. Another crucial role fulfilled by miRNAs is intercellular signaling. In the three decades since the discovery of miRNAs, they have been under intense investigation to understand their role in biological processes like diseases or as biomarkers [62, 63]. Countless scientists have investigated these opportunities and their evidences suggest that miRNAs could play a pivotal role in almost every medical field including cancer, Alzheimer's disease, in spinal cord injuries, epilepsy, acute cardiovascular diseases or heart failure and sepsis [64–70]. Especially, their role as biomarkers has been of exceptional interest, when it was discovered that extracellular miRNAs could be stably detected. Although, miRNAs are mostly found inside the cell, there are populations that migrate outside and can be found in various body fluids, including blood, urine, cerebrospinal fluid, saliva, and tears [62, 71]. These miRNAs are called circulating miRNAs. They can be released through active passage, in microvesicles, exosomes, or through being bound to a protein [72–75]. In addition, they may also be passively released during cell injury, thereby potentially serving as biomarkers of injuries causing acute pain or chronic pain, like most cases of polyneuropathy [76].

1.3 Polyneuropathy

Polyneuropathies (PNP) are prevalent, often demanding, and sometimes disabling or even lethal. They are generalized disorders that result in injury to nerves within the peripheral nervous system. Peripheral neuropathies are the most common type of disorder of the peripheral nervous system in adults, and especially in elderly [77]. In Europe, the prevalence is about 5.5% and with rising age up to 9.4% [78]. In 2013, diagnostic testing of these disorders by neurologists costed $357 million with electrodiagnostic tests ($205 million, 57%) and magnetic resonance imaging ($135 million, 38%) accounting for most of the costs [79, 80]. Most peripheral neuropathies are chronic and usually develop over several months. The symptoms usually begin in the toes, followed by the fingers and finally spread proximally. The distribution of these neurological symptoms is often referred to as stocking-glove pattern [81]. Peripheral neuropathies are best categorized by the localization of the nerve injury. One of the most common localizations is called distal symmetric polyneuropathy (DSP), a diffuse, length-dependent process [82]. Patients with DSP are associated with altered sensory sensation, pain and weakness. These patients usually suffer from numbness, burning or electric shock–like pain, are at risk of falls, ulcerations and even amputations, especially those with diabetes [83]. DSP can be induced by a wide array of conditions including metabolic (diabetes), idiopathic, toxic (alcohol), nutritional

(vitamin deficiency), medication (chemotherapy) and autoimmune (Sjogren's syndrome) [84]. For diagnosis, vibration perception and pressure sensation are used to discriminate those with and without large fiber neuropathy [85]. Large fiber (myelinated Aα/β-fibers) neuropathy manifests with the loss of pressure and vibration sense, whereas small fiber (thin myelinated Aδ-fibers or unmyelinated C-fibers) neuropathy manifests itself with the impairment of pain and temperature [86]. Diagnosis of these small fiber neuropathy patients utilizes pinprick and temperature sensation [87, 88]. For all confirmatory tests, reference values have to be adjusted for test site, age, sex, and population. For quantitative sensory testing (QST), multi-center reference data are available for different body regions in both sexes and a broad age range [89]. These reference data allow a transformation of a patient's data into Z-scores with a standard Gaussian distribution (zero mean and unity variance), provided the examiner has calibrated herself/himself for about 20 healthy subjects [89, 90]. Thus, making all confirmatory tests an extensive, long lasting and highly user dependent procedure. Importantly, objective instruments such as skin biopsies do not necessarily relate to the pain complaint of the patient. Although assessment of intraepidermal nerve fiber density through skin biopsy is validated for diagnostics of small fiber neuropathies [89, 91]. Thus, a fast and easy but also accurate and reliable method of detection is urgently needed for diagnostics of small fiber neuropathies. One approach could be the miRNA profiling of patients with chronic pain in polyneuropathy that could lead to a fast and easy but also accurate and reliable qPCR test. However, the most common cause of DSP is diabetic neuropathy (DN), accounting for 32–53% of cases, according to national guidelines, the prevalence of DN is 8%–54% in type 1 diabetes and 13%–46% in type 2 diabetes [80, 92, 93]. Risk factors for the development of DN can be grouped in diabetes related (blood sugar), vascular (arterial hypertension), nutritive (obesity) and general (age) [94]. The prevalence of chronic painful DSP amongst patients with diabetes in the United Kingdom is about 16.2% [95]. Various studies have investigated the pharmacologic treatment of neuropathic pain in DSP secondary to diabetes. The primary medications are tricyclic antidepressants such as amitriptyline, serotonin and norepinephrine reuptake inhibitors including duloxetine and voltage-gated calcium channel ligands such as gabapentin [84]. This neuropathic pain includes hyperalgesia (increased pain from a stimulus that usually provokes pain) and thermal as well as mechanical allodynia (pain due to a stimulus that does not usually provoke pain) [96]. It is caused by the sensitization of damaged axons including peripheral nociceptive axons and unmyelinated or thin myelinated axons (unmyelinated C- and thin myelinated Aδ-fibers/sensory neurons) in the DRGs [31]. Then, the neuropathic pain signal is mediated by upregulated sodium channels such as TRPV1, resulting in reduced threshold for activation and repetitive

signaling of DRGs in response to nociceptive stimuli (peripheral sensitization). In addition to the repetitive firing of DRGs, the effect of growth factors such as brain-derived neurotrophic factor (BDNF) and inflammatory mediators including tumor necrosis factor α (TNFα) result in the increased excitability of the dorsal horn neurons, finally leading to central sensitization and creating a self-maintaining loop of chronic pain [97]. This self-maintaining loop of chronic pain closes by microglia releasing TNFα, leading to increased expression of the cysteine-cysteine chemokine ligand (CCL2) by injured DRGs and astrocytes, resulting in depolarization of nociceptive afferents, astrocyte activation and upregulation of TRPV1 [98, 99].

1.4 TRPV1

The transient receptor potential vanilloid type 1 (TRPV1) channel is known as a molecular sensor for acid (pH < 5.9), heat (>43 °C), endogenous agonists like oxytocin and vanilloids, such as capsaicin that induces the “hot and burning” sensation which is associated with the consumption of chili peppers [100–103]. The family of TRP channels include approximately 30 proteins divided into six subfamilies: ankyrin (TRPA), canonical, melastatin (TRPM), mucolipin, polycystin, and vanilloid (TRPV). Nine of these TRP channels are highly sensitive to temperature and therefore called thermo-TRP channels. These thermo-TRP channels include the heat-activated TRPV1 to TRPV4, TRPM2, TRPM4 and TRPM5 as well as the cold-activated TRPA1 and TRPM8 [104, 105]. Activation of these nine thermo-TRP channels leads to a non-selective cationic inward/current that results in membrane depolarization [106]. Furthermore, each individual thermo-TRP channel is only activated within a relatively narrow temperature range but together they are able to cover a broad range of temperatures, from noxious cold to noxious heat [107]. However, TRPV1 is a ligand-gated non-selective cation channel and permeable to Ca^{2+}, Na^{+} as well as other monovalent cations [108]. It is highly expressed in unmyelinated C- and thin myelinated Aδ-fibers/sensory neurons within DRGs and is involved in inflammatory pain, neuropathic pain as well as hyperalgesia signaling [109, 110]. Activation of TRPV1 results in significant Ca^{2+} and Na^{+} influx, causing cell depolarization and resulting in action potentials in nociceptive DRG neurons (Figure 1.4.1: Activation of TRPV1 by capsaicin, heat and endogenous agonists). These nociceptive DRG neurons then convey the nociceptive information to the spinal dorsal horn. Thus, TRPV1 is considered to be one of the major contributors of nociception [111].

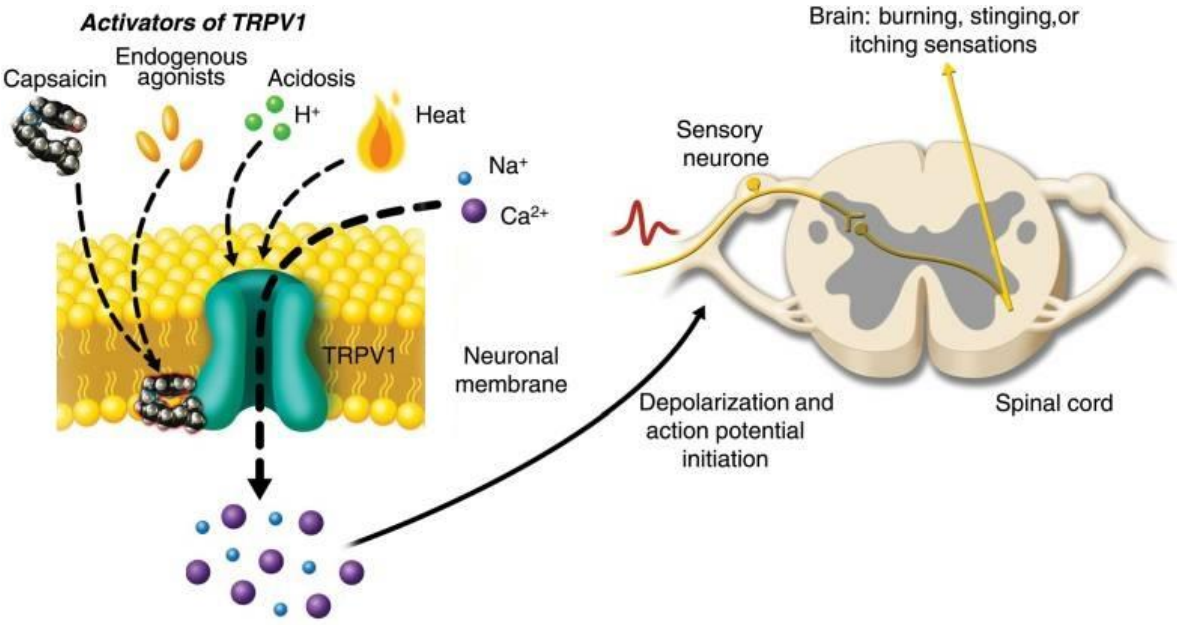

Figure 1.4.1: Activation of TRPV1 by capsaicin, heat and endogenous agonists
Activation of TRPV1 results in significant Ca^{2+} and Na^{+} influx, causing cell depolarization and generating action potentials in nociceptive DRG neurons of the spinal cord and resulting in the perception of pain/burning [112].

Each TRPV1 channel is composed of four subunits that form a homotetrameric non-selective cation channel with a high degree of Ca^{2+} permeability in the plasma membrane. Each TRPV1 subunit has six transmembrane domains with intracellular N- and C-termini that harbor several domains for interaction with modulatory factors including PKA, Protein kinase C (PKC), and Calcium/calmodulin-dependent protein kinase II (CaMKII) [113]. PKA, PKC, and CaMKII are known to phosphorylate TRPV1 at multiple sites within the N- and/or C-termini, resulting in sensitization of TRPV1 [114–116]. Remarkably, inflammation is known to increase PKC and PKA activity. Consequently, inflammation seems to promote the sensitized state of TRPV1 [117, 118]. However, PKA induced TRPV1 sensitization is mediated by the scaffolding protein A-Kinase anchoring protein 79 (AKAP79), which has binding sites for several kinases including PKA and binds to TRPV1. Thus, this facilitates the association of the kinase with its substrates at distinct subcellular loci and forming a signaling complex that promotes rapid as well as specific phosphorylation of sensitizing sites on TRPV1 [119]. Another potential sensitizing interaction partner of TRPV1 is the adaptor protein kinase D interacting substrate 220 kDa (KIDINS220) or also known as ankyrin-rich membrane spanning protein (ARMS) [120].

1.5 ARMS

Kinase-D interacting substrate of 220 kDa (KIDINS220), or also known as ankyrin repeat-rich membrane spanning (ARMS) was identified as the first physiological protein kinase D

substrate [121]. ARMS is a membrane protein expressed in the nervous system and acts as a signaling complex involved in many neural functions like differentiation, survival, and synaptic plasticity [122]. It interacts with membrane receptors, cytosolic signaling components, and cytoskeletal proteins including microtubule and actin, neurotrophin, and vascular endothelial growth factor as well as glutamate receptors and voltage-gated Na^+ channels [123, 124]. Furthermore, ARMS plays an important role in astrocytes, a key player in chronic neuropathic pain, modulating Ca^{2+} dynamics via TRPV4, survival and death pathways as well as astrocyte–neuron communication [125, 126]. ARMS has four transmembrane domains and intracellular N- and C-termini that contain several protein-protein interaction motives and mediate most of the known functions (Figure 1.5.1: Schematic structure of ARMS and its protein–protein interactions).

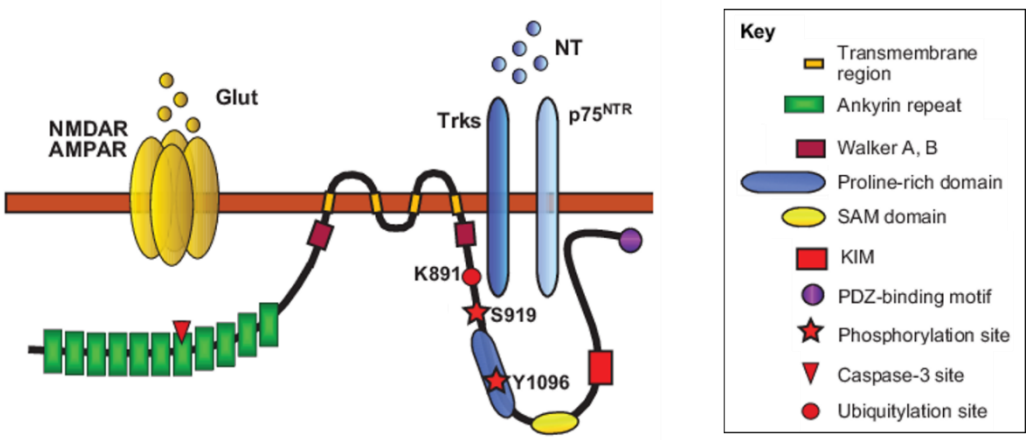

Figure 1.5.1: Schematic structure of ARMS and its protein–protein interactions
ARMS has four transmembrane domains and intracellular N- and C-termini that contain several protein-protein interaction motives and mediate most of the known functions like interaction with AMPA or NT receptors [123].

The N-terminus harbors 11 adjacent ankyrin repeats that mediate the rearrangement of the actin cytoskeleton induced by nerve growth factor (NGF) [123]. The C-terminus contains several residues dedicated to post-translational modifications including phosphorylation, ubiquitination and calpain cleavage [121, 127–129]. In addition, the C-terminal region contains different domains for the binding of several interaction partner including the mitogen-activated protein kinase (MAPK) pathway via the proline-rich domain, the molecular motor kinesin-1 via the kinesin-interacting motif (KIM) or the neurotrophin (NT) receptor $p75^{NTR}$ via the PSD-95/Disc large/Zonula occludens-1 (PDZ)-binding motif [130–132]. Other interactions like the interaction with AMPA receptor subunits and tropomyosin-related kinase (Trk)-type NT receptors seem to be mediated by ARMS trans-membrane domains [122, 133]. ARMS does not possess a catalytic function itself, but the interaction with target proteins seems to be modulated by phosphorylation as ARMS sensitizes TRPV1 towards capsaicin in a PKA-dependent manner [120]. While PKA phosphorylation sites of

TRPV1 are well known, further experiments have to be performed to identify ARMS – TRPV1 and ARMS – PKA interaction sites [134].

1.6 PKA

The cAMP-dependent protein kinase A (PKA) was discovered in 1968 and is considered to be one of the best characterized kinases [135]. While 2% of the genes of the human genome encode for protein kinases, approximately 30% of the proteome can be post-translational modified by phosphorylation [136]. Protein kinases are enzymatically active proteins that are able to transfer the γ-phosphate of ATP to a target protein. For this purpose, the free hydroxyl groups of amino acids including serine, threonine and tyrosine are used as phosphate group acceptors. Protein kinases are divided into serine/threonine and tyrosine kinases based on their target specificity. PKA belongs to the serine/threonine kinases. However, there are also dual-specific kinases such as the mitogen-activated protein kinase (MAP2K), which can phosphorylate both, serines/threonines and tyrosines [137]. Kinases can be monomers but can also consist of several subunits (catalytic and regulatory subunits). The regulatory subunits prevent unregulated activity of the kinase. Protein kinases are able to interfere with regulatory cell processes by altering the phosphorylation status of target proteins, resulting in increased or decreased target protein activity, sensitivity or specificity [138]. Post-translational modifications like phosphorylation are usually temporary and reversible, so-called protein phosphatases can dephosphorylate kinase targets [139]. In its inactive form, PKA consists of a heterotetrameric holoenzyme complex of two regulatory subunits and two catalytic subunits. To date, four regulatory subunits (RIα, RIβ, RIIα, and RIIβ) and four catalytic subunits (Cα, Cβ, Cγ, PrKX) have been identified. PKA is ubiquitously expressed, with a specific composition of regulatory and catalytic subtypes for each cell type/tissue [140–144]. It is activated via the cyclic adenosine monophosphate (cAMP) pathway. This pathway starts with an external stimulus like forskolin that activates a GPCR. The extracellular binding of a ligand to the GPCR results in a conformational change leading to the activation of an adenylate cyclase. The activation of adenylyl cyclase increases the concentration of the second messenger cAMP. The intracellular increase of the cAMP concentration leads to the binding of two cAMP molecules to the regulatory subunit of the PKA and thus to the release and activation of the catalytic subunit [145]. In its active form, the catalytic PKA subunits target a (**R**/K)-(**R**/K)-X-(**S**/T) Φ recognition sequence, where the bold letters code for preferential sites and Φ for any hydrophobic amino acid [146]. In addition, the catalytic subunits can also be inhibited by pseudo-substrates like H89 [147]. PKA mediates many physiological responses elicited by

GPCRs. These include regulation of gene transcription by phosphorylation and activation of transcription factors like cAMP response element-binding protein (CREB) [8]. PKA is also implicated in the process hippocampal long-term potentiation [148]. Furthermore, PKA is associated with diseases like cancer and is associated with pain including inflammatory pain and neuropathic pain, via the phosphorylation of ion channels like TRPV1 [118, 119, 149–151]. The regulatory subunits do not only take over the function of inactivating the catalytic subunit, but they also define the cellular location of the PKA. The regulatory subunit consists of an N-terminal docking and dimerization (D/D) domain that functions as binding site for the amphipathic α-helix anchoring motif common to all A kinase anchoring proteins (AKAPs) and lead the PKA to specific cellular locations. Thus, allowing site specific targeted phosphorylation of substrates by the active catalytic subunit mediated by AKAPs like AKAP79 [152].

1.7 AKAP79

The A kinase anchoring protein 79 (AKAP79) or also known as AKAP150 (human isoform 79, rodent isoform 150, bovine isoform 75) belongs to a family of proteins (AKAPs) that share the ability to bind the regulatory subunit of PKA [153]. In the neuronal cytosol a wide array of enzymes and signaling molecules exist that compete for substrates and binding partners. These interactions must be temporally and spatially restricted into accurate signaling cascades/compartments, to result in neuronal adaptation that occurs from environmental stimuli [154]. Many of these pathways include common and ubiquitous second messengers as well as enzymes with broad substrate specificity. Unsurprisingly, a vast number of neurological disorders are known to result from inaccurate signal transduction [155–158]. AKAPs are a large family of structurally diverse scaffolding proteins that are particularly important for this function and sequester enzymes as well as their effector proteins in selective cellular compartments. They affect the location and dynamics of signal transduction by tethering their interaction partners to a particular location in the cell [159]. The PKA binding amphipathic α-helix of AKAP79 was the first domain to be characterized and is located at the C-terminus [160]. The three N-terminal polybasic membrane targeting regions allow dynamic shuttling of AKAP79 between the plasma membrane and endosomal membrane compartments. In addition, the plasma membrane targeting of AKAP79 is also achieved through direct electrostatic interactions of the three polybasic domains with cadherin cell adhesion molecules and cortical F-actin [161–163]. In the nociceptive signaling, AKAP79 plays an essential role in maintaining TRPV1 activity by tethering several interaction partners to the receptor that alter its sensitivity and facilitate

crosstalk between TRPV1 and other membrane bound ion channels [164]. In sensory DRGs, AKAP79 is predominantly expressed in neurons of nociceptive unmyelinated C-fibers [165]. In these neurons, AKAP79 manages TRPV1 sensitivity induced by inflammatory mediators like prostaglandin E2 through tethering PKA that in turn phosphorylates TRPV1 to enhance its sensitivity [166]. AKAP79 also anchors adenylate cyclase to the TRPV1-AKAP79-PKA complex, providing PKA with cAMP [167]. Taken together, this highlights a central role for AKAP79 in nociceptive signaling complexes that are crucial for TRPV1 regulation.

1.8 Aim of the dissertation

This dissertation aimed to determine significant differential expressed miRNAs in the context of chronic pain in polyneuropathy. For this purpose, 30 patients with chronic painful polyneuropathy were compared with 30 age matched healthy patients. Polyneuropathy patients were selected with an average pain of ≥ 4 on a numerical scale (0-10), a chronification score on Mainz Pain Grading System (MPSS) of ≥ II and a pain duration ≥ 6 months. miRNAs were separated from serum for each patient. Isolated miRNAs were processed for sequencing as well as repeatedly quality controlled at relevant stages of the procedure. Finally, the sequenced samples/groups were compared via differential expression analysis. For significant differential expressed miRNAs a target prediction was performed. Since TRPV1 seems to be one of the major contributors of nociception and is associated with inflammatory pain as well as neuropathic pain, this dissertation also aimed to characterize the influence of PKA phosphorylated ARMS on the sensitivity of TRPV1 as well as to investigate the part of AKAP79 during PKA phosphorylation of ARMS. Therefore, potential PKA phosphorylation sites of ARMS were identified using a (R/K)-(R/K)-X-(S/T) pattern search and respective single PKA site/alanine mutants were synthetized. To characterize the phosphorylation status of each ARMS mutant and their interaction with TRPV1 as well as their influence on the sensitivity of TRPV1, each ARMS mutant was transfected with TRPV1 into HEK293 cells. The lysate of these transfected cells was analyzed by a FLEXMAP 3D analysis, immunoprecipitation, SDS-PAGE and Western Blot. For TRPV1 sensitivity determination, transfected cells were analyzed using a calcium flux analysis and the capsaicin induced EC_{50} for each TRPV1/ARMS mutant combination was calculated. Finally, ARMS specific shRNA was used to silence ARMS to demonstrate the involvement of ARMS in TRPV1 sensitization. These findings shed some light on pivotal miRNAs in the context of chronic pain in polyneuropathy and contributed to the understanding of the nociception relevant TRPV1/ARMS/AKAP79/PKA signaling complex.

2. Material and Methods

2.1 Material

2.1.1 Prokaryotic cells

Table 2.1.1.a: Prokaryotic cells

Strain	Description	Source
XL10-Gold® Ultracompetent Cells	Tet^{r}Δ(*mcrA*)*183* Δ(*mcrCB-hsdSMR-mrr*)*173* *endA1 supE44 thi-1 recA1 gyrA96 relA1 lac Hte [F' proAB lacI^{q}ZΔM15* Tn*10* (Tet^r) Amy Cam^r]	Agilent

2.1.2 Eukaryotic cells

Table 2.1.2.a: Eukaryotic cells

Cell line	Description	Source
HEK293	Human primary embryonal kidney cells	DSMZ

2.1.3 Antibodies

Table 2.1.3.a: Antibodies

Antibody	Species	Dilution	Cat No.	Source
AKAP79	Rabbit	1:1000	D28G3	Cell Signaling
ARMS	Mouse	1:1000	MA1-90667	Invitrogen
ARMS	Rabbit	1:1000	ab34790	abcam
mRPE	Goat	1:1000	P852	Invitrogen
pPKA-Substrate	Rabbit	1:1000	100G7E	Cell Signaling
rAlexaFluor555	Goat	1:1000	A-21428	Invitrogen
rRPE	Goat	1:1000	P2771MP	Invitrogen
TRPV1	Rabbit	1:1000	ACC-030	Alomone Labs

2.1.4 Protein and DNA ladder

Table 2.1.4.a: Protein and DNA ladder

Protein and DNA ladder	Cat. No.	Source
GeneRuler 1 kb DNA Ladder, ready-to-use	SM0314	Thermo Scientific
PageRuler™ Plus Prestained Protein Ladder	26619	Thermo Scientific

2.1.5 Oligonucleotides & Plasmids

Table 2.1.5.a: Oligonucleotides & Plasmids

Oligonucleotides & Plasmids	Sequence
ARMS UniProtKB - Q9EQG6 [168]	pcDNA 3.1 rARMS
$ARMS_0$	pcDNA 3.1. rARMS, S882A, T930A, S1251/52A, S1439/40A, S1526/27A
$ARMS_{S882}$	pcDNA 3.1. rARMS, T930A, S1251/52A, S1439/40A, S1526/27A
$ARMS_{S882, T903}$	pcDNA 3.1. rARMS, S1251/52A, S1439/40A, S1526/27A
$ARMS_{T903}$	pcDNA 3.1. rARMS, S882A, S1251/52A, S1439/40A, S1526/27A
$ARMS_{S1251/52}$	pcDNA 3.1. rARMS, S882A, T903A, S1439/40A, S1526/27A
$ARMS_{S1439/40}$	pcDNA 3.1. rARMS, S882A, T930A, S1251/52A, S1526/27A
$ARMS_{S1526/27}$	pcDNA 3.1. rARMS, S882A, T903A, S1251/52A, S1439/40A
S1439/40 for	5’ ctcccaggcaagaaatcctcagaacggcccagt 3’
S1439/40 rev	5’ actgggccgttctgaggatttcttgcctgggag 3’
shC (ARMS)	pRFP-C-RS, 5’ ctgttactgagttcaatgaccgtggatgt 3’
shS (scamble)	pRFP-C-RS, 5’ gcactaccagagctaactcagatagtact 3’
Sequencing Primer 1	5’ ccttgtaacttcagcaacaaatgg 3’
Sequencing Primer 2	5’ tagaaatgagaagtgtggaaagcc 3’
T903A for	5’ ctctcaacagaagggacgcttaccgcagaagacag 3’
T903A rev	5’ ctgtcttctgcggtaagcgtcccttctgttgagag 3’
TRPV1 UniProtKB - O35433 [169]	pcDNA 3.1 rTRPV1-YFP

2.1.6 Kits

Table 2.1.6.a: Kits

Kits	Cat. No.	Source
BluePippin, 3% Agarose Cassettes	342BDQ3010	Biozym
GeneJET Plasmid-Maxiprep-Kit	K0491	Thermo Scientific
High Sensitivity DNA Kit	5067-4626	Agilent
miRCURY LNA SYBR Green PCR Kit	339346	Qiagen
miRNeasy Serum/Plasma Advanced Kit	217204	Qiagen
MiSeq Reagent Kit v3 (150-cycle)	MS-102-3001	Illumina
Mix2Seq		Eurofins Genomics
peqGOLD Plasmid Miniprep Kit I	12-6942-02	VWR Peqlab
Pierce™ BCA Protein Assay Kit	23225	Thermo Scientific
QIAseq miRNA 48 Index IL	331595	Qiagen
QIAseq miRNA Library Kit	331505	Qiagen
QIAseq miRNA Library QC qPCR Assay Kit	331551	Qiagen
QIAshredder	79656	Qiagen
QuikChange Lightning	210518	Agilent

2.1.7 Instruments

Table 2.1.7.a: Instruments

Instruments	Source
Amersham™ Typhoon™ Biomolecular Imager	GE Healthcare
Bioanalyzer 2100	Agilent
Bio-Plex Pro II	Biorad
BluePippin	Sage Science
Centrifuge 5424 R	Eppendorf
Centrifuge 5804 R	Eppendorf
FLEXMAP 3D® System	Luminex Corporation
FLUOstar Omega	BMG Labtech
Incubators AvantgardeLine Model BD 56	Binder
LightCycler 2.0	Roche
LSM 510	Zeiss
MasterCycler Gradient Thermal Cycler	Eppendorf
Microwave MW7823	Severin
Mighty Small™ II SE250/SE260	Hoefer

MiSeq	Illumina
Nanodrop ND-1000	peqLab
Nikon ECLIPSE Ts2-FL	Nikon
pH 340i	WTW
PlateFuge	Biozym
Precision Balance LE6202P	Sartorius
PS300-B	Hoefer
Semi-Dry Transfer Unit TE77XP	Hoefer
Stuart™ Rock and Roller SRT6D Analogue Tube Roller	Bibby Scientific
ThermoStat plus	Eppendorf
Titramax 1000	Heidolph
Unimax 1010	Heidolph
Vortex Genie 2	Bender & Hobein AG

2.1.8 Chemicals and Consumables

Table 2.1.8.a: Chemicals and Consumables

Chemicals and Consumables	Cat. No.	Source
Acrylamide (37.5:1)	1.00639	Merck
Agar	20767.232	VWR Chemicals
Agarose	V3121	Promega
Ammonium persulfate	17874	Thermo Scientific
Ampicillin	J.60977.14	Thermo Fisher
Bacto Yeast Extract	212750	Difco
Blotting paper	TE76	GE Healthcare
Bovine Serum Albumin	8076.3	Carl Roth
BPKDi	2798	Axon
Bromophenol blue	B0126-25G	Sigma
Capsaicin	CAYM10010743-1	Cayman Chem
DMEM high glucose	F0415	Biochrom
DNA LoBind Tubes	0030108051	Eppendorf
DTT	D9779-5G	Sigma
EDC	77149	Pierce
EDTA	A1103.0250	AppliChem
Fetal Bovine Serum	S0115	Biochrom
Fluo-4, AM	F14201	Invitrogen

Forskolin	F6886-10MG	Sigma
Glycerol	A1123.1000	AppliChem
H89	FBM-10-2144	BIOZOL
Halt™ Protease and Phosphatase Inhibitor	78441	Thermo Fisher
IBMX	I5879-1G	Sigma
Isopropanol	0733.1	Carl Roth
L-Glutamine	K0302	Biochrom
LightCycler® Capillaries (20 µL)	04929292001	Roche
Loading Dye	R0611	Thermo Scientific
MagPlex-TAG Microspheres	MTAG-A012	Luminex Corporation
MES	M-8250	Sigma
Methanol	83638.320	VWR Chemicals
PDFV membrane	IPVH85R	Millipore
Protein G Mag Sepharose	28951379	Cytiva
Protein LoBind Tubes	0030108116	Eppendorf
RIPA	89900	Thermo Fisher
Sample Buffer Laemmli 2× Concentrate	S3401	Sigma
Sodium dodecyl sulfate	0183.3	Carl Roth
Sulfo-NHS	24520	Pierce
TEMED	17919	Invitrogen
Tetracycline	T-3383	Sigma
TransIT®-293 Transfection Reagent	MIR 2700	Mirus Bio LLC
TRIS	1.08219.1000	Merck
Trypsin EDTA (0.25 %)	15400054	Thermo Scientific
Tryptone	84610.0500	VWR Chemicals
Tween 20	A4974.0250	AppliChem
twin.tec™ LoBind 96-Well-PCR	0030129504	Eppendorf
β-Mercaptoethanol	4227.1	Carl Roth

2.1.9 Solvents, Buffer and Culture Media

Table 2.1.9.a: Solvents, Buffer and Culture Media

Solvents and Buffer	Composition
10x PBS	1.4 M Sodium chloride 27 mM Potassium chloride 78 mM Disodium phosphate

	15 mM Monopotassium phosphate
1x PBST	1x PBS 0.05 % Tween 20
5x SDS running buffer	623 mM Tris pH 8.3 6.3 M Glycine 0.5 % SDS
Blocking solution	1x PBST 5 % BSA (w/v)
Blotting buffer	4 mM Glycine 4.8 mM Tris pH 8.5 0.4 % SDS 20 % Methanol
HEK293 medium	87 % DMEM high glucose 10 % Fetal Bovine Serum 2 % L-Glutamine
HEK293 minus-medium	98 % DMEM high glucose 2 % L-Glutamine
LB-Agar	10 g Tryptone 10 g NaCl 5 g Yeast extract 15 g Agar ad 1 L H_2O
LB-Medium	10 g Tryptone 10 g NaCl 5 g Yeast extract ad 1 L H_2O

2.2 Methods

2.2.1 Patient selection, serum separation and storage

Patients were recruited at the University Hospital Schleswig-Holstein (Dr. P. Hüllemann) and the Marien Hospital Herne (Prof. N. Babel). In total, 30 patients with chronic painful polyneuropathy as well as 30 age matched healthy patients (ø 59 vs. ø 58 years) were selected. Polyneuropathy patients were selected with an average pain of ≥ 4 on a numerical scale (0-10), a chronification score on Mainz Pain Grading System (MPSS) of ≥ II and a pain duration ≥ 6 months [170, 171]. The serum of both groups was prepared accordingly to the miRNeasy Serum/Plasma Advanced Kit procedure for serum separation and storage. Therefore, whole blood in a primary blood collection tube without clot activator and without anticoagulants, such as EDTA or citrate, was collected. For complete clotting, tubes were left at room temperature for 30 min and subsequently centrifuged for 10 min at 1900 x g and 4 °C using a swinging bucket rotor. The upper (yellow) serum phase was transferred to a new tube with conical bottom and without disturbing the pellet containing cellular material. Serum samples in conical tubes were centrifuged again for 15 min at 3000 x g and 4 °C. After centrifugation, the cleared supernatant was carefully transferred to a new tube without disturbing the pellet, which usually formed a smear along the outer side of the centrifugation tube. For storage, the separated serum was kept frozen in aliquots at −80°C. Before processing, room temperature thawed serum samples were centrifuged for 5 min at 3000 x g and 4°C to remove cryoprecipitates [172].

2.2.2 miRNA purification

The miRNeasy Serum/Plasma Advanced Kit was used for purification of cell-free total RNA, primarily miRNA and other small RNA, from serum. The purification was performed accordingly to the manufacturer´s protocol with a starting volume of 200 µL serum. The basic procedure combined guanidine-based lysis of samples, an inhibitor removal centrifugation step and silica-membrane–based purification of total RNA. Buffer RPL, included in the kit, contained guanidine thiocyanate as well as detergents that facilitated lysis and denatured protein complexes and RNases. Therefore, RNA in samples lysed in buffer RPL were stable and protected from degradation. After thoroughly mixing to ensure a complete lysis, buffer RPP was added to precipitate inhibitors, mostly proteins that are highly concentrated in serum samples, by centrifugation. The supernatant containing the RNA was transferred to a new microcentrifuge tube, and isopropanol was added to provide appropriate binding conditions for all RNA molecules from approximately 18 nucleotides upwards. Then, the sample was applied to the silica-membrane spin column, where the

total RNA bound to the membrane and all contaminants were efficiently washed away. The purified total RNA was then eluted in 20 µL RNase-free water [172].

2.2.3 miRNA isolation pre library preparation quality control via qPCR

The primary purpose of the QIAseq miRNA Library QC PCR Panel Kit was to control the quality of the isolated RNA in any next-generation sequencing experiment. Addition of QIAseq miRNA Library QC Spike-Ins during RNA isolation enabled monitoring the comparability and reproducibility from RNA isolation to sequencing (Table 2.2.3.a and Table 2.2.8.a). The quality control was performed accordingly to the manufacturer´s protocol with 0.5 µL QIAseq miRNA Library QC Spike-Ins per 200 µL serum and 0.5 µL UniSp6 Spike-In per reverse transcription reaction.

Table 2.2.3.a: Assays included in the QIAseq miRNA Library QC PCR Panel Kit

qPCR assay	Recommended usage
UniSp100	RNA Isolation efficiency assessment
UniSp101	RNA Isolation efficiency assessment
miR-103a-3p	Endogenous control, serum/plasma
miR-191-5p	Endogenous control, serum/plasma
miR-30c-5p	Endogenous control, biofluids including urine
miR-451a	Hemolysis indicator serum/plasma
miR-23a-3p	Hemolysis indicator serum/plasma
UniSp6	Monitoring presence of inhibitory compounds

To avoid contamination, all samples were prepared as shown in Table 2.2.3.b under sterile conditions.

Table 2.2.3.b: Reaction setup for QIAseq miRNA Library QC PCR Panels with cDNA

Component	Volume per primer set [µL]
2x miRCURY SYBR Green Master Mix	5
PCR primer mix	1
cDNA template (undiluted)	0.1
RNase-free water	3.9

Each assay was transferred into a LightCycler® Capillary. The capillaries were capped and briefly centrifuged. Analysis of the samples was performed with the LightCycler 2.0 Instrument and the cycling conditions shown in Table 2.2.3.c.

Table 2.2.3.c: Cycling conditions

Step	Time	Temperature	Ramp rate
PCR initial heat activation	2 min	95°C	Maximal/fast mode
2-step cycling			
Denaturation	10 s	95°C	Maximal/fast mode
Combined annealing/extension	60 s	56°C	Maximal/fast mode
Number of cycles	40		
Melting curve analysis	60–95°C		

After conducting the qPCR-based quality control to detect the Spike-Ins and endogenous controls, the data were compared, outlier samples identified and considered for exclusion in the further library processing [173].

2.2.4 miRNA library preparation

The QIAseq miRNA Library Kit was utilized to enable unbiased next-generation sequencing of mature miRNAs on Illuminas MiSeq instrument for differential expression analysis of polyneuropathy vs. control serum samples. Therefore, the procedure integrated unique molecular indices into the reverse transcription process, enabling unbiased and accurate miRNome-wide quantification of mature miRNAs. The library preparation was performed accordingly to the manufacturer´s protocol with the recommended starting volume of 5 µL total RNA of the RNA eluate when 200 µL of serum has been processed using miRNeasy Serum/Plasma Advanced Kit. The basic procedure started with the sequentially adapter ligation to the 3' and 5' ends of miRNAs. Subsequently, universal cDNA synthesis with UMI assignment, cDNA cleanup, library amplification, and library cleanup were performed. During 3' ligation a preadenylated DNA adapter was ligated to the 3' ends of all miRNAs, while the 5' ligation ligated an RNA adapter to the 5' end of mature miRNAs. For cDNA synthesis, the reverse transcription primer contained an integrated UMI and bound to a region of the 3' adapter to facilitate conversion of the 3'/5' ligated miRNAs into cDNA, while assigning a UMI to every miRNA molecule. During reverse transcription, a universal sequence was also added that was recognized by the sample indexing primers during library amplification. After reverse transcription, a cleanup of the cDNA was performed using a magnetic bead-based method. Library amplification was accomplished using a universal

forward primer that was paired with 1 of 48 reverse primers to assign each sample a unique index. The unbiased amplification of all miRNAs in a single reaction ensured that sufficient target was present for next-generation sequencing. After library amplification, a cleanup of the miRNA library was performed using a magnetic bead-based method. The cleaned miRNA library was then subjected to the pre sequencing quality control via Agilent Bioanalyzer 2100 [174].

2.2.5 miRNA library pre sequencing quality control via Bioanalyzer 2100

The High Sensitivity DNA kit was used to provide quality control, sizing and quantitation of the cleaned miRNA Sequencing Library via electrophoresis with the Agilent Bioanalyzer 2100 system. Therefore, 1 µL of each miRNA Sequencing Library was analyzed on an Agilent Bioanalyzer 2100 instrument using a High Sensitivity DNA chip according to the manufacturer's instructions [175].

2.2.6 Adapter dimer removal via BluePippin

The BluePippin system is an automated gel electrophoresis platform and uses optical fluorescence detection of DNA separations to automatically collect size-selected fragments from pre-cast agarose gel cassettes. The sample lanes are physically separated, preventing any possibility of cross-contamination. DNA fractions are collected by electro-elution into a buffer-filled well using a branched channel configuration with switching electrodes. The timing of switching is determined by measuring the rate of DNA migration with optical detection of labelled markers. Therefore, the BluePippin instrument with 3 % agarose cassettes and internal standards was utilized to automatically separate the miRNA Sequencing Library from their adapter dimers. The BluePippin optical system was calibrated and the continuity test was accomplished before every run. The size selection was performed accordingly to the manufacturer´s protocol with the size selection mode set to tight 180 bp [176]. After adapter dimer removal, the cleaned miRNA Sequencing Library was subjected to the 2.2.5 miRNA library pre sequencing quality control via Bioanalyzer 2100 again.

2.2.7 Sequencing

The Illumina MiSeq was used to enable next-generation sequencing of mature miRNAs for differential expression analysis of polyneuropathy vs. control serum samples. Therefore, quality controlled miRNA Sequencing Libraries were diluted to 0.5 nM and four samples at a time were pooled accordingly to Illuminas Index Adapter Pooling Guide considering the Color Balance [177]. Subsequently, pooled 0.5 nM Libraries were denatured and diluted to

20 pM analogously to the NextSeq System Denature and Dilute Libraries Guide performing the Standard Normalization Method [178]. Denatured and diluted library pools were loaded onto a MiSeq Reagent Kit v3 cartridge with 13 pM and 1 % phiX accordingly to the MiSeq System Denature and Dilute Libraries Guide performing the Standard Normalization Method from step “Dilute Denatured 20 pM Library” [179]. The Sample Sheet, the flow cell, the PR2 bottle and the waste bottle as well as the reagent cartridge were prepared analogously to the MiSeq System Guide [180]. For sequencing, FASTQ Only and TruSeq Small RNA with a 75 bp single read was chosen to include the added unique molecular indices [174]. Resulting FASTQ files were analyzed with CLC Genomics Workbench 22 (QIAGEN) and the additional Biomedical Genomics Analysis plugin (22.0.4) [181, 182].

2.2.8 miRNA analysis

CLC Genomics Workbench 22 (QIAGEN) and the additional Biomedical Genomics Analysis plugin (22.0.4) was used to analyze the FASTQ file of each miRNA library and to perform a differential expression analysis [181, 182]. For quantification of the miRNA libraries, the QIAGEN miRNA Quantification workflow with default settings was utilized to count and annotate miRNAs using miRbase v22 [183]. The workflow outputted expression tables for each miRNA library. The "Grouped on mature" table had a row for each mature miRNA. The "Grouped on seed" table had a row for each seed sequence. The same seed sequence may be found in different mature miRNAs. For differential expression analysis of the miRNA libraries, the QIAseq miRNA Differential Expression workflow was used with the following settings:

- Expression tables: Grouped on mature
- Test differential expression due to: Group
- While controlling for: Age
- Comparisons: Against control group
- Control group: Control

The workflow calculated differential expressions for expression tables with associated metadata using multi-factorial statistics based on a negative binomial Generalized Linear Model. This created an expression browser table where each row includes the expression values of all samples and the contents of all the statistical comparison tables [184]. In addition, the comprehensive set of QIAseq miRNA Library QC Spike-Ins, added in 2.2.3 miRNA isolation pre library preparation quality control, allowed thorough quality control of the NGS data by assessing the reproducibility and linearity of the reads mapped to these exogenous sequences (Table 2.2.8.a). The 52 QIAseq miRNA Library QC Spike-Ins are synthetic 5’-phosphorylated miRNAs of plant origin and bear no significant homology to

human (hsa) miRNAs. Following mapping of the QIAseq miRNA Library QC Spike-In reads, they were normalized to the total number of reads per sample. After this simple normalization to individual sample reads was done for all Spike-Ins in all samples, they were tested for normality via Shapiro-Wilks Normality Test and a Spearman Correlation matrix was plotted for sample-to-sample comparisons using Prism 9.1.2 (GraphPad) [173, 185].

Table 2.2.8.a: Spike-In sequences

Spike-In	Sequence	Spike-In	Sequence
UniSp100	uugauucccaauccaagcaag	UniSp126	acaaacaccuuggauguucuu
UniSp101	uaccaaccuuucaucguuccc	UniSp127	aagcuuugcucguucauguuc
UniSp102	ucccaaauguagacaaagca	UniSp128	uaguccgguuuuggauacgug
UniSp103	ugaagcugccagcaugaucua	UniSp129	uuagaugaccaucaacaaacu
UniSp104	cagccaaggaugacuugccgg	UniSp130	ucuugcuuaaaugaguauucca
UniSp105	uccggcaaguugaccuuggcu	UniSp131	agcucugauaccaaaugauggaau
UniSp106	agaaucuugaugaugcugcau	UniSp132	ugaucucuucguacucuucuug
UniSp107	uuggcauucuguccaccucc	UniSp133	uguuuguuguacucggucuagu
UniSp108	uguguucucaggucaccccuu	UniSp134	uucuugcauauguucuuuauc
UniSp109	cgaaacuggugucgaccgaca	UniSp135	uccuguguuuccuuugaugcgugg
UniSp110	uucgaggccuauuaaaccucug	UniSp136	aucaguuucuuguucguuuca
UniSp111	uagaaugcuauuguaauccag	UniSp137	ucauggucagauccgucaucc
UniSp112	gguucguacguacacuguuca	UniSp138	ucgcucugauaccaaauugaug
UniSp113	uaaacuaaucacggaaaugca	UniSp139	uugaauugaagugcuugaauu
UniSp114	uuuuggaaauuuguccuuacg	UniSp140	ugacaugggacugccuaagcua
UniSp115	ugagccucugugguagcccuca	UniSp141	uaacuaaacauugguguagua
UniSp116	uuugcuuccagcuuuugucuc	UniSp142	uaagauccggacuacaacaaag
UniSp117	uugguuacccauauggccauc	UniSp143	uaauccuaccaauaacuucagc
UniSp118	uucgaugucuagcagugcca	UniSp144	gauggauaugucuucaaggac
UniSp119	ucuaagucuucuauugauguu	UniSp145	ccuuggagaaauaugcgucaa
UniSp120	uacgcauugaguuucguugcuu	UniSp146	uuaugucuuguugaucucaau
UniSp121	uggcuugguuuauguacaccg	UniSp147	uaaagucaauaauaccuugaag
UniSp122	uucugcuauguugcugcucau	UniSp148	uuuuuccucaaauuuauccaa
UniSp123	ugauuggaaauuucguugacu	UniSp149	augaauuuggaucuaauugag
UniSp124	ucuagcagcuguugagcaggu	UniSp150	auugguucaauucugguguug
UniSp125	uucuucgugaauaucuggcau	UniSp151	uaauuugguguuucuucgauc

2.2.9 Site-Directed Mutagenesis

The QuikChange Lightning kit was utilized to incorporate point mutations in $ARMS_{S882, T903}$ and $ARMS_{T903}$ to create $ARMS_0$, $ARMS_{S882}$ and $ARMS_{S1439/40}$. The Site-Directed Mutagenesis was performed accordingly to the manufacturer´s protocol. The basic procedure used a supercoiled double-stranded DNA vector with an insert of interest, in this case ARMS, and two synthetic oligonucleotide primers, both containing the desired mutation. The oligonucleotide primers, each complementary to opposite strands of the vector, were extended during temperature cycling, without primer displacement. Extension of the oligonucleotide primers generated a mutated plasmid containing staggered nicks. Following temperature cycling, the product was treated with Dpn I. The Dpn I endonuclease was specific for methylated and hemimethylated DNA and was used to digest the parental DNA template and to select for mutation-containing synthesized DNA. Then, the nicked vector DNA containing the desired mutations was transformed into XL10-Gold ultracompetent cells [186]. Transformation was performed with LB medium instead of NZY+ broth and spreaded on LB–Agar plates containing 50 µg/mL ampicillin and 5 µg/mL tetracycline. The transformation plates were incubated at 37°C for 16 hours.

2.2.10 Miniprep

The peqGOLD Plasmid Miniprep Kit I was used to isolate plasmid DNA from the Site-Directed Mutagenesis transformation plates. Therefore, single colonies were picked and incubated overnight at 37°C while shaking at 200-250 rpm in 6 mL LB medium containing 50 µg/mL ampicillin and 5 µg/mL tetracycline. 1 mL of the overnight culture was used to prepare a bacterial glycerol stock for long term storage of the plasmid. The plasmid isolation was performed accordingly to the manufacturer´s protocol. The basic procedure used alkaline-SDS lysis of bacterial cells to release the plasmid DNA. The released plasmid DNA bound to a silica membrane containing column, where it was purified from contaminants and enzyme inhibitors. The purified plasmid DNA was then eluted from the column with Elution Buffer [187]. Concentrations of the isolated plasmids were determined by Nanodrop ND-1000 and diluted to 100 ng/µL for sequencing with Sequencing Primer 1 or Sequencing Primer 2 via Eurofins Genomics Mix2Seq Kit. Sequencing results were aligned to wild type ARMS with SnapGene 6.0 from GSL Biotech LLC [188].

2.2.11 Maxiprep

The GeneJET Plasmid-Maxiprep-Kit was utilized to isolate plasmid DNA from successful Site-Directed Mutagenesis colonies. Therefore, the mutation verified bacterial glycerol stocks were used to inoculate a starter culture of 1 mL LB medium containing 50 µg/mL

ampicillin and 5 µg/mL tetracycline. After incubation for 8 hours at 37°C while shaking at 200-250 rpm, the starter culture was diluted in 400 mL LB medium containing 50 µg/mL ampicillin and 5 µg/mL tetracycline. The diluted starter culture was subsequently incubated overnight at 37°C while shaking at 200-250 rpm. Cells were harvested by centrifugation at 5.000 x g for 10 min and the supernatant discarded. The plasmid isolation was performed accordingly to the manufacturer´s protocol. The basic procedure used the resuspended bacterial cell pellet and subjected it to alkaline-SDS lysis to liberate the plasmid DNA. The resulting lysate was neutralized to re-anneal plasmid DNA and precipitate proteins and chromosomal DNA. Cell debris and SDS precipitate were pelleted by centrifugation. The supernatant containing plasmid DNA was loaded onto the purification column. The high salt concentration of the lysate created appropriate conditions for plasmid DNA binding to the silica membrane in the spin column. The adsorbed DNA was washed to remove contaminants and eluted with the Elution Buffer [189]. Concentrations of the isolated plasmids were determined by Nanodrop ND-1000.

2.2.12 HEK293 cultivation

This method served the cultivation of HEK293 cells. HEK293 cells are human primary embryonal kidney cells. All steps dealing with HEK293 cells were performed under sterile conditions. The cells were incubated with HEK293 medium in a cell culture flask (T75) at 37 °C, 5 % CO_2 and 90 % humidity. To ensure growth as an adherent monolayer and optimal nutrient supply, cells were split every 3-4 days, therefore not exceeding 80 % confluence. For this purpose, medium was removed, and cells were washed twice with 5 mL PBS to remove media residues, dead cells and cell debris. Subsequently, the cells were detached with 1 mL 0.25 % Trypsin-EDTA and incubated for about 5 min in the incubator. After incubation, 9 mL fresh HEK293 medium were added, cells were separated by pipetting up and down as well as counted with a Thoma-Hemocytometer. New T75 flasks were seeded with $1x10^6$ cells. As a last step, the new flask was refilled to 10 mL HEK293 medium and placed in the incubator. The part of the cells that was not used for further cultivation was either discarded or used for experiments.

2.2.13 HEK293 transfection and lysis

This method was used to transiently transfect HEK293 cells. Each well of a 6-well culture plate was seeded with $1x10^6$ cells in 2 mL HEK293 medium. Cells were incubated at 37 °C, 5 % CO_2 and 90 % humidity. After 24 h the HEK293 medium was renewed and cells were transfected with the transfection mix. This transfection mix contained 100 µL HEK293 minus-medium, 0.5 µg pcDNA3.1-TRPV1-YFP and/or 2.5 µg pcDNA3.1-ARMS and/or

1.75 µg pRFP-C-RS-sh and TransIT®-293 Transfection Reagent in a 3:1 ratio, which was incubated at RT for 30 min before use. The cells were placed in the incubator for 48 h until they were stimulated, inhibited or lysed. For stimulation or inhibition, the medium was removed, cells were washed with 1 mL PBS and 2 mL HEK293 minus-medium was added. After 2 h of incubation in the incubator 2 mL stimulation mix (HEK293 minus-medium with 50 µM forskolin and 100 µM IBMX) or inhibition mix (HEK293 minus-medium with 10 µM H89 or 1 µM BPKDi) was added and cells were incubated again for 20 min. Regardless of whether cells were stimulated, inhibited or none of both, in order to lyse cells, they were washed with 1 mL ice cold PBS and lysed with 300 µL RIPA containing 1x Halt Protease and Phosphatase Inhibitor on ice for 15 min while shaking at 75 rpm. After lysis, cell extracts were cleared from cell debris by centrifugation. Therefore, cell extracts were loaded onto QIAshredder tubes and centrifugated for 5 min at 3000 rpm, followed by another centrifugation step, in a new tube, for 20 min at 14.000 x g. The supernatant was again transferred to a new tube and used for BCA and FLEXMAP 3D® analysis.

2.2.14 BCA analysis

The Pierce™ BCA Protein Assay Kit was used for the colorimetric detection and quantitation of total protein in cleared cell extracts. The BCA analysis was performed accordingly to the manufacturer's manual. Therefore, samples were diluted 1:10 and subjected to the microplate procedure [190]. The absorbance of all standards and samples was measured at 562 nm on a FLUOstar Omega plate reader. Total protein concentrations were calculated, considering the dilution factor, via the standard curve.

2.2.15 Calcium flux analysis

This method was used to determine the calcium flux of transiently transfected HEK293 cells. Therefore, HEK293 cell were plated at a density of $4x10^4$/96 well and simultaneously transiently transfected with pcDNA3.1-TRPV1-YFP (0.5 µg/30 wells) and/or with pcDNA3.1-ARMS (2.5 µg/30 wells) and/or pRFP-C-RS-sh (1.75 µg/30 wells) using TransIT®-293 Transfection Reagent in a 3:1 ratio. 48 hours post transfection HEK 293 cells were washed with PBS and loaded with the fluorescent calcium indicator dye Fluo 4 AM (1 µM) in DMEM without phenol red for 1 hour. Baseline calcium flux was measured with FLUOstar® Omega Microplate Reader using bottom reading, 7x7 well scanning, 485 BP/510, orbital shaking and 37 °C. Calcium flux of TRPV1 was activated by capsaicin (0.1 nM – 10000 nM) and measured with FLUOstar® Omega Microplate Reader using the same settings [191]. Resulting dose-response curves were fitted via nonlinear regression and least squares fit using Prism 9.1.2 (GraphPad) [185].

2.2.16 xMAP® Antibody Coupling

The xMAP® Antibody Coupling method was utilized to covalently couple antibodies to MagPlex-TAG Microspheres for the development of a proteomic screening. MagPlex-TAG Microspheres are magnetic beads designed for coupling of antibodies enabling enrichment of target protein using immunoprecipitation The antibody coupling was performed accordingly to the manufacturer's manual with 10 µg of antibody per $1x10^6$ microspheres. The coupling procedure was achieved through a two-step carbodiimide reaction involving the primary amino groups on the antibody and the carboxyl functional groups on the microsphere surface. First, the carboxyl groups on the surface of the polystyrene microspheres must be activated with a carbodiimide derivative. EDC (1-Ethyl-3-[3-dimethylaminopropyl]carbodiimide hydrochloride) reacted with the carboxyl groups on the surface of the microspheres to form an active O-acylisourea intermediate. This intermediate formed a more stable ester using Sulfo-NHS (N-hydroxysulfosuccinimide). The final Sulfo-NHS-ester reacted with the primary amines of antibodies to form a covalent amide bond.

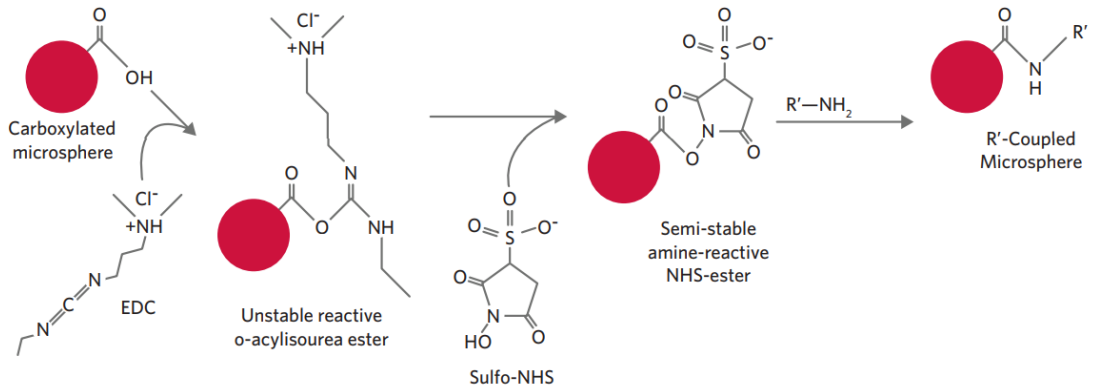

Figure 2.2.16.1: xMAP® Antibody Coupling Chemistry
Antibody coupling is performed via surface carboxyl groups of the microspheres and NHS/EDC chemistry [192].

Once the coupling reaction has been completed, the coupled microspheres were counted with the use of a hemacytometer. The successful antibody coupling reaction was then confirmed accordingly to the manufacturer's manual with a 1:1 dilution and a blank. Therefore, the coupled microspheres were incubated with a phycoerythrin (PE)- labeled antibody (anti-mRPE, goat, P852, Invitrogen) that bound to the coupled antibody. Used antibody dilutions are listed in Table 2.1.3.a: Antibodies. Next, this complex was then analyzed on a FLEXMAP 3D® instrument. The intensity of the fluorescent signal of this reaction is directly proportional to the amount of protein on the surface of the microspheres [192].

2.2.17 FLEXMAP 3D® analysis

This method was used for the detection and quantitation of immunoprecipitated protein of transfected cell extracts. 500 mg total protein of the cleared cell lysates were used for immunoprecipitation. Each sample was incubated overnight and end-to-end mixing with 10^4 anti-ARMS (mouse, MA1-90667, Invitrogen) coupled MagPlex-TAG Microspheres. Incubated MagPlex-TAG Microspheres were split into four sub-samples, washed twice with PBST using Bio-Plex Pro II and incubated for 1 hour at 900 rpm with anti-ARMS (rabbit, ab34790, abcam), anti-TRPV1 (rabbit, ACC-030, Alomone Labs), anti-AKAP79 (rabbit, D28G3, Cell Signaling) or Phospho-PKA substrate (rabbit, 100G7E, Cell Signaling). After antibody incubation, MagPlex-TAG Microspheres were washed twice with PBST using Bio-Plex Pro II, incubated for 1 hour at 900 rpm with anti-rRPE (goat, P-2771MP, Invitrogen) and washed twice with PBST using Bio-Plex Pro II again. Used antibody dilutions are listed in Table 2.1.3.a: Antibodies. MagPlex-TAG Microspheres were resuspended in PBST and analyzed on a FLEXMAP 3D® instrument with a threshold of at least 100 MagPlex-TAG Microspheres per sub-sample as well as a gating between 5000 and 20000 to exclude microsphere complexes of irregular size. Data was saved in comma separated values format. Outliers were identified and removed with ROUT method (Q = 1 %) using Prism 9.1.2 (GraphPad).

2.2.18 Immunoprecipitation with Protein G Mag Sepharose

This method was utilized for Western Blot analysis of immunoprecipitated protein of transfected cell extracts. Protein G Mag Sepharose are magnetic beads designed for coupling of antibodies enabling enrichment of target protein using immunoprecipitation for downstream analyses such as Western Blot [193]. Therefore, 25 µL Protein G Mag Sepharose were washed twice with RIPA Lysis and Extraction Buffer with Halt Protease and Phosphatase Inhibitor Cocktail and incubated 4 hours at 4°C with 1 µg anti-ARMS (mouse, MA1-90667, Invitrogen) by end-to-end mixing. Antibody incubated Protein G Mag Sepharose was washed twice, incubated overnight with 1 mg cleared cell lysate by end-to-end mixing and washed twice. Samples were eluted with 30 µL Sample Buffer Laemmli 2x Concentrate at 37°C for 30 min and subjected to SDS-PAGE using 8 % polyacrylamide gels.

2.2.19 SDS-PAGE

This method was used for protein separation by molecular weight under denaturing conditions. The gel consists of a resolving gel, which is covered with a stacking gel. For the stacking gel, a polymerization density of 5 % was used, for the resolving gel 8 %. The used

components are summarized in Table 2.2.19.a. 15 µL of each sample was loaded onto the gel, which was previously denatured with 30 µL Sample Buffer Laemmli 2x Concentrate at 37°C for 30 min. The voltage applied for the stacking gel was 80 V and 120 V for the resolving gel (Mighty Small™ II SE250/SE260).

Table 2.2.19.a: SDS-PAGE gel preparation (for 10 mL)

	Resolving Gel [8 %]	Stacking Gel [5 %]
H_2O	4.6	5.86
30% Acrylamide mix	2.6	1.34
1.5 M Tris (pH 8.8)	2.6	-
0.5 M Tris (pH 6.8)	-	2.6
10% SDS	0.1	0.1
10% APS	0.1	0.1
TEMED	0.01	0.01

2.2.20 Western Blot

This method served to detect antigen specific proteins. The proteins separated by SDS-PAGE were transferred to a methanol activated PVDF membrane (Semi-Dry Transfer Unit TE77XP, 0.5 mA/cm^2 for 2 hours). The blotting papers were adjusted to the size of the SDS-PAGE insert, soaked in blotting buffer and stacked as shown in Figure 2.2.20.1: Western Blot setup.

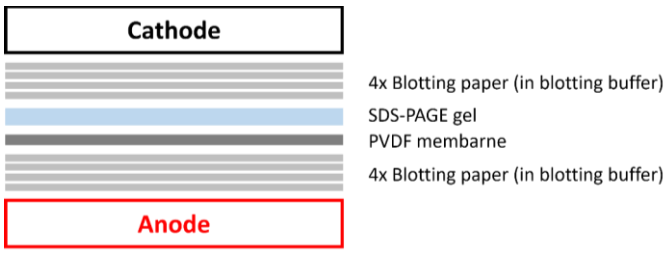

Figure 2.2.20.1: Western Blot setup
Soaked blotting papers were stacked above the anode followed by the PVDF membrane, the SDS-PAGE gel and soaked blotting papers.

After blotting, the membrane was blocked with 5 % BSA in PBST for 1 hour at RT and incubated for 1 hour at RT with the primary antibodies in PBST. After washing thrice for 5 min, the membrane was incubated with the secondary antibody in PBST for 1 hour at RT and washed thrice for 5 min. Used antibody dilutions are listed in Table 2.1.3.a: Antibodies. Protein bands were visualized using Amersham Typhoon Biomolecular Imager with Cy3 profile at 350 V.

3. Results

To determine significant differential expressed miRNAs in the context of chronic pain in polyneuropathy, 30 patients with chronic painful polyneuropathy were compared with 30 age matched healthy patients. Polyneuropathy patients were selected with an average pain of ≥ 4 on a numerical scale (0-10), a chronification score on Mainz Pain Grading System (MPSS) of ≥ II and a pain duration ≥ 6 months. miRNAs were separated from serum for each patient and subsequently quality controlled.

3.1 miRNA library preparation quality controls

3.1.1 Pre library preparation quality control

The primary purpose of the QIAseq miRNA Library QC PCR Panel Kit was to control the quality of the isolated RNA in any next-generation sequencing experiment. Addition of QIAseq miRNA Library QC Spike-Ins during RNA isolation enabled monitoring the comparability and reproducibility from RNA isolation to sequencing. The qPCR assay provided insight into RNA isolation efficiency (UniSp100 and UniSp101), cDNA synthesis efficiency (UniSp6) and controlled for endogenous miRNAs as well as for hemolysis. These endogenous miRNA controls were: miR-30c-5p (biofluids and urine), miR-103a-3p and miR-191-5p, which are well expressed in most tissues, as well as miR-451a and miR-23a-3p, which are found in plasma/serum and served as a hemolysis marker [173]. The complete data is provided in the Appendix under Pre library preparation quality control.

Table 3.1.1.a: RNA Isolation efficiency assessment (n=60)

	UniSp100	UniSp101	ΔC_T
Max	29.81	26.93	3.92
Min	26.95	24.01	2.06
Max-Min	2.86	2.92	-

The UniSp100 and UniSp101 RNA Spike-Ins were used to monitor the RNA isolation efficiency across all samples (Table 3.1.1.a: RNA Isolation efficiency assessment (n=60)). The typical C_T value should be in the range of 31–34 for UniSp100 and 25–28 for UniSp101. Every determined C_T value was below that expected range with a C_T range of 26.95-29.81 for UniSp100 and partly for UniSp101 with a C_T range of 24.01-26.93, indicating a more efficient isolation for UniSp100. Across all 60 samples a C_T deviation of 2.86 for UniSp100 and a C_T deviation of 2.92 for UniSp101 was calculated. The purification was considered

successful, as mentioned in the manufacturer´s protocol, as the C_T deviation across all samples was within a C_T deviation of <2-3. The ΔC_T of UniSp100-UniSp101 ranged between 2.06-3.92 across all 60 samples. However, a ΔC_T of 5-7 was expected accordingly to the manufacturer´s protocol.

Table 3.1.1.b: cDNA synthesis efficiency assessment (n=60)

	UniSp6
Max	17.96
Min	16.18
Max-Min	1.78

The UniSp6 RNA Spike-In was added during cDNA synthesis to monitor cDNA synthesis efficiency across all samples (Table 3.1.1.b: cDNA synthesis efficiency assessment (n=60)). The typical C_T values for UniSp6 should be below 20. Every determined C_T value was below the expected max. C_T of 20. Across all 60 samples a C_T deviation of 1.78 for UniSp6 was calculated. The cDNA synthesis efficiency was considered successful as the C_T deviation across all samples was within a C_T deviation of <1-2, accordingly to the manufacturer´s protocol.

Table 3.1.1.c: Hemolysis indicator (n=60)

	ΔC_T of miR-23a-5p - miR-451a
Max	6.85
Min	1.84

The endogenous controls miR-451a and miR-23a-3p served as a hemolysis marker for each sample (Table 3.1.1.c: Hemolysis indicator (n=60)). Across all 60 samples the ΔC_T of miR-23a-5p - miR-451a ranged between 1.84-6.85 and therefore were below the hemolytic border of ΔC_T <7 and considered successful, accordingly to the manufacturer´s protocol.

Table 3.1.1.d: Endogenous controls (n=60)

	miR-103a-3p	**miR-191-5p**	**miR-30c-5p**
Max	30.92	31.10	31.47
Min	21.25	23.93	24.45

The endogenous controls miR-103a-3p, miR-191-5p and miR-30c-5p served as biological markers for each sample (Table 3.1.1.d: Endogenous controls (n=60)). Across all 60 samples the C_T values of miR-103a-3p ranged between 21.25-30.92, while the C_T values of miR-191-5p varied between 23.93-31.10 and the C_T values of miR-30c-5p ranged between 24.45-31.47 respectively. Thus, purification was considered successful, accordingly to the manufacturer´s protocol, as all biological markers were present in all samples. Since all quality controls were successful, except the expected ΔC_T of UniSp100-UniSp101 of 5-7, and the UniSp100/UniSp101 Spike-Ins were added in a fixed/non-modifiable ratio per RNA isolation as well as UniSp100/UniSp101 showed comparable values across all samples, none of the samples was identified as outlier and no sample was excluded for library preparation (2.2.4 miRNA library preparation).

3.1.2 Pre sequencing quality control

The High Sensitivity DNA kit was used to provide quality control, sizing and quantitation of the prepared and cleaned miRNA Sequencing Library with the Agilent Bioanalyzer 2100 system. Figure 3.1.2.1: Electropherogram of P20 [Index 15] illustrates a representative electropherogram. All further electropherograms, after the automated size selection, are shown in the Appendix under Pre sequencing quality control.

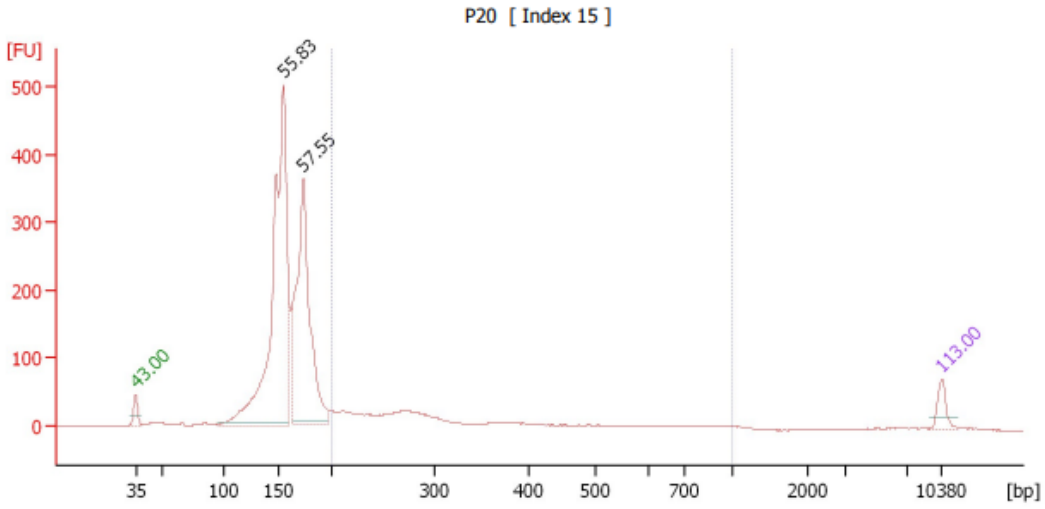

Peak table for sample 4 : P20

Peak	Size [bp]	Conc. [pg/µl]	Molarity [pmol/l]	Observations
1	35	125.00	5,411.2	Lower Marker
2	155	2,988.45	29,214.9	
3	174	1,917.93	16,721.8	
4	10,380	75.00	10.9	Upper Marker

Figure 3.1.2.1: Electropherogram of P20 [Index 15]
The electropherogram of P20 [Index 15] shows base pair (bp) on the x-axis and fluorescence units (FU) on the y-axis. Four peaks were determined: the lower/upper marker and two peaks at 155 bp and 174 bp.

The electropherogram of P20 [Index 15] shows base pair (bp) on the x-axis and fluorescence units (FU) on the y-axis. The peak table harbors four peaks: Peak 1 with a size of 35 bp, a concentration of 125 pg/µL and a molarity of 5411.2 pmol/L was identified as a lower marker by the Agilent Bioanalyzer 2100 system. Peak 2 with a size of 155 bp, a concentration of 2988.45 pg/µL and a molarity of 29214.9 pmol/L was classified as adapter dimer peak as well as Peak 3 with a size of 174 bp, a concentration of 1917.93 pg/µL and a molarity of 16721.8 pmol/L was categorized as miRNA-sized library in the QIAseq miRNA Library Kit Handbook [174]. Peak 4 with a size of 10380 bp, a concentration of 75 pg/µL and a molarity of 10.9 pmol/L was identified as an upper marker by the Agilent Bioanalyzer 2100 system. For all samples, in case of peaks showing at approximately 155 bp (adapter dimers), or in case of other undesired bands, automated size selection via BluePippin (2.2.6 Adapter dimer removal via BluePippin) on the remainder of the miRNA Sequencing Library was performed to select the specific library of interest.

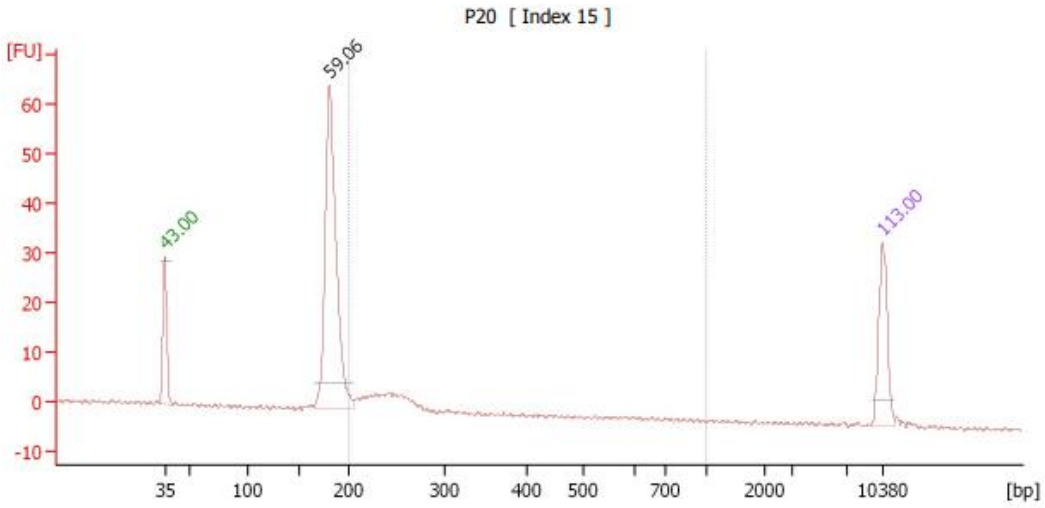

Peak table for sample 5 : P20

Peak		Size [bp]	Conc. [pg/µl]	Molarity [pmol/l]	Observations
1	◀	35	125.00	5,411.3	Lower Marker
2		181	603.79	5,054.9	
3	▶	10,380	75.00	10.9	Upper Marker

Figure 3.1.2.2: Electropherogram of P20 [Index 15] after BluePippin size selection
The electropherogram of P20 [Index 15] shows base pair (bp) on the x-axis and fluorescence units (FU) on the y-axis. Three peaks were determined: the lower/upper marker and one peak at 181 bp.

The electropherogram of P20 [Index 15] after BluePippin size selection shows base pair (bp) on the x-axis and fluorescence units (FU) on the y-axis. The peak table harbors three peaks: Peak 1 with a size of 35 bp, a concentration of 125 pg/µL and a molarity of 5411.3 pmol/L was identified as a lower marker by the Agilent Bioanalyzer 2100 system. Peak 2 with a size of 181 bp, a concentration of 603.79 pg/µL and a molarity of

5054.9 pmol/L was classified as selected miRNA-sized library. Peak 3 with a size of 10380 bp, a concentration of 75 pg/µL and a molarity of 10.9 pmol/L was identified as an upper marker by the Agilent Bioanalyzer 2100 system. Since all samples were free of adapter dimers after BluePippin size selection and reached the minimum molarity of 0.5 nM for further processing, all samples were subjected to sequencing (2.2.7 Sequencing).

3.2 Sequencing

The Illumina MiSeq was used to enable next-generation sequencing of mature miRNAs for differential expression analysis of polyneuropathy vs. control serum samples. Therefore, quality controlled miRNA Sequencing Libraries were diluted to 0.5 nM and four samples at a time were pooled. Pooled 0.5 nM libraries were denatured and diluted to 20 pM as well as loaded onto a MiSeq Reagent Kit v3 cartridge with 13 pM and 1 % phiX. For sequencing, FASTQ Only and TruSeq Small RNA with a 75 bp single read was chosen. Table 3.2.a: Sequencing run summary and Table 3.2.b: Sequencing run indexing show a representative sequencing result, all further sequencing results are attached in the Appendix under Sequencing statistic. The sequencing run resulted in a density of 1236±31 K/mm^2 (of clusters detected by image analysis) with a cluster PF of 89.25±1.56 % (percentage of clusters passing filtering) leading to 26.37 M reads PF (number of clusters passing filtering) with 97.13 % ≥ Q30 (percentage of bases with a quality score of 30 or higher, meaning ≥ 99.9 % base call accuracy) and equal index distribution between 22.03-27.44 %. Phas/Prephas (percentage of molecules in a cluster for which sequencing falls behind, phasing, or jumps ahead, prephasing) were 0.191/0.052 %. The percentage that aligned to the phiX genome was 0.68±0.02 %.

Table 3.2.a: Sequencing run summary

Density (K/mm2)	Cluster PF (%)	Phas/Prephas (%)	Reads PF (M)	≥ Q30 (%)	Aligned (%)
1236±31	89.25±1.56	0.191/0.052	26.37	97.13	0.68±0.02

Table 3.2.b: Sequencing run indexing

Index	% Reads Identified (PF)
TGACCA	27.44
ACAGTG	24.59
CAGATC	22.03
GATCAG	22.57

3.2.1 Sample-to-sample comparison

Resulting FASTQ files were analyzed and the reads mapped as well as counted. The comprehensive set of 52 QIAseq miRNA Library QC Spike-Ins, added in 2.2.3 miRNA isolation pre library preparation quality control, allowed thorough quality control of the NGS data by assessing the reproducibility of the reads mapped to these exogenous sequences. Following mapping of the 52 QIAseq miRNA Library QC Spike-In reads, they were normalized to the total number of reads per sample. After this simple normalization to individual sample reads was done for all Spike-Ins in all samples, they were evaluated for normality and a correlation matrix was plotted for sample-to-sample comparison. The corresponding data is attached in the Appendix under Sample-to-sample comparison.

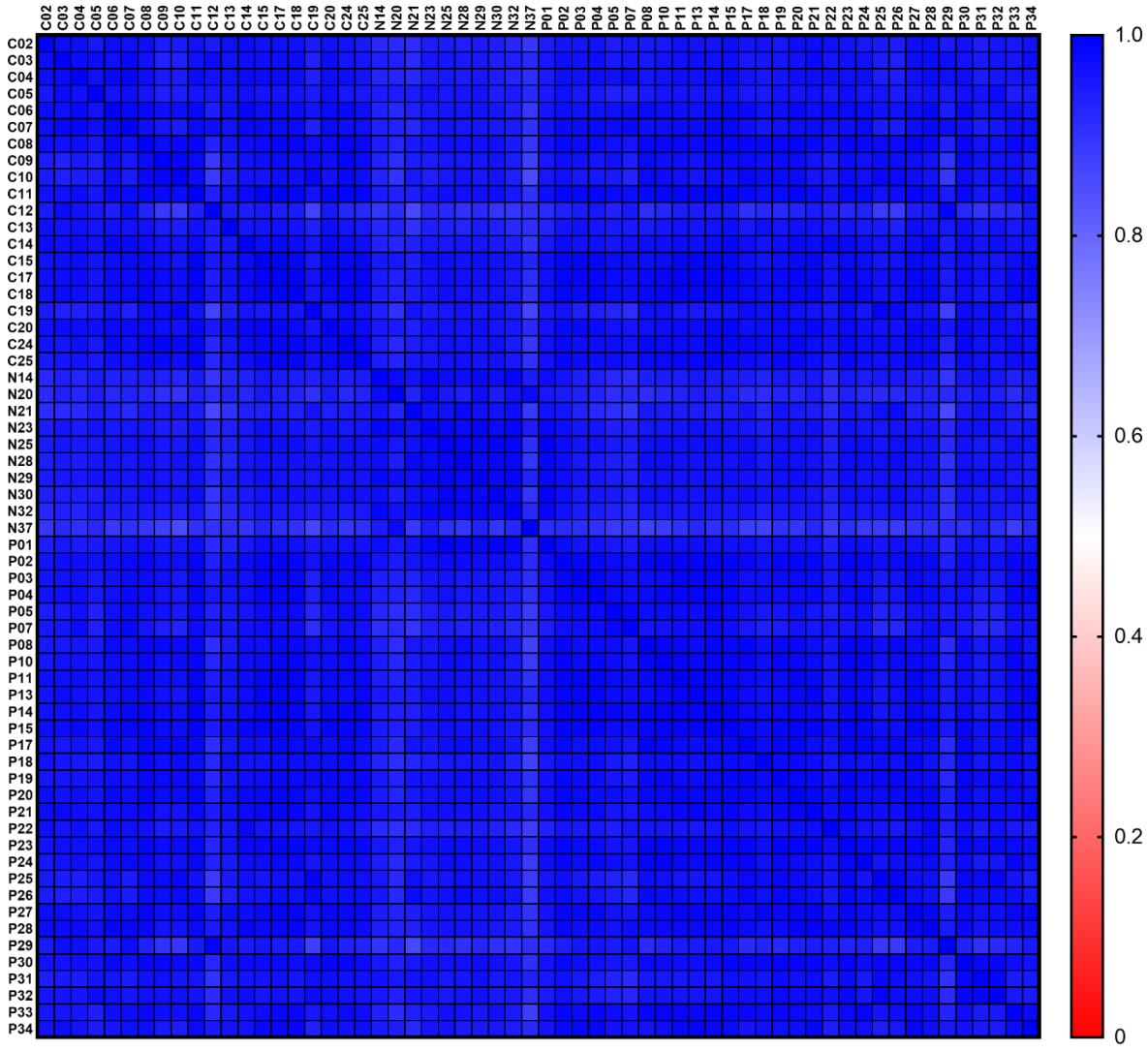

Figure 3.2.1.1: Normalized sample-to-sample spearman correlation matrix

52 QIAseq miRNA Library QC Spike-Ins were added to each sample. After sequencing, Spike-In reads were normalized to the total number of reads per sample. For all samples the spearman r values ranged from 0.86-0.99.

Figure 3.2.1.1: Normalized sample-to-sample spearman correlation matrix illustrates the spearman correlation matrix for all samples. For all samples the spearman r values ranged from 0.86-0.99. According, to the QIAseq™ miRNA Library QC PCR Handbook, the expected correlation should be R^2 = 0.95–0.99 within a batch of samples purified on the same day and a bit weaker when comparing day-to-day correlation. Samples that deviate from these values, should be considered technical outliers and should potentially be excluded from downstream analysis [173]. Since this would require normal distribution of the data to calculate R^2 from pearson r and the performed Shapiro-Wilks Normality Test did not show normality, the evaluation suggested in the manufacturer´s protocol could not be considered [194–196]. Thus, a new acceptable range of r = 0.85-0.99 was defined. This range is usually associated with strong correlation [197, 198]. Finally, all samples were used for miRNA analysis/differential expression analysis.

3.2.2 miRNA analysis

The resulting FASTQ file of each miRNA library was analyzed and used to perform a differential expression analysis. The FASTQ files are attached in the Appendix under Sequencing FASTQ. For quantification of the miRNA libraries, the miRNA reads were counted and annotated. For differential expression analysis, the resulting quantification of each miRNA library was utilized and grouped based on polyneuropathy/control. Despite age matched groups, differential expression analysis controlled for age to rule out age-based false positive differential miRNA expression (2.2.8 miRNA analysis). Table 3.2.2.a: Differential expression analysis shows the filtered results, fold change > 2 or fold change < -2 and Bonferroni corrected p-value < 0.05, of the differential expression analysis. In fold change analysis, 2 or 1.5 is often used as the cutoff to determine differentially expressed genes [199, 200]. In multiple hypothesis testing, the Bonferroni correction is a conservative method for multiple-comparison correction, used when several statistical tests are performed simultaneously, to control the occurrence of false positives [201]. The hsa-miR-3135b was determined with the largest fold change of -6.30 and a highly significant Bonferroni corrected p-value of 5.94E-11. Two other miRNAs were downregulated as well: hsa-miR-584-5p with the smallest fold change of -2.62 and a Bonferroni corrected p-value of 1.43E-6 as well as hsa-miR-12136 with a fold change of -3.80 and a Bonferroni corrected p-value of 7.50E-4. The only upregulated miRNA was hsa-miR-550a-3p with a fold change of 4.27 and a significant Bonferroni corrected p-value of 0.02, respectively.

Table 3.2.2.a: Differential expression analysis

	Fold change	Bonferroni
hsa-miR-3135b	-6.30	5.94E-11
hsa-miR-584-5p	-2.62	1.43E-6
hsa-miR-12136	-3.80	7.50E-4
hsa-miR-550a-3p	4.27	0.02

3.2.3 miRNA target prediction

The differentially expressed and filtered miRNAs were subjected to miRDB to perform a target prediction (human). miRDB is an online database for miRNA target prediction and functional mapping. All the targets in miRDB are predicted by MirTarget which was developed by analyzing thousands of miRNA-target interactions. From these interactions, common features associated with miRNA binding/target downregulation have been identified and used to predict miRNA targets with machine learning methods [202]. Table 3.2.3.a to Table 3.2.3.d show the top 3 predictions for each differentially expressed and filtered miRNA.

Table 3.2.3.a: hsa-miR-3135b target prediction

Target Detail	Target Rank	Target Score	Gene Symbol	Gene Description
Details	1	99	LRRC27	leucine rich repeat containing 27
Details	2	96	FMNL3	formin like 3
Details	3	96	TTC21B	tetratricopeptide repeat domain 21B

Table 3.2.3.a: hsa-miR-3135b target prediction contains the gene leucine rich repeat containing 27 (LRRC27) at target rank 1 with a target score of 99. LRRC27 is expressed in platelets and its overexpression is associated with preeclampsia, which among other symptoms manifests in elevated blood pressure [203]. With a target score of 96, target rank 2 is assigned to the gene formin like 3 (FMNL3). FMNL3 is expressed in endothelial cells and is a known cytoskeletal regulator of angiogenesis [204, 205]. Thus, modulating the maintenance of epithelial cohesion during dynamic processes, such as wound repair [206]. Finally, target rank 3 harbors the gene tetratricopeptide repeat domain 21B (TTC21B) with a target score of 96. TTC21B is expressed in the primary cilium and missense variants are associated with the tubuloglomerular kidney disease and arterial hypertension [207].

Table 3.2.3.b: hsa-miR-584-5p target prediction

Target Detail	Target Rank	Target Score	Gene Symbol	Gene Description
Details	1	96	USP6NL	USP6 N-terminal like
Details	2	95	AVPR1A	arginine vasopressin receptor 1A
Details	3	94	SETD5	SET domain containing 5

Table 3.2.3.b: hsa-miR-584-5p target prediction harbors the gene USP6 N-terminal like (USP6NL) at target rank 1 with a target score of 96. USP6NL is a GTPase-activating protein that functions as a deubiquitinating enzyme, regulating endocytosis and signal transduction. It is expressed in various cancer types and seems to promote the growth and proliferation of cancer cells. Cancer cells with high levels of USP6NL experienced delayed endocytosis and degradation of EGFR [208]. With a target score of 95, target rank 2 is assigned to the gene arginine vasopressin receptor 1A (AVPR1A). AVPR1A is expressed in peripheral blood vessels encoding a receptor for arginine vasopressin, a vasoconstricting hormone. Thus, modulating and elevating blood pressure [209]. Finally, target rank 3 with a target score of 94 is the gene SET domain containing 5 (SETD5). SETD5 is a ubiquitously expressed protein and related to the syndromic autism spectrum disorder. It seems to control neural cell proliferation and synaptic activity/connectivity [210–212].

Table 3.2.3.c: hsa-miR-12136 target prediction

Target Detail	Target Rank	Target Score	Gene Symbol	Gene Description
Details	1	100	IGSF11	immunoglobulin superfamily member 11
Details	2	100	DAAM1	dishevelled associated activator of morphogenesis 1
Details	3	100	STXBP5	syntaxin binding protein 5

Table 3.2.3.c: hsa-miR-12136 target prediction contains the gene immunoglobulin superfamily member 11 (IGSF11) at target rank 1 with a target score of 100. IGSF11 is preferentially expressed in the brain and functions as adhesion molecule, interacting with the postsynaptic scaffolding protein PSD-95 and AMPAR glutamate receptors [213]. It is required for synaptic development and overexpression of IGSF11 enlarges the presynaptic boutons as well as induces ectopic synapses [214]. Target rank 2 with a target score of 100 is assigned to the gene disheveled associated activator of morphogenesis 1 (DAAM1). The

formin DAAM1 has been shown to aid in the development of neuronal systems, through nucleating, elongating and possibly, bundling actin. The dynamic assembly of filamentous actin plays an essential role in the assembly of presynaptic boutons and the fusion, mobilization as well as recycling of synaptic vesicles during activity-dependent neurotransmitter release [215, 216]. Finally, target rank 3 with a target score of 100 is the gene syntaxin binding protein 5 (STXBP5). STXBP5 is expressed in human endothelial cells and is associated with venous thromboembolism that manifests in impaired blood flow, vessel walls and coagulation factors. It seems to induce venous thromboembolism through inhibition of endothelial exocytosis and promotion of platelet secretion/thrombosis [217].

Table 3.2.3.d: hsa-miR-550a-3p target prediction

Target Detail	Target Rank	Target Score	Gene Symbol	Gene Description
Details	1	98	MYH10	myosin heavy chain 10
Details	2	98	SYT4	synaptotagmin 4
Details	3	95	MYT1L	myelin transcription factor 1 like

Table 3.2.3.d: hsa-miR-550a-3p target prediction harbors the gene myosin heavy chain 10 (MYH10) at target rank 1 with a target score of 98. MYH10 belongs to the group of non-muscle myosin II and induces cell migration by regulating the localization of the centriole and the Golgi apparatus. It has been found that MYH10 participates in the critical developmental process of coronary vessel formation as well as that MYH10 is able to interact with sodium channels, modulating their current density and gating properties [218, 219]. With a target score of 98, target rank 2 is assigned to the gene synaptotagmin 4 (SYT4). SYT4 regulates membrane traffic in neurons and seems to be important for dendrite growth, since overexpression of SYT4 in melanocytes resulted in dendrite extension [220]. Finally, target rank 3 with a target score of 95 is the gene myelin transcription factor 1 like (MYT1L). MYT1L is mainly expressed in neurons including dorsal root ganglia. MYT1L is the only known transcription factor that is specifically expressed in all neurons throughout life, indicating that repression is critical for maintaining neuronal identity. It promotes axonal development/differentiation, neurite outgrowth/proliferation, synaptic transmission and extracellular matrix composition as well as remyelination after induced demyelination [221–223].

3.3 TRPV1, ARMS, PKA and AKAP79 signaling complex

Since TRPV1 seems to be one of the major contributors of nociception and is associated with neuropathic pain, the influence of PKA phosphorylated ARMS on the sensitivity of TRPV1 as well as the role of AKAP79 during PKA phosphorylation of ARMS was characterized.

3.3.1 TRPV1/ARMS co-immunoprecipitation

Initially, possible PKA-sites in the sequence of ARMS were identified using a (R/K)-(R/K)-X-(S/T) pattern search [168]. This revealed five canonical PKA-sites: S882 (RRVSQ), T903 (RRDTY), S1251/52 (RRSSH), S1439/40 (KKSSE) and S1526/27 (KKDSSD), illustrated in Figure 3.3.1.1: Schematic structure of ARMS and its potential PKA sites. To investigate possible functional and physical interactions between ARMS and TRPV1, TRPV1 and PKA-site-deficient ARMS mutants were co-expressed in HEK293 cells. Therefore, point mutations were incorporated into ARMS, resulting in each ARMS mutant only containing their denoted single PKA-site, while all other PKA-sites were mutated to containing alanine instead of serine or threonine (2.2.9 Site-Directed Mutagenesis). Additionally, in mutant $ARMS_0$ all PKA-sites were eliminated. Mutations were confirmed by sequencing via Eurofins Genomics Mix2Seq Kit and alignment to wild type ARMS with SnapGene 6.0 from GSL Biotech LLC. Alignments are attached in the Appendix under Mutation confirmation.

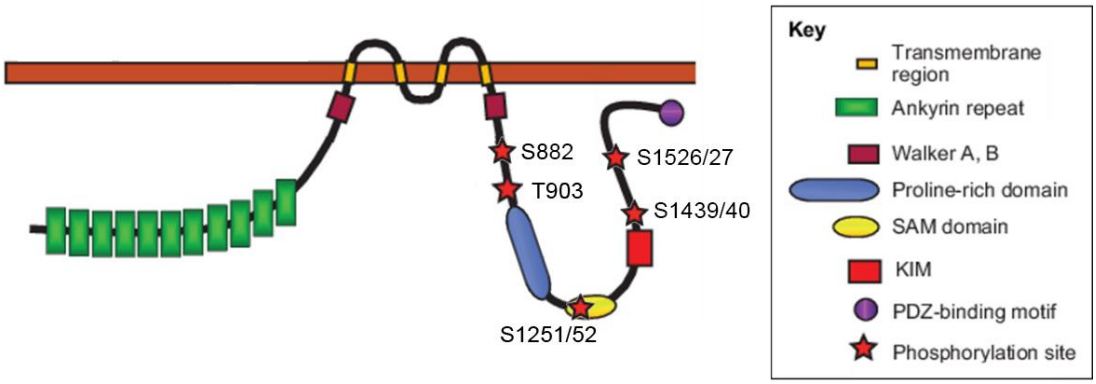

Figure 3.3.1.1: Schematic structure of ARMS and its potential PKA sites
ARMS has four transmembrane domains and intracellular N- and C-termini that contain several protein-protein interaction motives and five potential PKA phosphorylation sites [123].

Transfection efficiency of TRPV1 and PKA-site mutant or wild type ARMS was controlled by TRPV1-YFP excitation at 470 ± 20 nm and emission at 534 ± 27.5 nm, resulting in equal transfection efficiencies among all transfection combinations. Figure 3.3.1.2: HEK293 transfection efficiency 48 h post-transfection shows a representative transfection result:

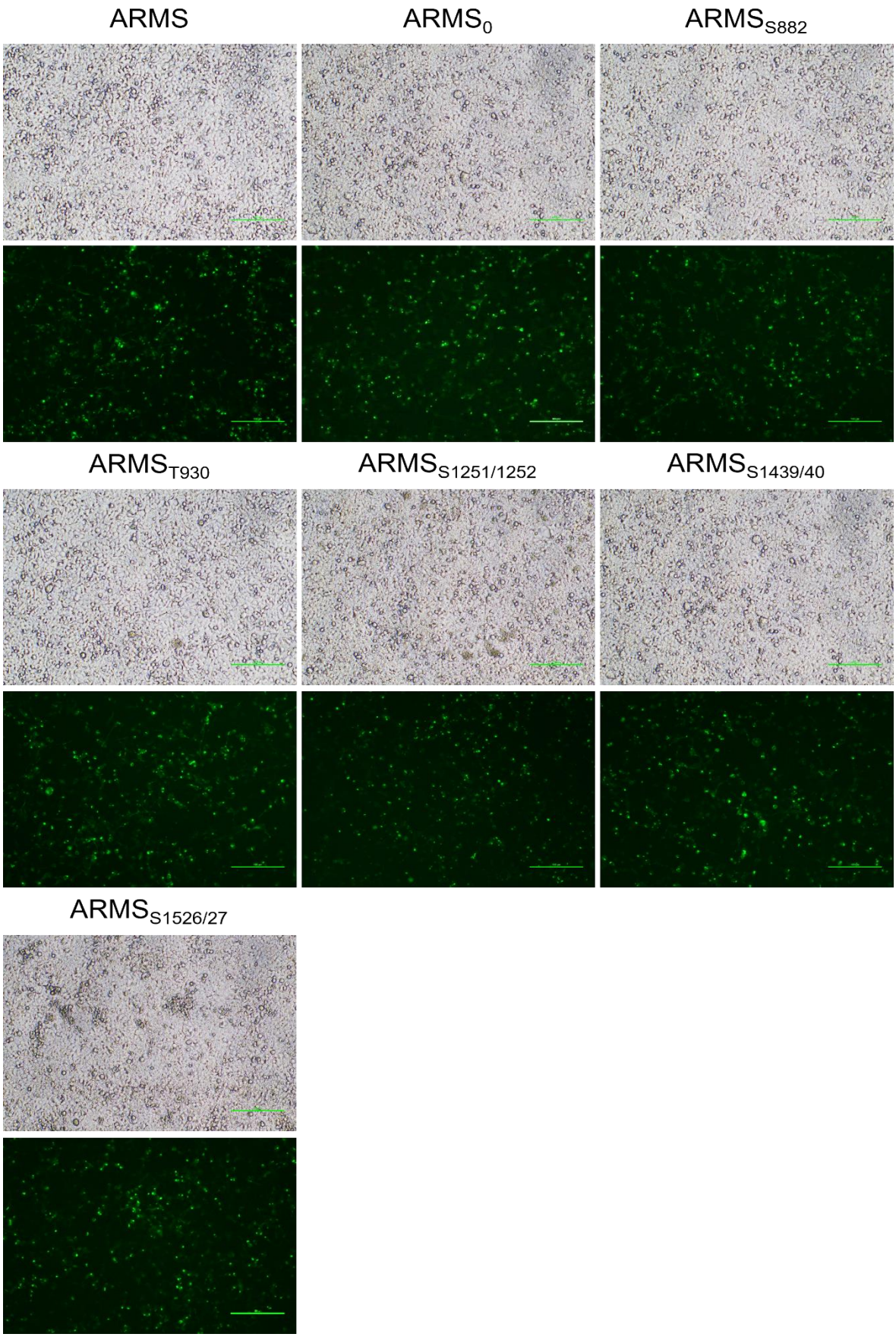

Figure 3.3.1.2: HEK293 transfection efficiency 48 h post-transfection
Nikon ECLIPSE Ts2-FL 10x/0.3, 20 ms (bright field) & 200 ms (FITC), 100 µm scale

Co-immunoprecipitation experiments were performed with an antibody directed against ARMS (mouse, MA1-90667, Invitrogen). The precipitate was further analyzed by the Luminex FlexMap3D platform with antibodies against ARMS (rabbit, ab34790, abcam) and TRPV1 (rabbit, ACC-030, Alomone Labs). For the assessment of the native interaction rate of TRPV1 and ARMS, the transfected HEK293 cells did not undergo any additional treatments. To determine the influence of PKA phosphorylation in terms of a decreasing or increasing interaction rate, transfected HEK293 cells were additionally treated with the PKA inhibitor H89 (10 µM), PKD inhibitor BPKDi (1 µM) or with the cAMP pathway activator forskolin (50 µM), which activates the synthesis of cAMP by directly stimulating adenylyl cyclase, together with IMBX (100 µM; an inhibitor of cyclic nucleotide phosphodiesterase). Results were then baseline corrected and transformed into percent of TRPV1 and ARMS interaction by dividing TRPV1 mean fluorescence intensity (MFI) by ARMS MFI for each mutant as well as the wild type:

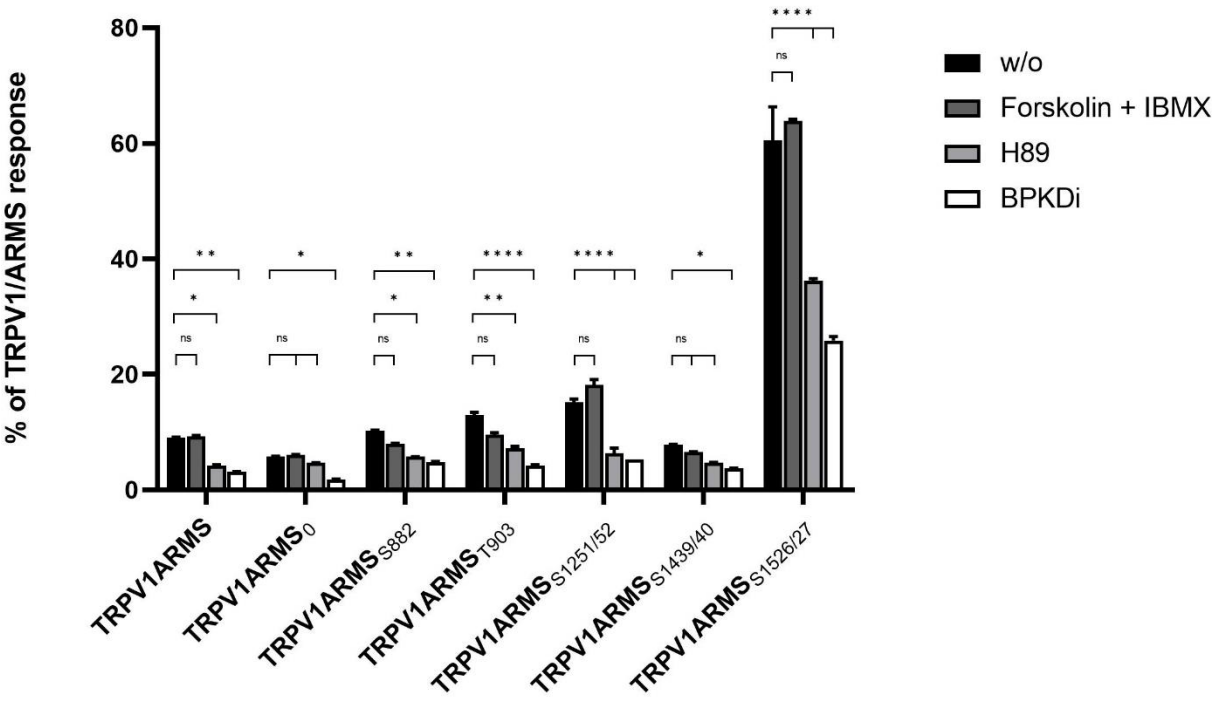

Figure 3.3.1.3: Co-immunoprecipitation of TRPV1/ARMS in transfected HEK293
Histogram of TRPV1/ARMS response in %. Data are presented as means ± SEM. *n* = 3. Statistical significance is denoted as ns = not significant, p<0.05 (*), p<0.01 (**), p<0.001 (***), p<0.0001 (****). BLACK: without stimulation or inhibition, DARK GREY: PKA stimulated with forskolin and IBMX, GREY: PKA inhibited with H89, WHITE: PKD inhibited with BPKDi. Interaction ratio was calculated: TRPV1 divided by ARMS (MFI). PKA stimulation does not alter the interaction. PKA/PKD inhibition decreases the interaction.

The screening confirmed the known native interaction of TRPV1 and wild type ARMS and showed differences regarding the ARMS mutants. About 9 % of wild type ARMS MFI was associated with TRPV1 MFI, while 5 % of $ARMS_{0}$, 10 % of $ARMS_{S882}$, 12 % of $ARMS_{T903}$, 15 % of $ARMS_{S1251/52}$, 7 % of $ARMS_{S1439/40}$ and 60 % of $ARMS_{S1526/27}$ were correlated with

TRPV1 MFI. For all mutants except $ARMS_{S1526/27}$, the relative MFI ranged in a narrow window between 5-15 %. In contrast, $ARMS_{S1526/27}$ showed a significantly increased association of 60 % with TRPV1. However, even $ARMS_0$, with all potential PKA-sites eliminated, showed a minimal association of 5 % with TRPV1. Thus, indicating an additional PKA-independent factor for interaction. Therefore, PKA was stimulated via forskolin and IBMX to force PKA mediated phosphorylation. Stimulation did not significantly increase the MFI association of TRPV1 with $ARMS_0$ (6 %), $ARMS_{S1251/52}$ (18 %) or $ARMS_{S1526/27}$ (63 %), while the MFI association of $ARMS_{S882}$ (7 %), $ARMS_{T903}$ (9 %), $ARMS_{S1439/40}$ (6 %) and TRPV1 did not significantly decrease, compared to the native untreated condition. Wild type ARMS, with all native PKA-sites, showed an unchanged association of 9 % with TRPV1. Thus, indicating that PKA mediated phosphorylation does not alter the interaction with TRPV1 or that ARMS is already basal phosphorylated. Since PKA stimulation via forskolin and IBMX did not alter the interaction with TRPV1, the PKA inhibitor H89 was used to induce an interaction change with the potentially basal phosphorylated ARMS. The PKA inhibitor H89 did not significantly decreased the MFI rate of $ARMS_0$ with TRPV1 to 4 % and of $ARMS_{S1439/40}$ to 4 % but significantly decreased the rate of wild type ARMS with TRPV1 to 4 %, of $ARMS_{S882}$ to 5 %, of $ARMS_{T903}$ to 7 %, of $ARMS_{S1251/52}$ to 6 % and of $ARMS_{S1526/27}$ to 36 %. Thus, resulting in a MFI interaction drop affecting most mutants and the wild type compared to the condition without PKA inhibitor. As this drop of MFI interaction affected the wild type and most mutants, halving the native MFI interaction rate, but not $ARMS_0$, H89 results indicate a PKA dependent interaction decrease by inhibiting basal PKA phosphorylation of ARMS. Nevertheless, these results indicate an additional factor that enables interaction with TRPV1, as already inferred with untreated $ARMS_0$. Since untreated $ARMS_0$ and H89 results indicated an additional factor that induces interaction between TRPV1 and ARMS, the effect of PKD inhibitor BPKDi was determined. Surprisingly, the PKD inhibitor BPKDi decreased the MFI rate significantly of the wild type and all mutants. Meaning, the MFI rate of wild type ARMS with TRPV1 decreased to 3 %, the rate of $ARMS_0$ to 2 %, of $ARMS_{S882}$ to 4 %, of $ARMS_{T903}$ to 4 %, of $ARMS_{S1251/52}$ to 5 %, of $ARMS_{S1439/40}$ to 3 % and of $ARMS_{S1526/27}$ to 25 %. Thus, resulting in a significant MFI interaction decrease affecting all mutants and the wild type, similar to the effect of H89. Especially, the significant decrease of $ARMS_0$ indicates that the additional factor that enables interaction between TRPV1 and ARMS could be PKD mediated phosphorylation.

3.3.2 ARMS phosphorylation sites

The phosphorylation status of each ARMS mutant as well as the wild type was determined via pPKA substrate antibody (rabbit, 100G7E, Cell Signaling). For the assessment of ARMS native phosphorylation status, the transfected HEK293 cells did not undergo any additional treatments. However, to determine PKA mediated ARMS phosphorylation under PKA stimulation/inhibition, transfected HEK293 cells were additionally treated with the PKA inhibitor H89 (10 µM), PKD inhibitor BPKDi (1 µM) or with the cAMP pathway activator forskolin (50 µM), which activates the synthesis of cAMP by directly stimulating adenylyl cyclase, together with IMBX (100 µM) an inhibitor of cyclic nucleotide phosphodiesterase (: Phosphorylation status of ARMS in HEK293):

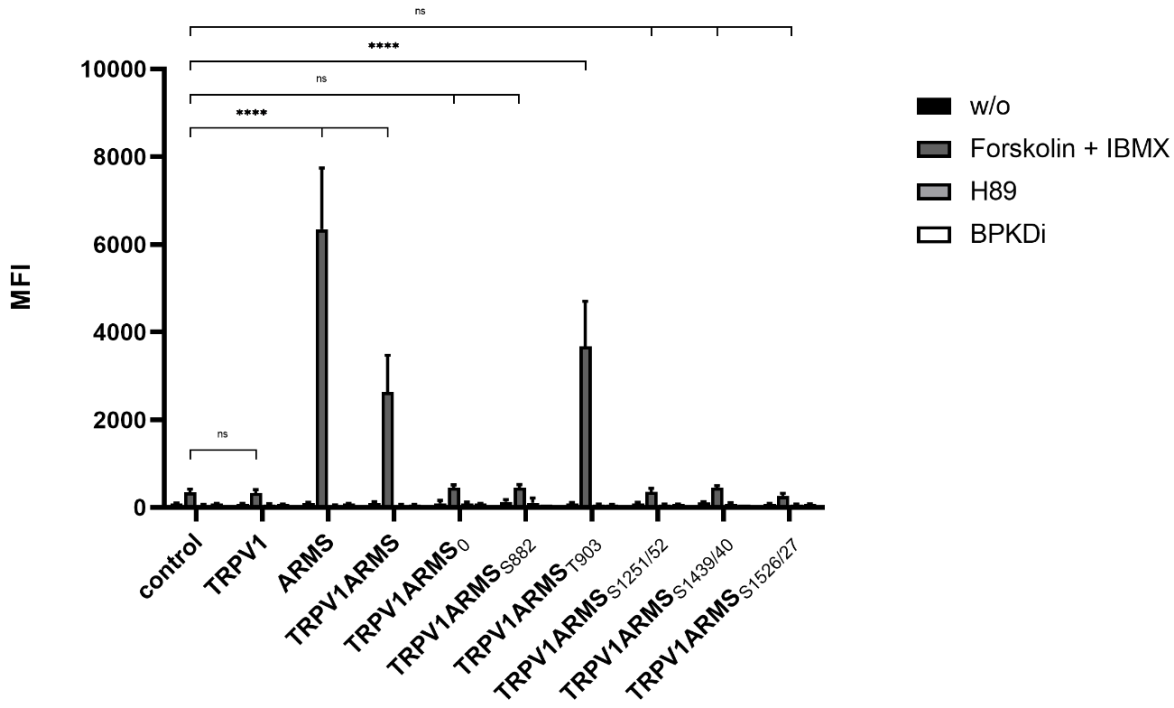

Figure 3.3.2.1: Phosphorylation status of ARMS in HEK293
Histogram in MFI. Data are presented as means ± SEM. *n* = 3. Statistical significance is denoted as ns = not significant, p<0.05 (*), p<0.01 (**), p<0.001 (***), p<0.0001 (****). BLACK: without stimulation or inhibition, DARK GREY: PKA stimulated with forskolin and IBMX, GREY: PKA inhibited with H89, WHITE: PKD inhibited with BPKDi. ARMS is phosphorylated at T903 during PKA stimulation.

The screening revealed that wild type ARMS and the ARMS mutants are, under native conditions and during PKA inhibition with H89 or PKD inhibition with BPKDi, presumably not phosphorylated. This refutes the assumed conclusion of already basal phosphorylated ARMS in 3.3.1 TRPV1/ARMS co-immunoprecipitation. PKA stimulation, via forskolin and IBMX, resulted in the phosphorylation of ARMS, TRPV1/ARMS and TRPV1/ARMS$_{T903}$. However, TRPV1 double transfections with ARMS$_0$, ARMS$_{S882}$, ARMS$_{S1251/52}$, ARMS$_{S1439/40}$

or $ARMS_{S1526/27}$ exposed that they are probably not phosphorylated, even under PKA stimulation via forskolin and IBMX. This shows that ARMS is a PKA target and that ARMS is phosphorylated by PKA at the amino acid T903, even if only with PKA stimulation via forskolin and IBMX. Together with the results from 3.3.1 TRPV1/ARMS co-immunoprecipitation, this leads to the conclusion that PKA mediated phosphorylation does not alter the interaction of TRPV1/ARMS. Since forced PKA stimulation via forskolin and IBMX did not significantly increase or decrease the MFI association of TRPV1 with wild type ARMS or all ARMS mutants. Thus, indicating a PKA independent TRPV1/ARMS interaction. However, this would also mean that the decreasing interaction effect of H89 is presumably unspecific, possibly inhibiting other kinases like PKD, and therefore being PKA independent, as well. On the other hand, this would indicate that TRPV1/ARMS interaction is presumably mediated by PKD phosphorylation as the decreasing interaction effect of BPKDi assumes.

3.3.3 ARMS/AKAP79 co-immunoprecipitation

Since AKAP79 was found to be important in PKA-dependent sensitization of TRPV1, the role of AKAP79 in the phosphorylation of ARMS was explored. As the pPKA substrate screening revealed, only PKA stimulation via forskolin and IBMX seemed to result in the phosphorylation of ARMS. Therefore, TRPV1 and PKA-site mutant ARMS were co-expressed in HEK293 cells and stimulated via forskolin (50 µM) and IBMX (100 µM). Cell lysates were verified to contain endogenous AKAP79 by Western Blot. Co-immunoprecipitation experiments were performed with an antibody directed against ARMS (mouse, MA1-90667, Invitrogen). The precipitate was further analyzed by the Luminex FlexMap3D platform with antibodies against TRPV1 (rabbit, ACC-030, Alomone Labs), ARMS (rabbit, ab34790, abcam), pPKA substrate (rabbit, 100G7E, Cell Signaling) and AKAP79 (rabbit, D28G3, Cell Signaling). The screening confirmed the previously observed phosphorylation pattern of ARMS and its mutants via forskolin and IBMX stimulation as well as the known interaction of TRPV1/ARMS. Furthermore, the screening revealed that AKAP79 was not detectable under the chosen conditions by the Luminex FlexMap3D platform (Figure 3.3.3.1: Co-immunoprecipitation of ARMS/AKAP79 in HEK293):

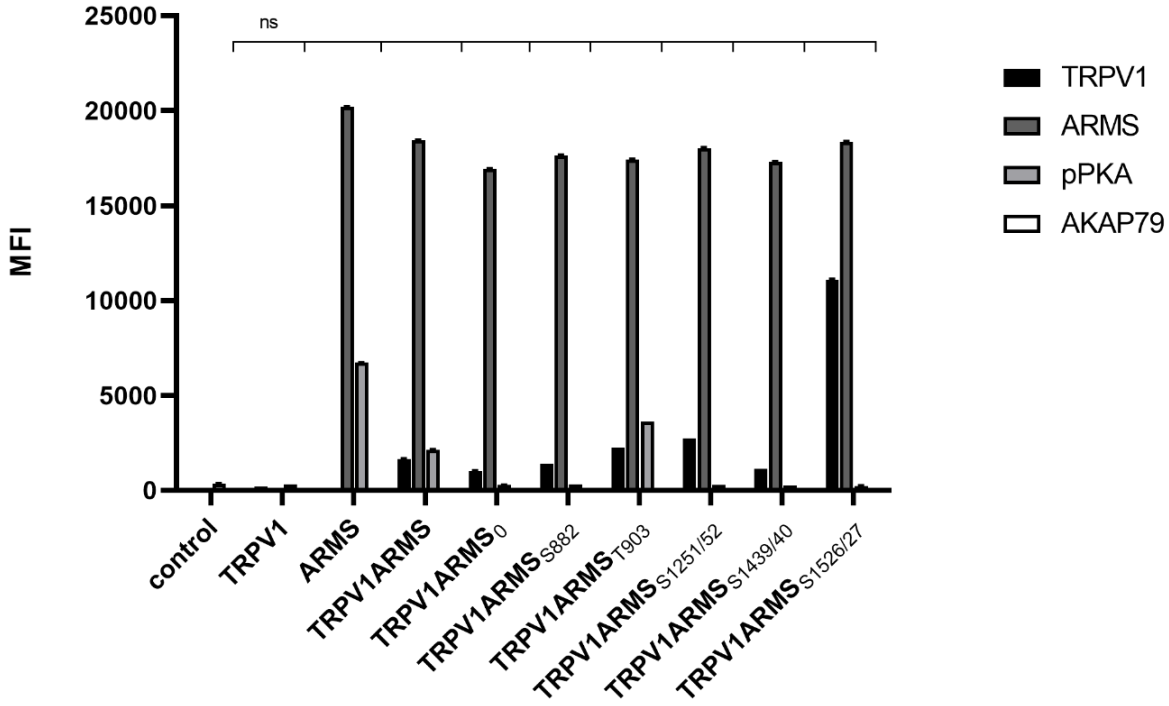

Figure 3.3.3.1: Co-immunoprecipitation of ARMS/AKAP79 in HEK293
TRPV1/ARMS transfected, PKA stimulated and detection via anti-TRPV1, anti-ARMS, anti-AKAP79 and pPKA substrate antibody. Histogram in MFI. Data are presented as means ± SEM. *n* = 3. Statistical significance is denoted as ns = not significant, p<0.05 (*), p<0.01 (**), p<0.001 (***), p<0.0001 (****). AKAP79 was not detectable.

To exclude epitope masking as a reason for this native technique, a denaturing western blot analysis was performed. Therefore, TRPV1 and PKA-site mutant ARMS were co-expressed in HEK293 cells and stimulated via forskolin (50 µM) and IBMX (100 µM). Cell lysates were incubated with anti-ARMS (mouse, MA1-90667, Invitrogen) coupled Protein G Mag Sepharose and subjected to SDS-PAGE/Western Blot. The membrane was probed with the primary antibodies: anti-ARMS (rabbit, ab34790, abcam), anti-TRPV1 (rabbit, ACC-030, Alomone Labs) and anti-AKAP79 (rabbit, D28G3, Cell Signaling). The secondary antibody, anti-Rabbit Alexa Fluor 555 (goat, A-21428, Invitrogen), was visualized using Amersham Typhoon Biomolecular Imager (GE Healthcare). The western blot analysis confirmed the previously observed TRPV1 and ARMS interaction (: Western blot analysis of TRPV1/ARMS/AKAP79 in HEK293). More importantly, AKAP79 seems to be involved in the TRPV1/ARMS/PKA signaling complex, regardless of transfected wild type ARMS or ARMS mutants. However, even without transfected TRPV1 AKAP79 and ARMS seem to interact with each other, indicating AKAP79 mediated PKA phosphorylation of ARMS:

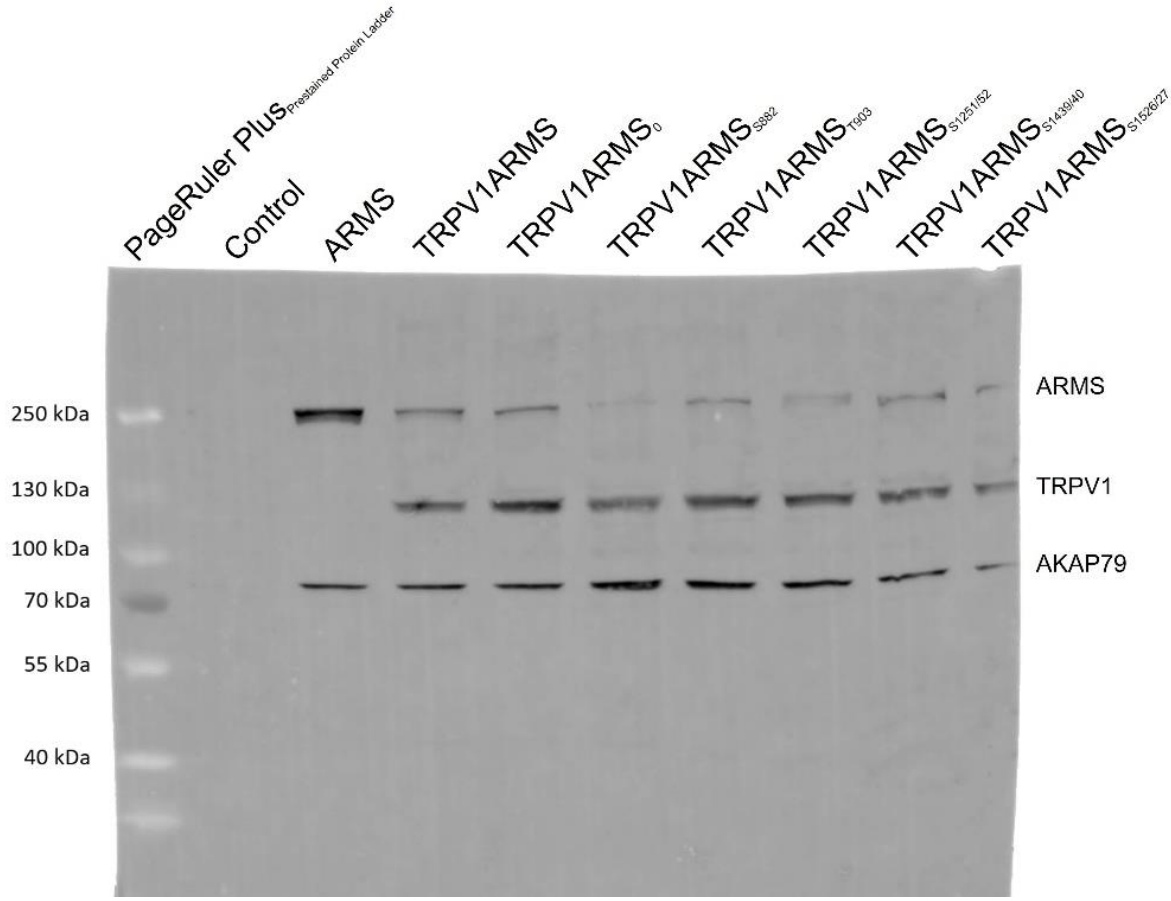

Figure 3.3.3.2: Western blot analysis of TRPV1/ARMS/AKAP79 in HEK293
TRPV1/ARMS transfected, PKA stimulated and detection via anti-TRPV1, anti-ARMS and anti-AKAP79. LANE 1: PageRuler Plus Prestained Protein Ladder, LANE 2: control, LANE 3: ARMS, LANE 4: TRPV1ARMS, LANE 5: $TRPV1ARMS_{0}$, LANE 6: $TRPV1ARMS_{S882}$, LANE 7: $TRPV1ARMS_{T903}$, LANE 8: $TRPV1ARMS_{S1251/52}$, LANE 9: $TRPV1ARMS_{S1439/40}$, LANE 10: $TRPV1ARMS_{S1526/27}$, BANDS at ~79 kDa: AKAP79, BANDS at ~120 kDa: TRPV1, BANDS at ~220 kDa: ARMS; AKAP79 is part of the TRPV1/ARMS/PKA signaling complex.

3.3.4 Calcium flux measurements

To determine a possible TRPV1 sensitizing or desensitizing effect of the newly discovered interaction ratios (3.3.1 TRPV1/ARMS co-immunoprecipitation), TRPV1 and PKA-site mutated ARMS plasmids were co-transfected into HEK293 cells. Calcium flux measurements were performed 48 h post transfection with the fluorescent calcium indicator dye Fluo 4 AM. TRPV1 was activated by capsaicin (0.1 nM – 10000 nM) and calcium flux was measured using a FLUOstar® Omega Microplate Reader (BMG LABTECH). The measurements confirmed the known sensitizing effect of ARMS on TRPV1 (Figure 3.3.4.1: Dose response curves of TRPV1/ARMS in transfected HEK293):

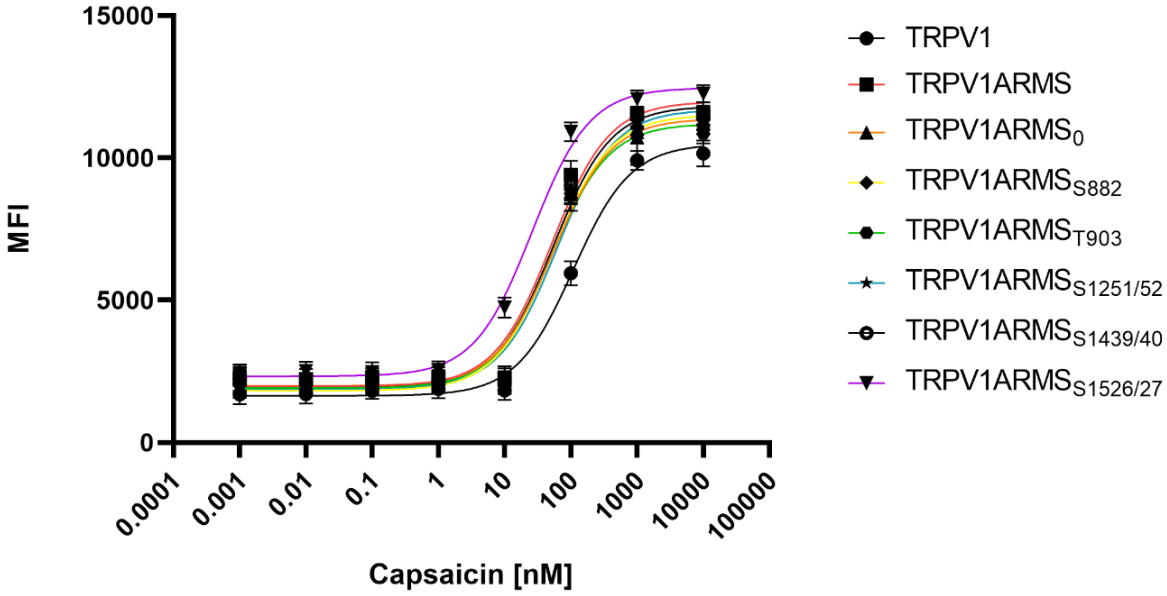

Figure 3.3.4.1: Dose response curves of TRPV1/ARMS in transfected HEK293
MFI Data was plotted against capsaicin concentration via nonlinear regression using least squares fit and is presented as means ± SEM. *n* = 3. ARMS sensitizes TRPV1, $ARMS_{S1526/27}$ sensitizes TRPV1 even more.

While TRPV1 showed an EC_{50} of 109 nM for capsaicin, ARMS was able to sensitize TRPV1 significantly to an EC_{50} of 51 nM for capsaicin. $ARMS_0$ with an EC_{50} of 54 nM, $ARMS_{S822}$ (EC_{50} of 53 nM), $ARMS_{T903}$ (EC_{50} of 51 nM) and $ARMS_{S1439/40}$ (EC_{50} of 54 nM) seemed to have a similar significant effect on TRPV1 as wild type ARMS during capsaicin treatment. On the other hand, the sensitizing effect of $ARMS_{S1251/52}$ on TRPV1 was slightly decreased with an EC_{50} of 65 nM for capsaicin. However, $ARMS_{S1526/27}$ showed an even greater sensitizing effect on TRPV1 as the wild type, TRPV1/$ARMS_{S1526/27}$ exhibited an EC_{50} of 26 nM for capsaicin. Together with the results from 3.3.1 TRPV1/ARMS co-immunoprecipitation, this indicates an interaction rate dependent sensitization of TRPV1, where a high TRPV1/ARMS or ARMS mutant interaction rate equals a high sensitization of TRPV1. For the assessment of the native sensitization of TRPV1, the transfected HEK293 cells were not additionally treated. To determine the influence of PKA mediated ARMS phosphorylation in terms of a decreasing or increasing sensitization, transfected HEK293 were additionally treated with the PKA inhibitor H89 (10 µM), the PKD inhibitor BPKDi (1 µM) or with forskolin (50 µM) combined with IBMX (100 µM). Native condition results from Figure 3.3.4.1: Dose response curves of TRPV1/ARMS in transfected HEK293 and treated condition results are summarized in : EC50 histogram of TRPV1/ARMS in transfected HEK293:

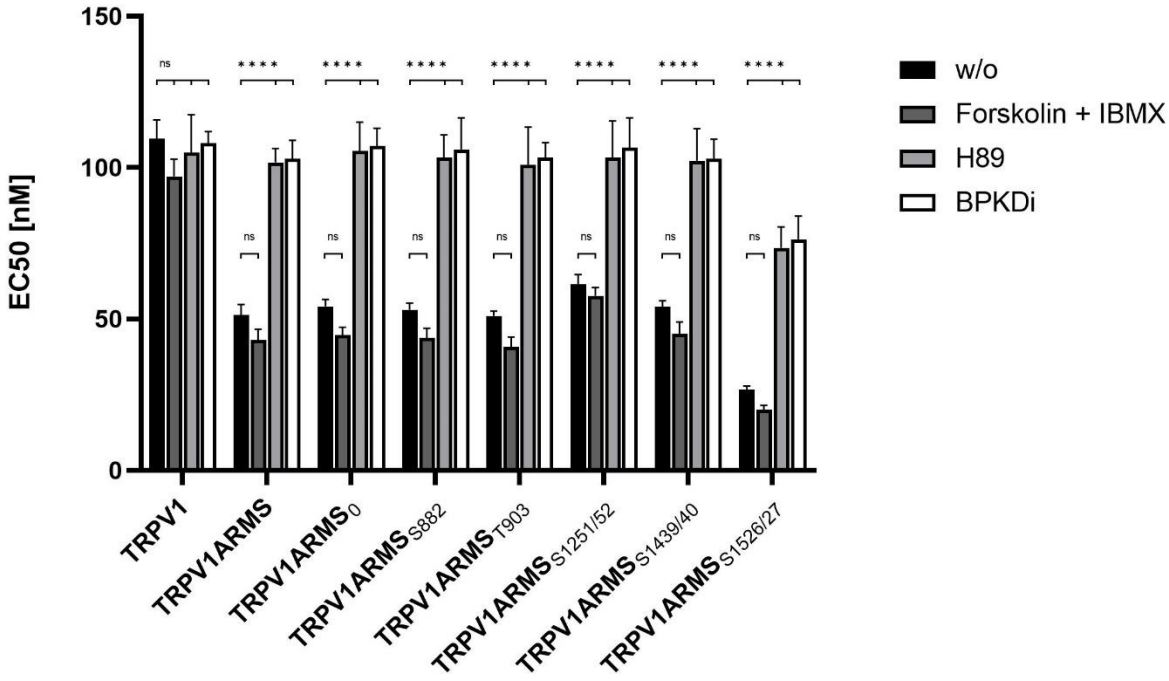

Figure 3.3.4.2: EC_{50} histogram of TRPV1/ARMS in transfected HEK293
Data are presented as means ± SEM. *n* = 21. Statistical significance is denoted as ns = not significant, p<0.05 (*), p<0.01 (**), p<0.001 (***), p<0.0001 (****). BLACK: without stimulation or inhibition, DARK GREY: PKA stimulated with forskolin and IBMX, GREY: PKA inhibited with H89, WHITE: PKD inhibited with BPKDi. PKA phosphorylation does not alter TRPV1 sensitization. PKA/PKD inhibition reverses TRPV1 sensitization.

PKA stimulation, via forskolin and IBMX, did not significantly alter the calcium flux or the EC_{50} of TRPV1 for capsaicin compared to the native condition in any case. Thus, maintaining the known sensitizing effect of ARMS and the newly discovered sensitizing effects of its mutants. In contrast, the PKA inhibitor H89 as well as the PKD inhibitor BPKDi significantly decreased the calcium flux of TRPV1 and therefore increased the EC_{50} of TRPV1 for capsaicin when compared to the native condition. Thus, the sensitizing effects of wild type ARMS, $ARMS_0$, $ARMS_{S822}$, $ARMS_{T903}$, and $ARMS_{S1251/52}$ and $ARMS_{S1439/40}$ were reversed by H89 or BPKDi treatment. However, the calcium flux or the EC_{50} of TRPV1 for capsaicin of single transfected TRPV1 did not significantly alter in the treated conditions compared to the native condition. Thus, indicating that the determined effects are mediated by ARMS and independent of TRPV1. While the sensitizing effect of ARMS and its mutants on TRPV1 was reversed by H89 or BPKDi treatment, the sensitizing effect of $ARMS_{S1526/27}$ on TRPV1 was not fully reversed. Even under H89 or BPKDi treatment, $ARMS_{S1526/27}$ had a sensitizing effect on TRPV1. Together with the results from 3.3.1 TRPV1/ARMS co-immunoprecipitation and 3.3.2 ARMS phosphorylation sites, this indicates an interaction rate dependent sensitization of TRPV1, where PKA mediated phosphorylation does not alter the interaction of TRPV1/ARMS. Since forced PKA stimulation via forskolin and IBMX

did not significantly increase or decrease the MFI association of TRPV1 with wild type ARMS or all ARMS mutants and therefore did not alter the sensitization of TRPV1. Thus, indicating a PKA independent TRPV1/ARMS interaction and sensitization of TRPV1. However, this would also mean that the decreasing interaction effect of H89 and therefore the reversal of TRPV1 sensitization is presumably unspecific, possibly inhibiting other kinases like PKD, and therefore being PKA independent as well. On the other hand, this would indicate that TRPV1/ARMS interaction is presumably mediated by PKD phosphorylation as the decreasing interaction effect and the reversal of TRPV1 sensitization of BPKDi assumes.

3.3.5 shRNA mediated ARMS silencing

To demonstrate the involvement of ARMS in TRPV1 sensitization, ARMS was silenced by shRNA. The shRNA plasmid shC (ARMS specific) was determined to be the most effective/silencing out of four different ARMS targeting shRNA plasmids. The shRNA plasmid shS (scrambled control) served as negative control. TRPV1, ARMS and shRNA plasmids were singly and/or co-transfected into HEK293 cells. Immunoprecipitation experiments (Figure 3.3.5.1: Immunoprecipitation of TRPV1/ARMS in transfected HEK293) were performed with antibodies directed against ARMS or TRPV1. The precipitate was further analyzed by the Luminex FlexMap3D platform with antibodies against ARMS for the ARMS precipitate and TRPV1 for the TRPV1 precipitate. The ARMS screening confirmed the significant silencing effect of shC on ARMS, which was decreased by a factor of 2.65, while shS showed a non-significant and negligible effect on ARMS expression. On the other hand, the TRPV1 screening revealed that neither of the shRNA plasmids had a significant effect on TRPV1 expression. Thus, indicating that TRPV1/ARMS interaction and respectively ARMS mediated TRPV1 sensitization could be modulated by shRNA:

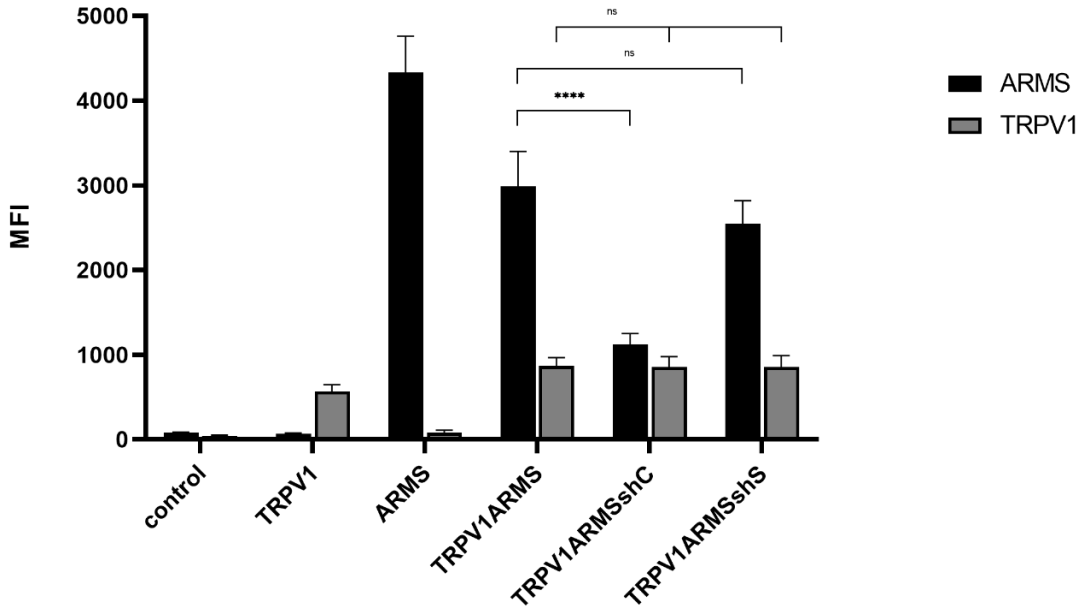

Figure 3.3.5.1: Immunoprecipitation of TRPV1/ARMS in transfected HEK293
Histogram of ARMS and TRPV1 response in MFI. Data are presented as means ± SEM. *n* = 3. Statistical significance is denoted as ns = not significant, p<0.05 (*), p<0.01 (**), p<0.001 (***), p<0.0001 (****). BLACK, ARMS. GREY, TRPV1. ARMS expression is reduced via shC without affecting TRPV1 expression.

To determine if the shRNA-induced ARMS decrease correlates with a desensitizing effect of TRPV1, TRPV1, ARMS and shRNA plasmids were co-transfected into HEK293 cells. Calcium flux measurements (: Dose response curves of TRPV1/ARMS in shRNA transfected HEK293) were performed 48 h post transfection with the fluorescent calcium indicator dye Fluo 4 AM. TRPV1 was activated by capsaicin (0.1 nM – 10000 nM) and calcium flux was measured using a FLUOstar® Omega Microplate Reader (BMG LABTECH). In addition to dose response curves, results are shown as histogram in : EC50 histogram of TRPV1/ARMS in shRNA transfected HEK293. The measurements confirmed the known and significantly sensitizing effect of ARMS on TRPV1 (EC_{50} of 109 nM vs. 49 nM for capsaicin). Triple transfection with shC lead to a significantly decreased ARMS-mediated TRPV1 sensitization with an EC_{50} of 91 nM for capsaicin compared to the TRPV1/ARMS transfection, indicating the reversal of the ARMS-mediated TRPV1 sensitization (TRPV1 – TRPV1ARMSshC: not significant). In addition, shS triple transfections, which served as shRNA negative control, showed no significant effect (EC_{50} 56 nM for capsaicin) on the sensitization of TRPV1 compared to the TRPV1/ARMS transfection. Thus, confirming the assumption that TRPV1/ARMS interaction and respectively ARMS mediated TRPV1 sensitization can be specifically modulated by shRNA.

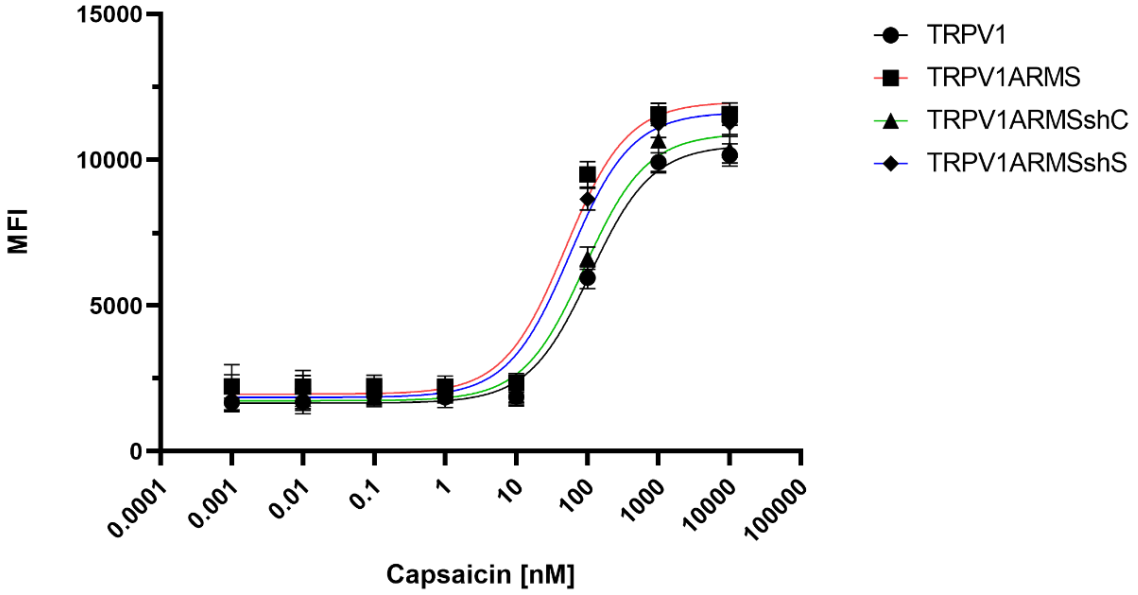

Figure 3.3.5.2: Dose response curves of TRPV1/ARMS in shRNA transfected HEK293
MFI Data was plotted against capsaicin concentration via nonlinear regression using least squares fit and is presented as means ± SEM. *n* = 3. TRPV1 sensitization induced by ARMS is reversed via shC.

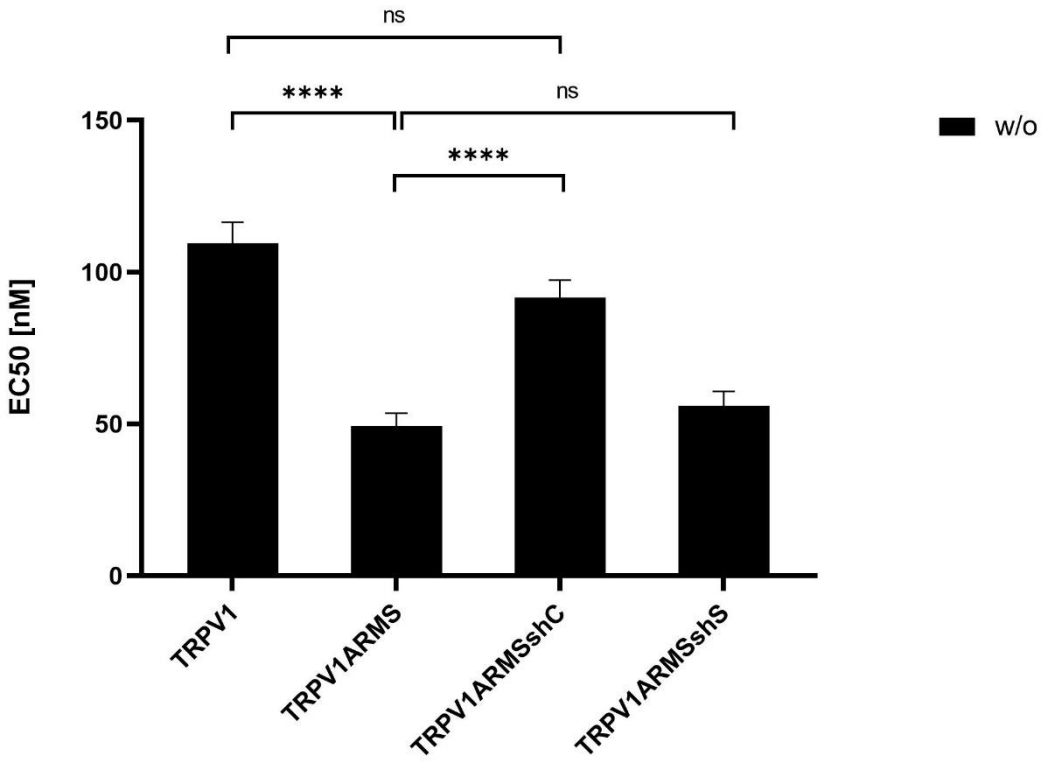

Figure 3.3.5.3: EC_{50} histogram of TRPV1/ARMS in shRNA transfected HEK293
Data are presented as means ± SEM. *n* = 3. Statistical significance is denoted as ns = not significant, p<0.05 (*), p<0.01 (**), p<0.001 (***), p<0.0001 (****). BLACK: without stimulation. TRPV1 sensitization induced by ARMS is reversed via shC.

4. Discussion

This dissertation aimed to determine differential expressed miRNAs in the context of chronic pain in polyneuropathy. For this purpose, the miRNA profiles of 60 age matched patients were sequenced and a differential expression analysis as well as a target prediction was performed. Furthermore, the pain relevant interaction of TRPV1 and ARMS was characterized based on potential PKA phosphorylation sites of ARMS. Therefore, single PKA phosphorylation site/alanine ARMS mutants were synthetized and characterized in terms of PKA/AKAP79 mediated ARMS phosphorylation and TRPV1 sensitivity via transfection of HEK293 cells, FLEXMAP 3D analysis, immunoprecipitation, SDS-PAGE, Western Blot, calcium flux analysis and shRNA silencing.

4.1 miRNA library preparation quality control

To enable comparability and reproducibility from RNA isolation to sequencing, in any next-generation sequencing experiment, quality control Spike-Ins were added during RNA isolation/cDNA synthesis and verified via qPCR. After library preparation, libraries were quality controlled, sized and quantified via the Agilent Bioanalyzer 2100 system.

The UniSp100 and UniSp101 RNA Spike-Ins were used to monitor the RNA isolation efficiency across all samples. The typical C_T value should be in the range of 31–34 for UniSp100 and 25–28 for UniSp101. Every determined C_T value was below that expected range with a C_T range of 26.95-29.81 for UniSp100 and partly for UniSp101 with a C_T range of 24.01-26.93, indicating a more efficient isolation of UniSp100. However, the manufacturer´s handbook mentions, that the concentration of UniSp100 Spike-In corresponds to moderately abundant miRNAs and the concentration of UniSp101 Spike-In corresponds to highly abundant miRNAs in a biofluid. In addition, it mentions that the C_T values will vary depending on experimental settings and the method used as well as the elution volume and RNA input [173]. Since these parameters were not changed and exactly performed as stated in the manufacturer´s protocol, the low C_T values indicate efficient RNA isolations even for low abundant miRNAs. The C_T deviation of 2.86 for UniSp100 and the C_T deviation of 2.92 for UniSp101 were within the acceptable range of <2-3, meaning that all isolations were performed with similar efficiencies. However, the ΔC_T of UniSp100-UniSp101 ranged between 2.06-3.92 and did not meet the expected range of 5-7 as mentioned in the manufacturer´s protocol, which is a consequence of the more efficient isolation of UniSp100, shifting the expected range to lower values [173]. Since the UniSp100/UniSp101 Spike-Ins were added in a fixed/non-modifiable ratio per RNA isolation

and UniSp100/UniSp101 showed comparable values across all samples as well as Qiagen's Product & Technical Support could not explain the more efficient RNA isolation either, samples were further quality controlled. The UniSp6 RNA Spike-In was added during cDNA synthesis to monitor cDNA synthesis efficiency. With all determined C_T values being below 20 and a C_T deviation of 1.78 for UniSp6, the parameters were within the acceptable range of C_T deviation <1-2 and C_T < 20, accordingly to the manufacturer´s protocol [173]. This indicates that all cDNA syntheses and qPCRs were performed with similar efficiencies and no sample was affected by inhibitors of cDNA synthesis or qPCR. A major source of variation in plasma and serum is potential cellular-derived miRNA contamination, including hemolysis. After extensive data analysis on human serum and plasma samples, it was found that the red blood cell specific miR-451a and the stable miR-23a could be used to monitor hemolysis. A ΔC_T (miR-23a – miR-451a) lower than 7 in human serum or plasma represents non-hemolyzed samples [173]. Across all samples the ΔC_T of miR-23a-5p – miR-451a ranged between 1.84-6.85 and therefore were below the hemolytic border of ΔC_T <7 and considered successful. The endogenous controls miR-103a-3p, miR-191-5p and miR-30c-5p served as biological markers for each sample and were present in all samples. Since all quality controls were successful, except the UniSp100/UniSp101 related ones, none of the samples was identified as an outlier and no sample was excluded for library preparation (Figure 4.1.1: Decision tree).

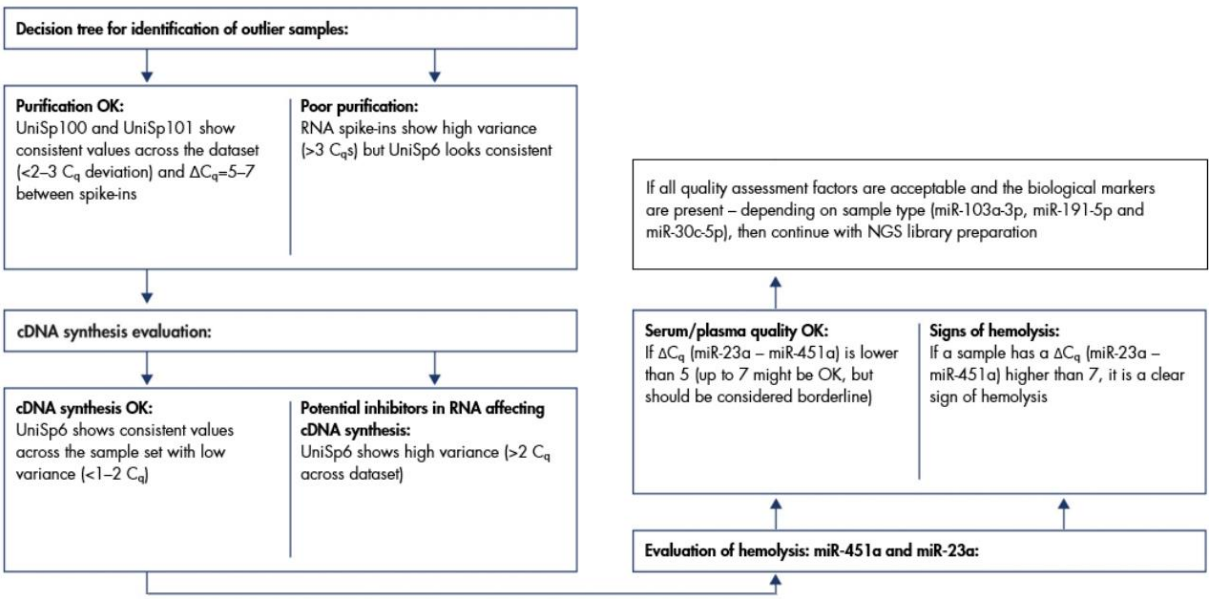

Figure 4.1.1: Decision tree

Decision tree for identification of outlier samples via QIAseq miRNA Library QC PCR Panel Kit. Purification was OK with a C_T deviation <2-3 for UniSp100 & UniSp101. cDNA synthesis was OK with a C_T deviation <1-2 for UniSp6. Hemolysis was OK with a ΔC_T <7 for miR-23a – miR-451a. Presence of miR-103a-3p, miR-191-5p and miR-30c-5p is required [173].

After library preparation, libraries were quality control controlled, sized and quantified via the Agilent Bioanalyzer 2100 system. However, the Agilent Bioanalyzer 2100 system should only be used for quantifying libraries with narrow size distributions such as small RNA libraries due to decreasing accuracy with increasing library fragment size distributions [224]. Almost all electropherograms showed an additional/unexpected Peak with the size of 155 bp that was classified as adapter dimer peak in the QIAseq miRNA Library Kit Handbook [174]. For all samples, in case of peaks showing at approximately 155 bp (adapter dimers), or in case of other undesired bands, automated size selection via BluePippin on the remainder of the miRNA Sequencing Library was performed to select the specific miRNA library at approximately 177 bp. However, the manufacturer´s handbook mentions that when a prominent adapter dimer peak is observed, one should ensure that the QIAseq miRNA NGS RT Initiator has been added as indicated, between the 5' ligation and RT reactions, and the correct temperature profile has been set up for the initiation as well as to ensure that 3' ligation and 5' ligation components were added to their respective reactions in the order listed. RT reaction setup as well as 3' ligation and 5' ligation reaction setups were double checked and were as they should. In addition, it mentions to use 1 ng or more of total RNA to prevent adapter dimerization. This only leaves one conclusion: the recommended starting amount of total RNA, 5 µL of the RNA eluate when 200 µL of serum have been processed using the miRNeasy Serum/Plasma Advanced Kit, did not contain the required amount of total RNA. For example, it is recommended to dilute the 3’ ligation adapter 1:5 for serum samples, while it is also diluted 1:5 for 10 ng total RNA. On the other hand, it is diluted 1:10 for 1 ng total RNA [174]. Thus, being below the expected total RNA amount leads to a uneven RNA/adapter ratio resulting in adapter dimers during library preparation. This adapter dimer formation does not affect the quality of the final miRNA library but does add an additional size selection step. Since all samples were free of adapter dimers after BluePippin size selection and reached the minimum molarity for further processing, all samples were subjected to sequencing.

4.2 Sequencing

The Illumina MiSeq was used to enable next-generation sequencing of mature miRNAs. The resulting FASTQ file of each miRNA library was quality controlled, analyzed and used to perform a differential expression analysis of polyneuropathy vs. control samples. Finally, the differentially expressed and filtered miRNAs were subjected to miRDB to perform a target prediction (human).

The sequencing runs usually resulted in a density of 1236±31 K/mm^2 (of clusters detected by image analysis) with a cluster PF of 89.25±1.56 % (percentage of clusters passing filtering) leading to 26.37 M reads PF (number of clusters passing filtering) with 97.13 % ≥ Q30 (percentage of bases with a quality score of 30 or higher, meaning ≥ 99.9 % base call accuracy) and equal index distribution between 22.03-27.44 %. Illumina recommends an optimal raw cluster density of 1200-1400 K/mm^2 for v3 reagents and a cluster PF >80 % to ensure optimal clustering [225, 226]. The MiSeq Reagent Kit v3 is advertised with 25 M reads and > 85% bases higher than Q30 [227]. In addition, when sequencing quality reaches Q30, virtually all of the reads will be error-free. This is why Q30 is considered benchmark for quality in NGS [228]. Phas/Prephas (percentage of molecules in a cluster for which sequencing falls behind, phasing, or jumps ahead, prephasing) were 0.191/0.052 %. For Phas/Prephas a low percentage (<0.5%) is desired [229]. There are several possible causes for poor phasing/prephasing: unbalanced base composition (≠ 25% of each base), that can be fixed by adding extra phiX control or, assuming base composition is not the problem, the most likely causes are the reagents or the flow cell. Therefore, the use-by date of reagents, the fluidics and not too high temperatures during the run should be checked [230]. All in all, the mentioned sequencing parameters above were in their optimal range. The only parameter that was not in its expected range was the percentage that aligned to the phiX genome (0.68±0.02 %). The expected percentage of alignment to the phiX genome should have been 1 %, because this amount was used during loading the MiSeq Reagent Kit v3 cartridge. Illumina recommends, for most libraries a low concentration of phiX control (1%) as a sequencing control but for low diversity libraries, as mentioned above, the concentration of phiX control can be increased to at least 5%. However, the same denatured and diluted 20 pM phiX library was used for all sequencing runs . This denatured 20 pM phiX library can be stored up to 3 weeks at -15°C to -25°C and due to multiple freeze/thaw cycles cluster numbers tended to decrease towards the end of this timeframe [178, 231]. Since the phiX library was used as a sequencing control for phasing and prephasing calculations as well as examining the overall performance of the MiSeq (cluster generation, sequencing and alignment), the lower than expected alignment percentage does not affect the quality of the final sequencing result.

Resulting FASTQ files were analyzed and reads mapped/counted. Following mapping of the quality control Spike-In reads, they were normalized to the total number of reads per sample. After this simple normalization to individual sample reads was done for all Spike-Ins in all samples, they were tested for normality via Shapiro-Wilks Normality Test and a Spearman Correlation matrix was plotted for sample-to-sample comparisons. For all samples the spearman r values ranged from 0.86-0.99. According, to the QIAseq™ miRNA

Library QC PCR Handbook, the expected correlation should be R^2 = 0.95–0.99 within a batch of samples purified on the same day and a bit weaker when comparing day-to-day correlation. Samples that deviate from these values, should be considered technical outliers and should potentially be excluded from downstream analysis [173]. Since this would require normal distribution of the data to calculate R^2 from pearson r and the performed Shapiro-Wilks Normality Test did not show normality, the evaluation suggested in the manufacturer´s protocol was not considered [194–196]. Thus, a new acceptable range of r = 0.85-0.99 was defined. This range is usually associated with strong correlation in medical research [197, 198]. Finally, all samples were used for miRNA analysis/differential expression analysis.

For differential expression analysis, the resulting quantification of each miRNA library was utilized and grouped based on polyneuropathy/control with a sample size of 30 each group (n=30). Recent miRNA expression studies used similar sample sizes in the context of amyotrophic lateral sclerosis (n=12), tetralogy of fallot (n=22) or vascular health (n=36) [232–234]. Thus, indicating a robust and diagnostically conclusive sample size. Despite age matched groups, differential expression analysis controlled for age to rule out age-based false positive differential miRNA expression. Results of the differential expression analysis were filtered: fold change > 2 or fold change < -2 and Bonferroni corrected p-value < 0.05, respective. In fold change analysis, 2 or 1.5 is often used as the cutoff to determine differentially expressed genes [199, 200]. While in multiple hypothesis testing, the Bonferroni correction is a conservative method for multiple-comparison correction, used when several statistical tests are performed simultaneously, to control the occurrence of false positives [201].

Extensive manual literature research via PubMed/PubMed Central with search terms like “miRNA polyneuropathy” and “miRNA”, where miRNA is the corresponding differentially expressed and filtered miRNA, did not yield results to verify the determined miRNAs in the context of polyneuropathy/chronic pain [235]. However, literature research yielded first hints for their involvement in hemorheological abnormalities like hypertension/coronary artery calcification (hsa-miR-3135b), pulmonary arterial hypertension (hsa-miR-584-5p), angiogenesis/hypoxia (hsa-miR-12136) and damaged vascular smooth muscles (has-miR-550a-3p) [236–241]. Nonetheless, Crawler-based literature research (Figure 4.2.1: Crawler-based literature research and Figure 4.2.2: Crawler-based literature research result table) via PubMed Central with the search term “Polyneuropathy miRNA” yielded 978 paper and showed that the top 3 mentioned miRNAs (in total 93 different miRNAs were mentioned) in this context are: miR-155 (10 times mentioned), miR-124 (6 times mentioned) and miR-146a (6 times mentioned). Examination of the mentions

showed that these miRNAs are found in the context of polyneuropathy but only a tiny fraction of these mentions were really related to polyneuropathy/neuropathic pain.

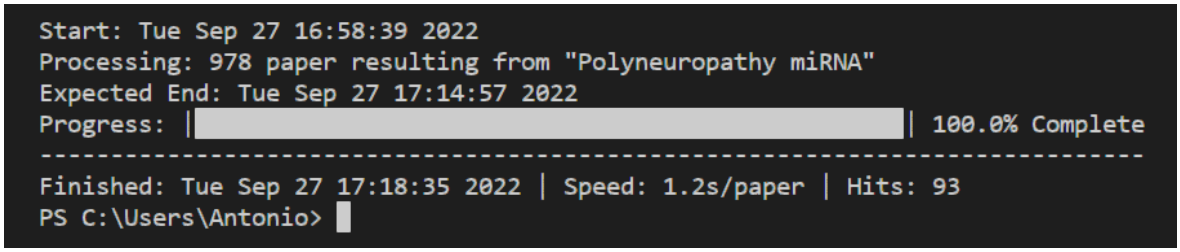

Figure 4.2.1: Crawler-based literature research
Crawler-based literature research via PubMed Central with the search term “Polyneuropathy miRNA” yielded 978 paper and resulted in 93 different miRNAs that were mentioned in the abstracts.

93 hits	Count	PMIDs	Sentence
miR-155	10	9082251	-
		9082748	+
		8520483	-
		8535125	-
		8293470	-
		8137895	-
		7606596	+
		6475967	-
		5598142	-
		5029065	-

Figure 4.2.2: Crawler-based literature research result table
Crawler-based literature research result table showing that 93 different miRNAs (hits) were mentioned in the abstracts. The most mentioned miRNA was miR-155 with 10 counts, the PMIDs of the corresponding mentions were saved and “+” under “Sentence” indicates a correlation with “chronic” in the abstract.

The complete list as well as the crawler is provided in the Appendix under Crawler-based literature research. However, the differentially expressed and filtered miRNAs (hsa-miR-3135b, hsa-miR-584-5p, hsa-miR-12136 and hsa-miR-550a-3p) were not mentioned in any of the 978 papers. Thus, confirming the extensive manual literature research. Nevertheless, the top 3 mentioned miRNAs and the determined differentially expressed and filtered miRNAs showed similarities. In the context of polyneuropathy, the mentioned miRNAs also showed involvement in hemorheological abnormalities like hypertension (miR-155/ miR-146a) and hypoxia (miR-124) [242–244]. Thus, matching with the literature results of the determined miRNAs and seeming to effect similar hemorheological pathways.
Subsequently, the differentially expressed and filtered miRNAs were subjected to miRDB to perform a target prediction (human). Three of those four miRNAs were downregulated: hsa-miR-3135b (-6.30 fold change), hsa-miR-584-5p (-2.62 fold change) and has-miR-12136 (-3.80 fold change). Downregulation of hsa-miR-3135b, hsa-miR-584-5p, hsa-miR-12136 and therefore upregulation of target genes/mRNAs were associated with high blood pressure (LRRC27), angiogenesis (FMNL3), arterial hypertension (TTC21B),

elevated blood pressure (AVPR1A), impaired blood flow, vessel walls and coagulation (STXBP5) and delayed endocytosis and degradation of EGFR (USP6NL) or associated with neural cell proliferation and synaptic activity/connectivity (SETD5), synaptic development (IGSF11) and the development of neuronal systems (DAAM1) [203–205, 207–217]. Thus, grouping the miRNA downregulation effects in vasoconstriction/high blood pressure related and neural activity related ones. The only upregulated miRNA was hsa-miR-550a-3p (4.27 fold change). Upregulation of hsa-miR-550a-3p and therefore downregulation of target genes/mRNAs were associated with developmental process of coronary vessel formation (MYH10), dendrite extension (SYT4) and maintaining neuronal identity (MYT1L), also grouping the miRNA upregulation effects in vasoconstriction/high blood pressure related and neural activity related ones [218, 220, 222, 223]. This leads to the conclusion that chronic pain in polyneuropathy results of a combination of high blood flow/pressure and neural activity dysregulations/disbalances. One could speculate that vasoconstriction/high blood pressure induced by upregulation of LRRC27, AVPR1A, TTC21B, STXBP5 and downregulated coronary vessel formation (MYH10) as well as overactive angiogenesis/EGFR (FMNL3/USP6NL) leads to the degeneration of small sensory neurons due to the lack of nourishment/restricted blood flow (Figure 4.2.3: Vasoconstriction leading to nerve damage) [203, 205, 207–209, 217, 218]. Thus, resulting in the neuropathy typical proximal numbness, burning or electric shock–like pain [83].

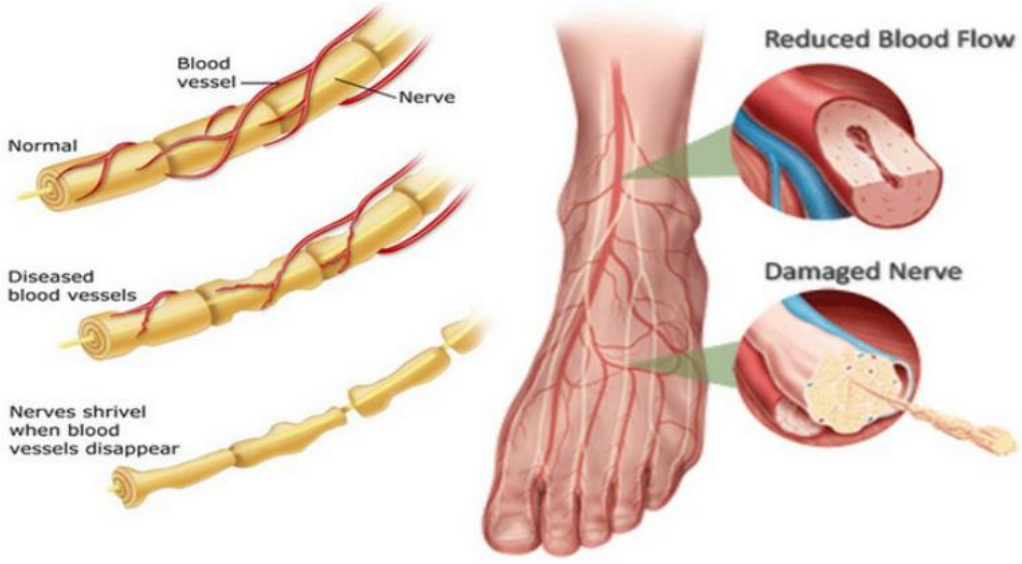

Figure 4.2.3: Vasoconstriction leading to nerve damage
Healthy blood vessels ensure normal blood flow and efficient nerves. Diseased blood vessels can lead to reduced blood flow resulting in damaged nerves as nerves shrivel when blood vessels disappear due to the lack of nourishment [245].

In addition, neural dysregulation in terms of overactive synaptic development/proliferation and activity/connectivity mediated by upregulation of SETD5, IGSF11 and DAAM1 as well as downregulated dendrite extension/maintenance of neuronal identity (SYT4/MYT1L) could contribute to the degeneration of sensory neurons as well [211, 213, 215, 220, 223]. Meaning, overactive synaptic development/proliferation and activity/connectivity as well as the lack of nourishment/restricted blood flow due to vasoconstriction/high blood pressure could lead to the degeneration of small sensory neurons resulting in the neuropathy typical numbness/pain that begins in the toes, followed by the fingers and finally spreads proximally. This hypothesis is encouraged by investigations on biopsy material from patients with mild to severe neuropathy. These patients showed graded structural changes in nerve microvasculature including basement membrane thickening, pericyte degeneration and endothelial cell hyperplasia. Thus, leading to vasoconstriction/high blood pressure and resulting in nerve hypoxia and reduced nerve blood flow [246]. However, basement membrane thickening, pericyte degeneration and endothelial cell hyperplasia could also be a maladaptive response to hypoxia causing reduced diffusion capacity. Thus, exacerbating the initial hypoxia. Studies showed that endothelial hyperplasia leads to a reduction in luminal area [247]. In conjunction with hemorheological abnormalities including cytoskeletal dislocation (FMNL3/MYH10), vasoconstriction (AVPR1A), platelet activation (LRRC27) and coagulation (STXBP5) this could cause vessel occlusion, endoneural hypoxia and neuropathy [203, 204, 209, 217, 218]. Since, the degree of neuropathy is closely correlated with the numbers of closed vessels [248]. Nonetheless, studies showed that neuropathy can develop from various diseases causing hypoxia, for example: chronic obstructive pulmonary disease. Neuropathological changes in chronic obstructive pulmonary disease were similar to those found in metabolic induced neuropathies like diabetic neuropathy [249]. However, overactive synaptic development/proliferation and activity/connectivity (SETD5, IGSF11 and DAAM1) as well as downregulated dendrite extension/maintenance of neuronal identity (SYT4/MYT1L) could additionally contribute to chronify painful neuropathies [211, 213, 215, 220, 223]. Since, adult neurogenesis is involved in the maintenance of long-lasting neuropathic chronic pain and becomes a major contributor at later stages of pain chronicity [250]. In addition, studies showed that the upregulation of hippocampal neurogenesis (learning and memory) results in the prolongation of persistent pain and facilitates the development of chronic pain [251]. Moreover, it could be shown that the number of new neurons is enhanced by persistent pain, suggesting that adult neurogenesis is an pain induced process [252]. As, chronic pain is considered to develop as a result of the persistence of pain memory and the inability to erase pain memory after injury [253]. On the other hand, neuroplastic processes are considered to occur in the

central nervous system during neuropathic pain and cause an imbalance between excitatory and inhibitory processes [254]. Furthermore, recent studies have shown that neuroplasticity is able to cause additional neuropathic pain, which may occur adjacent to or remotely from the site of injury, and that such alterations in pain perception are often mediated by structural and functional neuroplasticity of the spinal dorsal horn (Figure 4.2.4: Pain induced neuroplasticity and neurogenesis) [255].

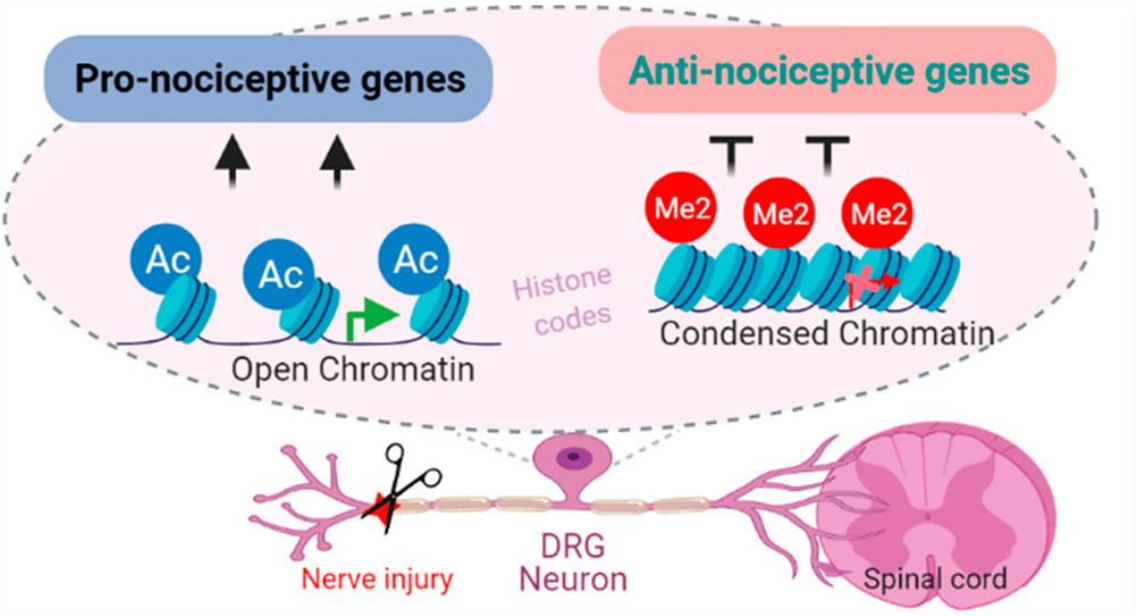

Figure 4.2.4: Pain induced neuroplasticity and neurogenesis
Nerve injuries can induce neuroplasticity and neurogenesis of DRG neurons by epigenetic mechanisms like histone acetylation and methylation, resulting in opened or condensed chromatin. Thus, increasing pro-nociceptive gene expression and decreasing anti-nociceptive gene expression, leading to alterations in pain perception [256].

Taken together, this strong correlation between miRNA mechanisms and chronic pain in polyneuropathy could encourage the promising indication that hsa-miR-3135b, has-miR-584-5p, hsa-miR-12136 and hsa-miR-550a-3p are potential biomarkers with high accessibility, specificity and sensitivity for the diagnosis of chronic pain in polyneuropathy.

4.3 TRPV1, ARMS, PKA and AKAP79 signaling complex

Since TRPV1 seems to be one of the major contributors of nociception and is associated with neuropathic pain the influence of PKA phosphorylated ARMS on the sensitivity of TRPV1 as well as the part of AKAP79 during PKA phosphorylation of ARMS was

characterized. Finally, ARMS specific shRNA was used to silence ARMS to demonstrate the involvement of ARMS in TRPV1 sensitization.

Initially, possible PKA-sites in the sequence of ARMS were identified using a (R/K)-(R/K)-X-(S/T) pattern search [168]. This revealed five canonical PKA-sites: S882 (RRVSQ), T903 (RRDTY), S1251/52 (RRSSH), S1439/40 (KKSSE) and S1526/27 (KKDSSD). To investigate possible functional and physical interactions between ARMS and TRPV1, TRPV1 and PKA-site-deficient ARMS mutants were co-expressed in HEK293 cells. Transfection efficiency of TRPV1 and PKA-site mutant or wild type ARMS was controlled by TRPV1-YFP excitation at 470 ± 20 nm and emission at 534 ± 27.5 nm, resulting in equal transfection efficiencies among all transfection combinations. Since, co-transfection studies using two auto fluorescent reporter genes showed that transfection efficiencies are depending on the ratio of the plasmids themselves and on the ratio of the plasmids to transfection reagent, which were identical between conditions and already published/used by *Kasper et al.* [120, 257]. Subsequently, co-immunoprecipitation experiments were performed with an antibody (mouse) directed against ARMS. The precipitate was further analyzed by the Luminex FlexMap3D platform with antibodies (rabbit) against ARMS, TRPV1 and pPKA substrate (Figure 4.3.1: Schematic structure of ARMS and its confirmed PKA site). The pPKA substrate antibody is according to its manufacture able to detect a RRXS*/T* PKA phosphorylation pattern [258]. Thus, possible PKA-sites like S1439/40 (KKSSE) and S1526/27 (KKDSSD) would not be detected. However, experiments from our own lab showed that the antibody is also able to detect a KKXS*/T* PKA phosphorylation pattern [259].

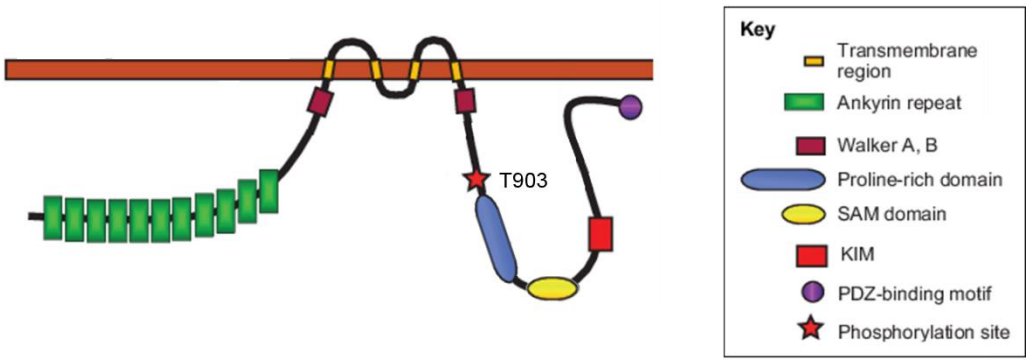

Figure 4.3.1: Schematic structure of ARMS and its confirmed PKA site
ARMS has four transmembrane domains and intracellular N- and C-termini that contain several protein-protein interaction motives as well as a newly discovered and experimentally confirmed PKA phosphorylation site: T903 (RRDTY) [123].

For the assessment of the native interaction rate of TRPV1 and ARMS, the transfected HEK293 cells did not undergo any additional treatments. To determine the influence of PKA phosphorylation in terms of a decreasing or increasing interaction rate, transfected HEK293 cells were additionally treated with H89 (PKA inhibition), BPKDi (PKD inhibition) or forskolin together with IMBX (PKA stimulation). The single PKA-site mutants of ARMS revealed that PKA-mediated ARMS phosphorylation does not seem to influence the interaction rate of TRPV1/ARMS. While phosphorylation of $ARMS_{T903}$ does not increase the interaction rate with TRPV1, $ARMS_{S1526/27}$ is probably not phosphorylated and leads to an increased interaction rate. Resulting from these findings and additional H89 as well as BPKDi experiments, which were both able to decrease the interaction of TRPV1/ARMS, it is likely that the TRPV1/ARMS interaction is independent of PKA phosphorylation of ARMS. This leads to the conclusion, that the H89 and BPKDi effect is either mediated via protein kinase D (PKD) inhibition or via TRPV1 phosphorylation. Meaning, PKA phosphorylation is required for TRPV1/ARMS interaction on the site of TRPV1. While PKA phosphorylation sites of TRPV1 have been established, further studies should be performed to identify PKA relevant sites of TRPV1 that may mediate TRPV1/ARMS interaction [260, 261]. On the other hand, ARMS is known to be a PKD substrate and in addition to the BPKDi results, one can conclude that the interaction with TRPV1 is driven by PKD phosphorylation [121]. This hypothesis is encouraged by investigations that showed that H89, which is marketed as a selective and potent inhibitor of PKA, is able to target several other kinases including PKD [262]. In addition, one could speculate that myr-PKI 14-22 (myr-GRTGRRNAI) used by *Kasper et al.* also inhibits PKD [120]. Since, PKD and PKA share similarities in their consensus sequence: (R/K)-(R/K)-X-(S/T) for PKA and (L/I/V)-X-(R/K)-X-X-(S/T) for PKD [146, 263]. As, PKD prefers hydrophobic amino acids (L/I/V) at the -5 position of its substrates, the T within myr-PKI 14-22 at this position does not entirely fit to substitute the quite similar V, due to the hydroxyl group making T a polar/uncharged amino acid. Nevertheless, the myristylation (myristic acid is covalently attached to a N-terminal glycine residue) adds the said hydrophobicity and could enable inhibition of PKD. However, while other studies showed that ARMS is able to modulate the phosphorylation of the AMPA receptor subunit GluA1, a more recent study identified ARMS as a modulating interaction partner of voltage-gated sodium channels in the brain [122, 124]. These studies, in addition to the results above, underline the ability of ARMS to modulate the activity and phosphorylation status of ion channels like TRPV1.

To determine a possible TRPV1 sensitizing or desensitizing effect of the newly discovered interaction ratios, TRPV1 and PKA-site mutated ARMS plasmids were co-transfected into HEK293 cells and calcium flux measurements with Fluo 4 AM were performed. TRPV1 was

activated by capsaicin (0.1 nM – 10000 nM). The results suggest that TRPV1/ARMS interaction sensitizes TRPV1 (TRPV1-EC_{50}: 109 nM vs. TRPV1/ARMS-EC_{50}: 51 nM). The calcium flux measurements indicate that the higher the interaction rate of TRPV1/ARMS, the lower the EC_{50} for capsaicin of TRPV1 and capsaicin induced TRPV1 currents, independent of the PKA phosphorylation status of ARMS. Thus, phosphorylation of $ARMS_{T903}$ does not increase the interaction rate with TRPV1 and it does not alter the EC_{50} for capsaicin of TRPV1 compared to wild type ARMS. On the other hand, $ARMS_{S1526/27}$ is not phosphorylated and leads to an increased interaction rate, resulting in a decreased EC_{50} for capsaicin of TRPV1 and increased capsaicin induced TRPV1 current compared to wild type ARMS. However, single transfected TRPV1 did not show a significant sensitization during PKA stimulation and thus being in line with other data suggesting a basal PKA phosphorylation of TRPV1 [119, 264]. Recent whole cell patch-clamp studies showed that EC_{50} values for activating TRPV1 (capsaicin) expressed in mammalian cell lines are between 0.1–0.25 µM and therefore much lower than those in native capsaicin-sensitive sensory neurons (0.68–1.1µM), while experiments measuring Ca^{2+} influx induced by capsaicin in DRG neurons are between 0.072-0.2 µM and those in HEK-TRPV1 are between 0.016 – 0.098 µM [265]. Thus, being in line with determined results above. However, calcium flux measurements in the presence of H89 or BPKDi show, that this ARMS mediated TRPV1 sensitization can be reversed. Especially, the similar H89 and BPKDi effect on $ARMS_0$ empowers the conclusion that this ARMS mediated TRPV1 sensitization is dependent on PKD phosphorylation. Since, all PKA sites are mutated to alanine in $ARMS_0$ and there is still interaction/sensitization. Additionally, the assumption, that $ARMS_{S1526/27}$ is not PKA phosphorylated leads to the conclusion, that the H89 effect is either mediated via TRPV1 phosphorylation or like in the case of $ARMS_0$, via inhibition of PKD and completely independent of PKA phosphorylation of ARMS. Thus, interaction of ARMS and TRPV1 leads to the sensitization of TRPV1 but is independent of PKA phosphorylation of ARMS and seems to be dependent on PKA phosphorylation of TRPV1 or PKD. Substantial interaction of TRPV1 and PKA has already been demonstrated by others. For PKA it was shown that it is involved in the insertion of functional TRPV1 tetramers into the plasma membrane by forming a complex of AKAP79, PKA and TRPV1 [266]. It was shown that AKAP79 can arrange TRPV1, adenylyl cyclase and PKA to form a sophisticated complex vital for TRPV1 sensitization [167, 267].

Since AKAP79 was found to be important in PKA-dependent sensitization of TRPV1, the role of AKAP79 in the phosphorylation of ARMS was explored. As the pPKA substrate screening revealed, only PKA stimulation via forskolin and IBMX seemed to result in the phosphorylation of ARMS. Therefore, TRPV1 and PKA-site mutant ARMS were co-

expressed in HEK293 cells and stimulated via forskolin and IBMX. Cell lysates were verified to contain endogenous AKAP79 by Western Blot. Co-immunoprecipitation experiments were performed with an antibody directed against ARMS. The precipitate was further analyzed by the Luminex FlexMap3D platform with an antibody against AKAP79. The screening confirmed the previously observed phosphorylation pattern of ARMS and its mutants via forskolin and IBMX stimulation. Furthermore, the screening revealed that AKAP79 is not detectable under the chosen conditions by the Luminex FlexMap3D platform. However, to exclude epitope masking as a reason for this native technique, a denaturing western blot analysis was performed. Conditions for cell treatment and lysate preparation remained that same. The western blot analysis confirmed the previously observed TRPV1 (95 kDa + 22 kDa YFP) and ARMS (195 kDa) interaction [168, 169, 268]. More importantly, AKAP79 (79 kDa) seems to be involved in the TRPV1/ARMS/PKA signaling complex, regardless of transfected ARMS wild type or ARMS mutants [269]. However, even without transfected TRPV1, AKAP79 and ARMS seem to interact with each other. By showing physical and functional interactions between TRPV1, ARMS, PKA and AKAP79, the results suggest that all four proteins are part of a sophisticated signaling complex that sensitizes TRPV1 towards capsaicin (Figure 4.3.2: Schematic model of the TRPV1/ARMS/PKA/AKAP79 complex).

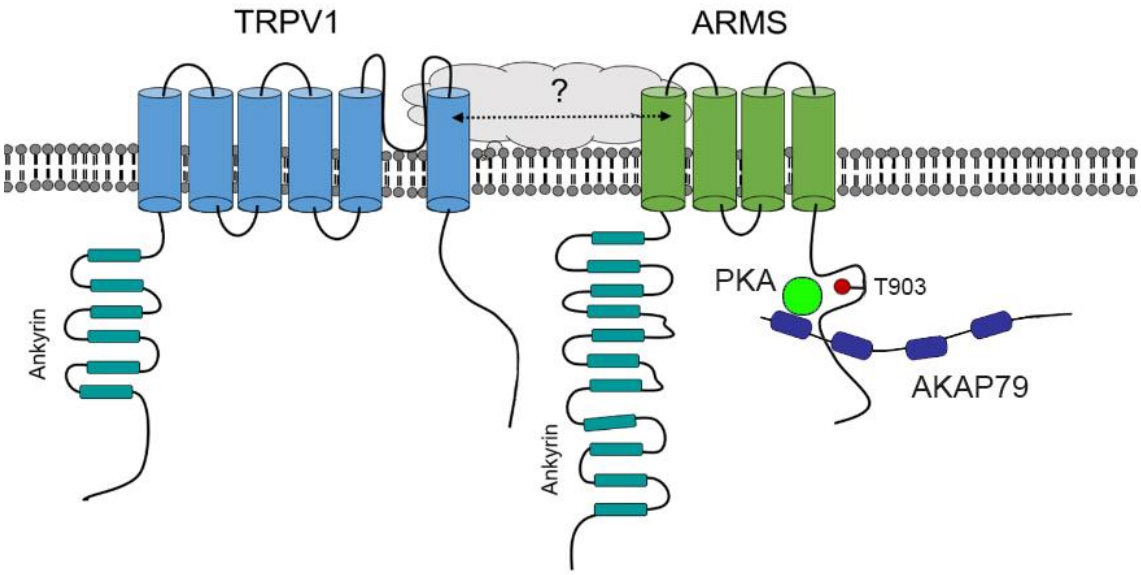

Figure 4.3.2: Schematic model of the TRPV1/ARMS/PKA/AKAP79 complex
Schematic model of the sophisticated TRPV1/ARMS/PKA/AKAP79 signaling complex. AKAP79 mediates PKA phosphorylation of ARMS at the amino acid T903. TRPV1 and ARMS interaction seems independent on PKA phosphorylation of ARMS and results in sensitization of TRPV1 towards capsaicin. The actual sensitizing mechanism of ARMS on TRPV1 remains unknown [270].

Since the TRPV1-sensitizing effect of the ARMS/PKA/AKAP79 complex seems to be independent of PKA phosphorylation, but dependent on interaction, a drastically reduced interaction should stop sensitization of TRPV1. To overcome the problem of ARMS-mediated TRPV1 sensitization by interaction, ARMS was silenced by shRNA. ARMS silencing resulted in a restored TRPV1 desensitization without affecting the TRPV1 expression and therefore could be used as new topical therapeutic analgesic alternative to stop ARMS mediated TRPV1 sensitization. In the past, targeting TRPV1 directly with antagonists was not very successful. Many compounds have been developed that inhibit TRPV1 but none of them are in routine clinical practice. Nevertheless, TRPV1 antagonists have been shown to provide pain relief in some animal models/clinical trials but not in all studies. In addition, they suffer from major limitations and side effects like accidental burns and hyperthermia [271]. On the other hand, the approval of the first small interfering RNA drug Patisiran by FDA in 2018 marks a new era of RNA interference therapeutics [272]. Given the concerns of on-target side-effects (without constrained organ-specific delivery, they may cause severe on-target side-effects), siRNAs administered locally clearly avoid these obstacles. For example, Sylentis Pharmaceuticals´ SYL1001 (Tivanisiram) is under investigation in a phase III clinical trial in more than 30 European hospitals and 300 patients [273]. Tivanisiram silences TRPV1 to treat dry eye syndrome. No systemic adverse effects were observed at any time in pre-clinical and phase I trials [274]. However, experiments showed that miR-4638-5p is able to regulate ARMS and that shRNA-mediated knockdown of ARMS phenocopied miR-4638-5p restoration. Furthermore, they found that miR-4638-5p, through regulating ARMS and the downstream activity of VEGF and PI3K/AKT pathway, influences prostate cancer progression via angiogenesis [275].

Taken together, the results shed some light on PKA phosphorylation of ARMS. Furthermore, a functional and physical interaction of TRPV1, ARMS and PKA as well as AKAP79 in HEK293 cells was identified/verified, resulting in sensitization of TRPV1 towards capsaicin, independent on PKA but dependent on interaction rate. This underlines the underestimated role of signaling complex formation and their interaction, which may be relevant to pain sensitization. When considering the development of new analgesics, it might be necessary to examine not only single proteins, but also signaling complexes including their interaction rates. Pain relief solutions based on shRNA could be used as new topical therapeutic analgesic alternative to stop ARMS mediated TRPV1 sensitization. In addition, these investigations could show that TRPV1/ARMS are linked to neuropathic pain/polyneuropathy via angiogenesis and similar determined miRNA mechanisms above. Making shRNA based ARMS silencing a possible/potential treatment to stop chronifying/chronic pain in polyneuropathy and other neuropathic pain conditions.

4.4 Outlook

Since the strong correlation between miRNA mechanisms and chronic pain in polyneuropathy encourages the promising indication that hsa-miR-3135b, hsa-miR-584-5p, hsa-miR-12136 and hsa-miR-550a-3p could be potential biomarkers with high accessibility, specificity and sensitivity for the diagnosis of chronic pain in polyneuropathy, the following experiments should be addressed: new chronic painful polyneuropathy patients as well as new healthy patients should be recruited and tested for hsa-miR-3135b, hsa-miR-584-5p, hsa-miR-12136 and hsa-miR-550a-3p via qPCR to verify the sequencing results. In these experiments qPCR should be the method of choice, because for the ease of use and to cut down costs/time for each test, without losing specificity and sensitivity. Each test could be performed in less than three hours from sample to result, enabling reliable diagnosis of chronic pain in polyneuropathy. On the other hand, therapeutics based on hsa-miR-3135b, hsa-miR-584-5p, hsa-miR-12136 and hsa-miR-550a-3p could be investigated to reverse the miRNA mediated disbalance causing chronic pain in polyneuropathy. Therefore, miRNA mimics or in case of hsa-miR-550a-3p an antisense miRNA could be used to adjust the miRNA disbalance that could hopefully soften or reverse chronic pain symptoms in polyneuropathy.

Since the functional and physical interaction of TRPV1, ARMS and PKA as well as AKAP79 in HEK293 cells was identified/verified, resulting in sensitization of TRPV1 to capsaicin, independent on PKA but dependent on interaction rate, the following experiments should be addressed: immunoprecipitation of TRPV1, ARMS and PKA as well as AKAP79 from DRG neurons. This experiment would verify the interaction of the addressed signaling complex in a context that harbors all four proteins in a native manner. On the other hand, experiments should be performed to investigate whether PKD facilitates ARMS mediated TRPV1 sensitization. Therefore, PKD sites in ARMS should be determined via pattern search and single PKD site ARMS mutants should be cloned. A phosphorylation screening could show which PKD sites in ARMS are phosphorylated and if these PKD sites are important for the TRPV1/ARMS interaction. Furthermore, the effect of the specific PKA inhibitor myr-PKI 14 22 (myr-GRTGRRNAI) on PKD should be investigated. Since, this could explain the results by Kasper et al. and results obtained by H89/BPKDi experiments. However, to verify and overcome the problem of ARMS-mediated TRPV1 sensitization by interaction, ARMS should be silenced in the mouse chronic constriction injury model of neuropathic pain. Therefore, shRNA could be used to stop ARMS mediated TRPV1 sensitization. Such a new therapeutic could be applied as topical analgesic to minimize systematic off target effects. In addition, these investigations could show that TRPV1/ARMS are linked to chronic neuropathic pain/polyneuropathy as well as a possible treatment.

5. Abstract

This dissertation aimed to determine differential expressed miRNAs in the context of chronic pain in polyneuropathy. For this purpose, patients with chronic painful polyneuropathy were compared with age matched healthy patients. Taken together, all miRNA pre library preparation quality controls were successful and none of the samples was identified as an outlier or excluded for library preparation. Pre sequencing quality control showed that library preparation worked for all samples as well as that all samples were free of adapter dimers after BluePippin size selection and reached the minimum molarity for further processing. Thus, all samples were subjected to sequencing. The sequencing control parameters were in their optimal range and resulted in valid sequencing results with strong sample to sample correlation for all samples. The resulting FASTQ file of each miRNA library was analyzed and used to perform a differential expression analysis. The differentially expressed and filtered miRNAs were subjected to miRDB to perform a target prediction. Three of those four miRNAs were downregulated: hsa-miR-3135b, hsa-miR-584-5p and hsa-miR-12136, while one was upregulated: hsa-miR-550a-3p. miRNA target prediction showed that chronic pain in polyneuropathy might be the result of a combination of miRNA mediated high blood flow/pressure and neural activity dysregulations/disbalances. Thus, leading to the promising conclusion that these four miRNAs could serve as potential biomarkers for the diagnosis of chronic pain in polyneuropathy.

Since TRPV1 seems to be one of the major contributors of nociception and is associated with neuropathic pain, the influence of PKA phosphorylated ARMS on the sensitivity of TRPV1 as well as the part of AKAP79 during PKA phosphorylation of ARMS was characterized. Therefore, possible PKA-sites in the sequence of ARMS were identified. This revealed five canonical PKA-sites: S882, T903, S1251/52, S1439/40 and S1526/27. The single PKA-site mutants of ARMS revealed that PKA-mediated ARMS phosphorylation seems not to influence the interaction rate of TRPV1/ARMS. While phosphorylation of $ARMS_{T903}$ does not increase the interaction rate with TRPV1, $ARMS_{S1526/27}$ is probably not phosphorylated and leads to an increased interaction rate. The calcium flux measurements indicated that the higher the interaction rate of TRPV1/ARMS, the lower the EC_{50} for capsaicin of TRPV1, independent of the PKA phosphorylation status of ARMS. In addition, the western blot analysis confirmed the previously observed TRPV1/ARMS interaction. More importantly, AKAP79 seems to be involved in the TRPV1/ARMS/PKA signaling complex. To overcome the problem of ARMS-mediated TRPV1 sensitization by interaction, ARMS was silenced by shRNA. ARMS silencing resulted in a restored TRPV1 desensitization without affecting the TRPV1 expression and therefore could be used as new topical therapeutic analgesic alternative to stop ARMS mediated TRPV1 sensitization.

5.1 Zusammenfassung

Ziel dieser Dissertation war es, differentiell exprimierte miRNAs im Kontext von chronischen Schmerzen bei Polyneuropathie zu bestimmen. Zu diesem Zweck wurden Patienten mit chronisch schmerzhafter Polyneuropathie und altersgleiche gesunde Patienten verglichen. Insgesamt waren alle Qualitätskontrollen zur Erstellung der miRNA-Bibliothek erfolgreich und keine der Proben wurde als Ausreißer identifiziert oder ausgeschlossen. Die Qualitätskontrolle vor der Sequenzierung zeigte, dass die Bibliothekserstellung für alle Proben funktionierte, sowie dass alle Proben frei von Adapterdimeren waren und die Mindestmolalität erreichten, woraufhin alle Proben sequenziert wurden. Die Kontrollparameter für die Sequenzierung lagen im optimalen Bereich und führten bei allen Proben zu gültigen Sequenzierungsergebnissen mit einer starken Korrelation zwischen den Proben. Die resultierende FASTQ-Datei jeder miRNA-Bibliothek wurde analysiert und für eine differenzielle Expressionsanalyse verwendet. Die differenziell exprimierten und gefilterten miRNAs wurden mittels miRDB analysiert, um eine Zielvorhersage zu erhalten. Drei dieser vier miRNAs wurden herunterreguliert: hsa-miR-3135b, hsa-miR-584-5p und hsa-miR-12136, während eine hochreguliert wurde: hsa-miR-550a-3p. Die miRNA-Zielvorhersage zeigte, dass chronische Schmerzen bei Polyneuropathie das Ergebnis von miRNA induziertem hohen Blutdruck und neuralen Aktivitätsdysregulationen sein könnten. Daraus ergibt sich die Schlussfolgerung, dass diese vier miRNAs als potenzielle Biomarker für die Diagnose von chronischen Schmerzen bei Polyneuropathie dienen könnten.

Da TRPV1 mit Nozizeption und neuropathischen Schmerzen in Verbindung gebracht wird, wurde der Einfluss von PKA-phosphoryliertem ARMS auf die Sensitivität von TRPV1 sowie die Rolle von AKAP79 während der PKA-Phosphorylierung von ARMS untersucht. Dazu wurden mögliche PKA-Stellen in der Sequenz von ARMS identifiziert. Dies ergab fünf kanonische PKA-Stellen: S882, T903, S1251/52, S1439/40 und S1526/27. Die einzelnen ARMS-Mutanten zeigten, dass die PKA-vermittelte ARMS-Phosphorylierung die Interaktion von TRPV1/ARMS nicht zu beeinflussen scheint. Während die Phosphorylierung von $ARMS_{T903}$ die Interaktionsrate mit TRPV1 nicht erhöht, wird $ARMS_{S1526/27}$ vermutlich nicht phosphoryliert und führt zu einer erhöhten Interaktionsrate. Zusätzlich zeigten Kalziumflussmessungen, dass der EC_{50} für Capsaicin von TRPV1 umso niedriger ist, je höher die Interaktionsrate von TRPV1/ARMS ist, unabhängig vom PKA-Phosphorylierungsstatus von ARMS. Darüber hinaus bestätigte die Western-Blot-Analyse, dass AKAP79 an dem TRPV1/ARMS/PKA-Signalkomplex beteiligt zu sein scheint. Letztlich sorgte die Stilllegung von ARMS mittels shRNA zu einer wiederhergestellten TRPV1-Desensibilisierung, ohne die TRPV1-Expression zu beeinträchtigen, und könnte als neue topische therapeutische Analgetika-Alternative verwendet werden.

6. References

[1] T. Ferenci, “Adaptation to life at micromolar nutrient levels: the regulation of Escherichia coli glucose transport by endoinduction and cAMP,” (eng), *FEMS microbiology reviews*, vol. 18, no. 4, pp. 301–317, 1996.

[2] S. E. Kotob, “"Review Article: An Overview of Cellular Signal Transduction Pathway"," *BJSTR*, vol. 38, no. 2, 2021.

[3] Y. He *et al.,* “Cell type specificity of signaling: view from membrane receptors distribution and their downstream transduction networks,” (eng), *Protein & cell*, vol. 3, no. 9, pp. 701–713, 2012.

[4] L. John Wiley & Sons, Ed., *Encyclopedia of life sciences*. Chichester: Wiley, 2005.

[5] E. J. Kodis *et al.,* “First Messengers,” in *Encyclopedia of life sciences*, L. John Wiley & Sons, Ed., Chichester: Wiley, 2005.

[6] E. Cao, M. Liao, Y. Cheng, and D. Julius, “TRPV1 structures in distinct conformations reveal activation mechanisms,” (eng), *Nature*, vol. 504, no. 7478, pp. 113–118, 2013.

[7] A. C. Newton, M. D. Bootman, and J. D. SCOTT, “Second Messengers,” (eng), *Cold Spring Harbor perspectives in biology*, vol. 8, no. 8, 2016.

[8] H. Zhang, Q. Kong, J. Wang, Y. Jiang, and H. Hua, “Complex roles of cAMP-PKA-CREB signaling in cancer,” (eng), *Experimental hematology & oncology*, vol. 9, no. 1, p. 32, 2020.

[9] O. Brandman and T. Meyer, “Feedback loops shape cellular signals in space and time,” (eng), *Science (New York, N.Y.)*, vol. 322, no. 5900, pp. 390–395, 2008.

[10] J. J. Cox *et al.,* “An SCN9A channelopathy causes congenital inability to experience pain,” (eng), *Nature*, vol. 444, no. 7121, pp. 894–898, 2006.

[11] International Association for the Study of Pain (IASP), *Terminology | International Association for the Study of Pain.* [Online] Available: https://www.iasp-pain.org/resources/terminology/#pain. Accessed on: Aug. 31 2022.

[12] International Association for the Study of Pain (IASP), *Definitions of Chronic Pain Syndromes - International Association for the Study of Pain (IASP).* [Online] Available: https://www.iasp-pain.org/advocacy/definitions-of-chronic-pain-syndromes/. Accessed on: Aug. 31 2022.

[13] R.-D. Treede *et al.,* “Chronic pain as a symptom or a disease: the IASP Classification of Chronic Pain for the International Classification of Diseases (ICD-11),” (eng), *Pain*, vol. 160, no. 1, pp. 19–27, 2019.

[14] C. A. Courtney, C. Fernández-de-las-Peñas, and S. Bond, “Mechanisms of chronic pain - key considerations for appropriate physical therapy management,” (eng), *The Journal of Manual & Manipulative Therapy*, vol. 25, no. 3, pp. 118–127, 2017.

[15] M.-A. Fitzcharles *et al.,* “Nociplastic pain: towards an understanding of prevalent pain conditions,” (eng), *The Lancet*, vol. 397, no. 10289, pp. 2098–2110, 2021.

[16] K. Meßlinger, “Was ist ein Nozizeptor?,” *Der Schmerz*, vol. 11, no. 5, pp. 353–366, 1997.

[17] A. I. Basbaum, D. M. Bautista, G. Scherrer, and D. Julius, “Cellular and molecular mechanisms of pain,” (eng), *Cell*, vol. 139, no. 2, pp. 267–284, 2009.

[18] D. Purves, Ed., *Neuroscience,* 3rd ed. Sunderland, Mass.: Sinauer Associates, 2004.

[19] J. E. Hall, *Guyton and Hall textbook of medical physiology: Student consult. Activate at studentconsult.com. Searchable full text online,* 12th ed. Philadelphia, Pa.: Saunders Elsevier, 2011.

[20] R. D'Mello and A. H. Dickenson, “Spinal cord mechanisms of pain,” (eng), *British journal of anaesthesia*, vol. 101, no. 1, pp. 8–16, 2008.

[21] D. Albe-Fessar, K. J. Berkley, L. Kruger, H. J. Ralston, and W. D. Willis, “Diencephalic mechanisms of pain sensation,” (eng), *Brain Research Reviews*, vol. 9, no. 3, pp. 217–296, 1985.

[22] S. Yang and M. C. Chang, “Chronic Pain: Structural and Functional Changes in Brain Structures and Associated Negative Affective States,” (eng), *International journal of molecular sciences*, vol. 20, no. 13, 2019.

[23] J. Ball, R. M. Bindler, and K. J. Cowen, *Principles of pediatric nursing: Caring for children*. Boston: Pearson, 2017.

[24] X. J. Song, S. J. Hu, K. W. Greenquist, J. M. Zhang, and R. H. LaMotte, “Mechanical and thermal hyperalgesia and ectopic neuronal discharge after chronic compression of dorsal root ganglia,” (eng), *Journal of neurophysiology*, vol. 82, no. 6, pp. 3347–3358, 1999.

[25] V. Gangadharan and R. Kuner, “Pain hypersensitivity mechanisms at a glance,” (eng), *Disease models & mechanisms*, vol. 6, no. 4, pp. 889–895, 2013.

[26] G. P. Dureja, R. N. Iyer, G. Das, J. Ahdal, and P. Narang, “Evidence and consensus recommendations for the pharmacological management of pain in India,” (eng), *Journal of pain research*, vol. 10, pp. 709–736, 2017.

[27] M. J. Caterina, T. A. Rosen, M. Tominaga, A. J. Brake, and D. Julius, “A capsaicin-receptor homologue with a high threshold for noxious heat,” (eng), *Nature*, vol. 398, no. 6726, pp. 436–441, 1999.

[28] D. C. Immke and N. R. Gavva, “The TRPV1 receptor and nociception,” (eng), *Seminars in cell & developmental biology*, vol. 17, no. 5, pp. 582–591, 2006.

[29] T. A. Nees *et al., The molecular mechanism and physiological role of silent nociceptor activation*, 2022.

[30] E. N. van den Broeke, C. Lenoir, and A. Mouraux, “Secondary hyperalgesia is mediated by heat-insensitive A-fibre nociceptors,” (eng), *The Journal of physiology*, vol. 594, no. 22, pp. 6767–6776, 2016.

[31] A. Latremoliere and C. J. Woolf, “Central sensitization: a generator of pain hypersensitivity by central neural plasticity,” (eng), *The journal of pain*, vol. 10, no. 9, pp. 895–926, 2009.

[32] H. Hou *et al.,* “Magnesium Acts as a Second Messenger in the Regulation of NMDA Receptor-Mediated CREB Signaling in Neurons,” (eng), *Molecular neurobiology*, vol. 57, no. 6, pp. 2539–2550, 2020.

[33] G. Chen, Y.-Q. Zhang, Y. J. Qadri, C. N. Serhan, and R.-R. Ji, “Microglia in Pain: Detrimental and Protective Roles in Pathogenesis and Resolution of Pain,” (eng), *Neuron*, vol. 100, no. 6, pp. 1292–1311, 2018.

[34] R.-R. Ji, T. A. Samad, S.-X. Jin, R. Schmoll, and C. J. Woolf, “p38 MAPK Activation by NGF in Primary Sensory Neurons after Inflammation Increases TRPV1 Levels and Maintains Heat Hyperalgesia,” *Neuron*, vol. 36, no. 1, pp. 57–68, 2002.

[35] S.-X. Jin, Z.-Y. Zhuang, C. J. Woolf, and R.-R. Ji, “p38 Mitogen-Activated Protein Kinase Is Activated after a Spinal Nerve Ligation in Spinal Cord Microglia and Dorsal Root Ganglion Neurons and Contributes to the Generation of Neuropathic Pain,” *J. Neurosci.*, vol. 23, no. 10, pp. 4017–4022, 2003.

[36] J. Wang, J. Chen, and S. Sen, “MicroRNA as Biomarkers and Diagnostics,” (eng), *Journal of cellular physiology*, vol. 231, no. 1, pp. 25–30, 2016.

[37] J. R. Chevillet, I. Lee, H. A. Briggs, Y. He, and K. Wang, “Issues and prospects of microRNA-based biomarkers in blood and other body fluids,” (eng), *Molecules*, vol. 19, no. 5, pp. 6080–6105, 2014.

[38] A. Etheridge, I. Lee, L. Hood, D. Galas, and K. Wang, “Extracellular microRNA: A new source of biomarkers,” (eng), *Mutation research*, vol. 717, no. 1-2, pp. 85–90, 2011.

[39] R. C. Lee, R. L. Feinbaum, and V. Ambros, “The C. elegans heterochronic gene lin-4 encodes small RNAs with antisense complementarity to lin-14,” (eng), *Cell*, vol. 75, no. 5, pp. 843–854, 1993.

[40] B. Wightman, I. Ha, and G. Ruvkun, “Posttranscriptional regulation of the heterochronic gene lin-14 by lin-4 mediates temporal pattern formation in C. elegans,” (eng), *Cell*, vol. 75, no. 5, pp. 855–862, 1993.

[41] R. C. Friedman, K. K.-H. Farh, C. B. Burge, and D. P. Bartel, “Most mammalian mRNAs are conserved targets of microRNAs,” (eng), *Genome Research*, vol. 19, no. 1, pp. 92–105, 2009.

[42] Applied Biological Materials (abm) Inc., *miRNA Introduction - Biogenesis, Nomenclature, and Experimental Workflow.* [Online] Available: https://old.abmgood.com/marketing/knowledge_base/miRNA_Introduction.php. Accessed on: Jul. 11 2022.

[43] Y. Lee *et al.,* "MicroRNA genes are transcribed by RNA polymerase II," (eng), *The EMBO Journal*, vol. 23, no. 20, pp. 4051–4060, 2004.

[44] Y. Lee *et al.,* "The nuclear RNase III Drosha initiates microRNA processing," (eng), *Nature*, vol. 425, no. 6956, pp. 415–419, 2003.

[45] R. Yi, Y. Qin, I. G. Macara, and B. R. Cullen, "Exportin-5 mediates the nuclear export of pre-microRNAs and short hairpin RNAs," (eng), *Genes & Development*, vol. 17, no. 24, pp. 3011–3016, 2003.

[46] T. P. Chendrimada *et al.,* "TRBP recruits the Dicer complex to Ago2 for microRNA processing and gene silencing," (eng), *Nature*, vol. 436, no. 7051, pp. 740–744, 2005.

[47] P. B. Kwak and Y. Tomari, "The N domain of Argonaute drives duplex unwinding during RISC assembly," (eng), *Nature structural & molecular biology*, vol. 19, no. 2, pp. 145–151, 2012.

[48] C. L. Noland and J. A. Doudna, "Multiple sensors ensure guide strand selection in human RNAi pathways," (eng), *RNA (New York, N.Y.)*, vol. 19, no. 5, pp. 639–648, 2013.

[49] J. O'Brien, H. Hayder, Y. Zayed, and C. Peng, "Overview of MicroRNA Biogenesis, Mechanisms of Actions, and Circulation," (eng), *Frontiers in Endocrinology*, vol. 9, p. 402, 2018.

[50] C. E. Condrat *et al.,* "miRNAs as Biomarkers in Disease: Latest Findings Regarding Their Role in Diagnosis and Prognosis," (eng), *Cells*, vol. 9, no. 2, 2020.

[51] C. Catalanotto, C. Cogoni, and G. Zardo, "MicroRNA in Control of Gene Expression: An Overview of Nuclear Functions," (eng), *International journal of molecular sciences*, vol. 17, no. 10, 2016.

[52] D. Didiano and O. Hobert, "Molecular architecture of a miRNA-regulated 3' UTR," (eng), *RNA (New York, N.Y.)*, vol. 14, no. 7, pp. 1297–1317, 2008.

[53] E. Huntzinger and E. Izaurralde, "Gene silencing by microRNAs: contributions of translational repression and mRNA decay," (eng), *Nature reviews. Genetics*, vol. 12, no. 2, pp. 99–110, 2011.

[54] H.-O. Iwakawa and Y. Tomari, "The Functions of MicroRNAs: mRNA Decay and Translational Repression," (eng), *Trends in cell biology*, vol. 25, no. 11, pp. 651–665, 2015.

[55] M. Arribas-Layton, D. Wu, J. Lykke-Andersen, and H. Song, “Structural and functional control of the eukaryotic mRNA decapping machinery,” (eng), *Biochimica et biophysica acta*, vol. 1829, no. 6-7, pp. 580–589, 2013.

[56] E. Wahle and G. S. Winkler, “RNA decay machines: deadenylation by the Ccr4-not and Pan2-Pan3 complexes,” (eng), *Biochimica et biophysica acta*, vol. 1829, no. 6-7, pp. 561–570, 2013.

[57] M. R. Fabian *et al.,* “miRNA-mediated deadenylation is orchestrated by GW182 through two conserved motifs that interact with CCR4-NOT,” (eng), *Nature structural & molecular biology*, vol. 18, no. 11, pp. 1211–1217, 2011.

[58] S. Gu and M. A. Kay, “How do miRNAs mediate translational repression?,” (eng), *Silence*, vol. 1, no. 1, p. 11, 2010.

[59] T. Nishihara, L. Zekri, J. E. Braun, and E. Izaurralde, “miRISC recruits decapping factors to miRNA targets to enhance their degradation,” (eng), *Nucleic Acids Research*, vol. 41, no. 18, pp. 8692–8705, 2013.

[60] K. Xu, J. Lin, R. Zandi, J. A. Roth, and L. Ji, “MicroRNA-mediated target mRNA cleavage and 3'-uridylation in human cells,” (eng), *Scientific reports*, vol. 6, p. 30242, 2016.

[61] A. Helwak, G. Kudla, T. Dudnakova, and D. Tollervey, “Mapping the human miRNA interactome by CLASH reveals frequent noncanonical binding,” (eng), *Cell*, vol. 153, no. 3, pp. 654–665, 2013.

[62] J. A. Weber *et al.,* “The microRNA spectrum in 12 body fluids,” (eng), *Clinical chemistry*, vol. 56, no. 11, pp. 1733–1741, 2010.

[63] K. Zen and C.-Y. Zhang, “Circulating microRNAs: a novel class of biomarkers to diagnose and monitor human cancers,” (eng), *Medicinal research reviews*, vol. 32, no. 2, pp. 326–348, 2012.

[64] M. F. Corsten *et al.,* “Circulating MicroRNA-208b and MicroRNA-499 reflect myocardial damage in cardiovascular disease,” (eng), *Circulation. Cardiovascular genetics*, vol. 3, no. 6, pp. 499–506, 2010.

[65] K. Kai, R. L. Dittmar, and S. Sen, “Secretory microRNAs as biomarkers of cancer,” (eng), *Seminars in cell & developmental biology*, vol. 78, pp. 22–36, 2018.

[66] R. Raoof *et al.,* “Dual-center, dual-platform microRNA profiling identifies potential plasma biomarkers of adult temporal lobe epilepsy,” (eng), *EBioMedicine*, vol. 38, pp. 127–141, 2018.

[67] S. Tigchelaar *et al.,* “MicroRNA Biomarkers in Cerebrospinal Fluid and Serum Reflect Injury Severity in Human Acute Traumatic Spinal Cord Injury,” (eng), *Journal of neurotrauma*, vol. 36, no. 15, pp. 2358–2371, 2019.

[68] A. J. Tijsen *et al.,* “MiR423-5p as a circulating biomarker for heart failure,” (eng), *Circulation research*, vol. 106, no. 6, pp. 1035–1039, 2010.

[69] J. T. Wiedrick *et al.,* “Validation of MicroRNA Biomarkers for Alzheimer's Disease in Human Cerebrospinal Fluid,” (eng), *Journal of Alzheimer's disease : JAD*, vol. 67, no. 3, pp. 875–891, 2019.

[70] B. Szilágyi, Z. Fejes, M. Pócsi, J. Kappelmayer, and B. Nagy, “Role of sepsis modulated circulating microRNAs,” (eng), *EJIFCC*, vol. 30, no. 2, pp. 128–145, 2019.

[71] X. Chen *et al.,* “Characterization of microRNAs in serum: a novel class of biomarkers for diagnosis of cancer and other diseases,” (eng), *Cell research*, vol. 18, no. 10, pp. 997–1006, 2008.

[72] H. Valadi *et al.,* “Exosome-mediated transfer of mRNAs and microRNAs is a novel mechanism of genetic exchange between cells,” (eng), *Nature cell biology*, vol. 9, no. 6, pp. 654–659, 2007.

[73] A. Turchinovich, L. Weiz, A. Langheinz, and B. Burwinkel, “Characterization of extracellular circulating microRNA,” (eng), *Nucleic Acids Research*, vol. 39, no. 16, pp. 7223–7233, 2011.

[74] J. D. Arroyo *et al.,* “Argonaute2 complexes carry a population of circulating microRNAs independent of vesicles in human plasma,” (eng), *Proceedings of the National Academy of Sciences of the United States of America*, vol. 108, no. 12, pp. 5003–5008, 2011.

[75] K. C. Vickers, B. T. Palmisano, B. M. Shoucri, R. D. Shamburek, and A. T. Remaley, “MicroRNAs are transported in plasma and delivered to recipient cells by high-density lipoproteins,” (eng), *Nature cell biology*, vol. 13, no. 4, pp. 423–433, 2011.

[76] A. Sakai and H. Suzuki, “microRNA and Pain,” (eng), *Advances in experimental medicine and biology*, vol. 888, pp. 17–39, 2015.

[77] C. Sommer *et al.,* “Polyneuropathies,” (eng), *Deutsches Ärzteblatt International*, vol. 115, no. 6, pp. 83–90, 2018.

[78] R. Hanewinckel *et al.,* “Prevalence of polyneuropathy in the general middle-aged and elderly population,” (eng), *Neurology*, vol. 87, no. 18, pp. 1892–1898, 2016.

[79] J. F. Burke, L. E. Skolarus, B. C. Callaghan, and K. A. Kerber, “Choosing Wisely: highest-cost tests in outpatient neurology,” (eng), *Annals of neurology*, vol. 73, no. 5, pp. 679–683, 2013.

[80] B. C. Callaghan *et al.,* “Role of neurologists and diagnostic tests on the management of distal symmetric polyneuropathy,” (eng), *JAMA neurology*, vol. 71, no. 9, pp. 1143–1149, 2014.

[81] R. A. C. Hughes, “Peripheral neuropathy,” (eng), *BMJ : British Medical Journal*, vol. 324, no. 7335, pp. 466–469, 2002.

[82] N. E. Bharucha, A. E. Bharucha, and E. P. Bharucha, “Prevalence of peripheral neuropathy in the Parsi community of Bombay,” (eng), *Neurology*, vol. 41, no. 8, pp. 1315–1317, 1991.

[83] A. I. Adler, E. J. Boyko, J. H. Ahroni, and D. G. Smith, “Lower-extremity amputation in diabetes. The independent effects of peripheral vascular disease, sensory neuropathy, and foot ulcers,” (eng), *Diabetes care*, vol. 22, no. 7, pp. 1029–1035, 1999.

[84] B. C. Callaghan, R. S. Price, and E. L. Feldman, “Distal Symmetric Polyneuropathy: A Review,” (eng), *JAMA*, vol. 314, no. 20, pp. 2172–2181, 2015.

[85] J. N. Kanji, R. E. S. Anglin, D. L. Hunt, and A. Panju, “Does this patient with diabetes have large-fiber peripheral neuropathy?,” (eng), *JAMA*, vol. 303, no. 15, pp. 1526–1532, 2010.

[86] U. K. Misra, J. Kalita, and P. P. Nair, “Diagnostic approach to peripheral neuropathy,” (eng), *Annals of Indian Academy of Neurology*, vol. 11, no. 2, pp. 89–97, 2008.

[87] D. Blackmore and Z. A. Siddiqi, “Pinprick Testing in Small Fiber Neuropathy: Accuracy and Pitfalls,” (eng), *Journal of clinical neuromuscular disease*, vol. 17, no. 4, pp. 181–186, 2016.

[88] A. Hovaguimian and C. H. Gibbons, “Diagnosis and treatment of pain in small-fiber neuropathy,” (eng), *Current pain and headache reports*, vol. 15, no. 3, pp. 193–200, 2011.

[89] D. C. Rosenberger, V. Blechschmidt, H. Timmerman, A. Wolff, and R.-D. Treede, “Challenges of neuropathic pain: focus on diabetic neuropathy,” (eng), *Journal of neural transmission (Vienna, Austria : 1996)*, vol. 127, no. 4, pp. 589–624, 2020.

[90] W. Magerl *et al.,* “Reference data for quantitative sensory testing (QST): refined stratification for age and a novel method for statistical comparison of group data,” (eng), *Pain*, vol. 151, no. 3, pp. 598–605, https://pubmed.ncbi.nlm.nih.gov/20965658/, 2010.

[91] G. Lauria *et al.,* “European Federation of Neurological Societies/Peripheral Nerve Society Guideline on the use of skin biopsy in the diagnosis of small fiber neuropathy. Report of a joint task force of the European Federation of Neurological Societies and the Peripheral Nerve Society,” (eng), *European journal of neurology*, vol. 17, no. 7, 903-12, e44-9, 2010.

[92] C. Khan *et al.,* “Nationale VersorgungsLeitlinie Neuropathie bei Diabetes im Erwachsenenalter,” *Diabetologie und Stoffwechsel*, vol. 7, no. 04, pp. 243–285, 2012.

[93] L. Johannsen *et al.,* “Evaluation of Patients With Symptoms Suggestive of Chronic Polyneuropathy,” *Journal of clinical neuromuscular disease*, vol. 3, no. 2, pp. 47–52, 2001.

[94] N. Papanas and D. Ziegler, “Risk Factors and Comorbidities in Diabetic Neuropathy: An Update 2015,” *Rev Diabet Stud*, vol. 12, no. 1-2, pp. 48–62, 2015.

[95] C. Daousi *et al.,* “Chronic painful peripheral neuropathy in an urban community: a controlled comparison of people with and without diabetes,” (eng), *Diabetic medicine : a journal of the British Diabetic Association*, vol. 21, no. 9, pp. 976–982, 2004.

[96] T. S. Jensen and N. B. Finnerup, “Allodynia and hyperalgesia in neuropathic pain: clinical manifestations and mechanisms,” *The Lancet Neurology*, vol. 13, no. 9, pp. 924–935, 2014.

[97] E. E. Benarroch, “Central neuron-glia interactions and neuropathic pain: overview of recent concepts and clinical implications,” (eng), *Neurology*, vol. 75, no. 3, pp. 273–278, 2010.

[98] D.-J. Kao *et al.,* “CC chemokine ligand 2 upregulates the current density and expression of TRPV1 channels and Nav1.8 sodium channels in dorsal root ganglion neurons,” (eng), *Journal of neuroinflammation*, vol. 9, p. 189, 2012.

[99] B. D. Semple, T. Kossmann, and M. C. Morganti-Kossmann, “Role of chemokines in CNS health and pathology: a focus on the CCL2/CCR2 and CXCL8/CXCR2 networks,” (eng), *Journal of Cerebral Blood Flow and Metabolism: Official Journal of the International Society of Cerebral Blood Flow and Metabolism*, vol. 30, no. 3, pp. 459–473, 2010.

[100] S.-E. Jordt and D. Julius, “Molecular Basis for Species-Specific Sensitivity to “Hot” Chili Peppers,” *Cell*, vol. 108, no. 3, pp. 421–430, 2002.

[101] S. E. Jordt, M. Tominaga, and D. Julius, “Acid potentiation of the capsaicin receptor determined by a key extracellular site,” (eng), *Proceedings of the National Academy of Sciences of the United States of America*, vol. 97, no. 14, pp. 8134–8139, 2000.

[102] D. H. Kwon *et al.,* “Heat-dependent opening of TRPV1 in the presence of capsaicin,” (eng), *Nature structural & molecular biology*, vol. 28, no. 7, pp. 554–563, 2021.

[103] M. Benítez-Angeles, S. L. Morales-Lázaro, E. Juárez-González, and T. Rosenbaum, “TRPV1: Structure, Endogenous Agonists, and Mechanisms,” (eng), *International journal of molecular sciences*, vol. 21, no. 10, 2020.

[104] A. Patapoutian, A. M. Peier, G. M. Story, and V. Viswanath, “ThermoTRP channels and beyond: mechanisms of temperature sensation,” (eng), *Nature reviews. Neuroscience*, vol. 4, no. 7, pp. 529–539, 2003.

[105] A. Dhaka, V. Viswanath, and A. Patapoutian, “Trp ion channels and temperature sensation,” (eng), *Annual review of neuroscience*, vol. 29, pp. 135–161, 2006.

[106] M. J. Caterina, “Transient receptor potential ion channels as participants in thermosensation and thermoregulation,” (eng), *American journal of physiology. Regulatory, integrative and comparative physiology*, vol. 292, no. 1, R64-76, 2007.

[107] A. A. Romanovsky, “Thermoregulation: some concepts have changed. Functional architecture of the thermoregulatory system,” (eng), *American journal of physiology. Regulatory, integrative and comparative physiology*, vol. 292, no. 1, R37-46, 2007.

[108] C. H. Munns, M.-K. Chung, Y. E. Sanchez, L. M. Amzel, and M. J. Caterina, “Role of the outer pore domain in transient receptor potential vanilloid 1 dynamic permeability to large cations,” (eng), *The Journal of biological chemistry*, vol. 290, no. 9, pp. 5707–5724, 2015.

[109] M. Morgan, S. Nencini, J. Thai, and J. J. Ivanusic, “TRPV1 activation alters the function of Aδ and C fiber sensory neurons that innervate bone,” (eng), *Bone*, vol. 123, pp. 168–175, 2019.

[110] A. Jara-Oseguera, S. A. Simon, and T. Rosenbaum, “TRPV1: on the road to pain relief,” (eng), *Current molecular pharmacology*, vol. 1, no. 3, pp. 255–269, 2008.

[111] Y. Wang *et al.,* “TRPV1 SUMOylation regulates nociceptive signaling in models of inflammatory pain,” (eng), *Nature communications*, vol. 9, no. 1, p. 1529, 2018.

[112] Oxford University Press, *Activation of TRPV1 by capsaicin.* [Online] Available: https://de.m.wikipedia.org/wiki/Datei:Activation_of_TRPV1_by_capsaicin.jpg#. Accessed on: Jul. 05 2022.

[113] S. Munjuluri *et al.,* “Capsaicin and TRPV1 Channels in the Cardiovascular System: The Role of Inflammation,” (eng), *Cells*, vol. 11, no. 1, 2021.

[114] J. Jung *et al.,* “Phosphorylation of vanilloid receptor 1 by Ca2+/calmodulin-dependent kinase II regulates its vanilloid binding,” (eng), *The Journal of biological chemistry*, vol. 279, no. 8, pp. 7048–7054, 2004.

[115] L. de Petrocellis *et al.,* “The vanilloid receptor (VR1)-mediated effects of anandamide are potently enhanced by the cAMP-dependent protein kinase,” (eng), *Journal of neurochemistry*, vol. 77, no. 6, pp. 1660–1663, 2001.

[116] L. S. Premkumar and G. P. Ahern, “Induction of vanilloid receptor channel activity by protein kinase C,” (eng), *Nature*, vol. 408, no. 6815, pp. 985–990, 2000.

[117] T. Leppänen, R. K. Tuominen, and E. Moilanen, “Protein kinase C and its inhibitors in the regulation of inflammation: inducible nitric oxide synthase as an example,” (eng), *Basic & clinical pharmacology & toxicology*, vol. 114, no. 1, pp. 37–43, 2014.

[118] K. O. Aley and J. D. Levine, “Role of Protein Kinase A in the Maintenance of Inflammatory Pain,” *J. Neurosci.*, vol. 19, no. 6, pp. 2181–2186, 1999.

[119] N. A. Jeske *et al.,* “A-kinase anchoring protein mediates TRPV1 thermal hyperalgesia through PKA phosphorylation of TRPV1,” (eng), *Pain*, vol. 138, no. 3, pp. 604–616, 2008.

[120] J. Peter *et al.,* “Ankyrin-rich membrane spanning protein as a novel modulator of transient receptor potential vanilloid 1-function in nociceptive neurons,” (eng), *European journal of pain (London, England)*, vol. 21, no. 6, pp. 1072–1086, 2017.

[121] T. Iglesias *et al.,* “Identification and cloning of Kidins220, a novel neuronal substrate of protein kinase D,” (eng), *The Journal of biological chemistry*, vol. 275, no. 51, pp. 40048–40056, 2000.

[122] J. C. Arévalo *et al.,* “The ARMS/Kidins220 scaffold protein modulates synaptic transmission,” (eng), *Molecular and cellular neurosciences*, vol. 45, no. 2, pp. 92–100, 2010.

[123] V. E. Neubrand, F. Cesca, F. Benfenati, and G. Schiavo, “Kidins220/ARMS as a functional mediator of multiple receptor signalling pathways,” (eng), *Journal of cell science*, vol. 125, no. Pt 8, pp. 1845–1854, 2012.

[124] F. Cesca *et al.,* “Functional Interaction between the Scaffold Protein Kidins220/ARMS and Neuronal Voltage-Gated Na+ Channels,” (eng), *The Journal of biological chemistry*, vol. 290, no. 29, pp. 18045–18055, 2015.

[125] F. Jaudon *et al.,* “Kidins220/ARMS controls astrocyte calcium signaling and neuron-astrocyte communication,” (eng), *Cell death and differentiation*, vol. 27, no. 5, pp. 1505–1519, 2020.

[126] Y.-J. Gao and R.-R. Ji, “Targeting astrocyte signaling for chronic pain,” (eng), *Neurotherapeutics : the journal of the American Society for Experimental NeuroTherapeutics*, vol. 7, no. 4, pp. 482–493, 2010.

[127] J. Scholz-Starke and F. Cesca, “Stepping Out of the Shade: Control of Neuronal Activity by the Scaffold Protein Kidins220/ARMS,” (eng), *Frontiers in cellular neuroscience*, vol. 10, p. 68, 2016.

[128] M. Andreazzoli *et al.,* “Kidins220/ARMS interacts with Pdzrn3, a protein containing multiple binding domains,” (eng), *Biochimie*, vol. 94, no. 9, pp. 2054–2057, 2012.

[129] C. López-Menéndez *et al.,* “Excitotoxic targeting of Kidins220 to the Golgi apparatus precedes calpain cleavage of Rap1-activation complexes,” (eng), *Cell death & disease*, vol. 10, no. 7, p. 535, 2019.

[130] J. C. Arévalo, D. B. Pereira, H. Yano, K. K. Teng, and M. V. Chao, “Identification of a switch in neurotrophin signaling by selective tyrosine phosphorylation,” (eng), *The Journal of biological chemistry*, vol. 281, no. 2, pp. 1001–1007, 2006.

[131] A. Bracale *et al.,* “Kidins220/ARMS is transported by a kinesin-1-based mechanism likely to be involved in neuronal differentiation,” (eng), *Molecular biology of the cell*, vol. 18, no. 1, pp. 142–152, 2007.

[132] H. Kong, J. Boulter, J. L. Weber, C. Lai, and M. V. Chao, “An Evolutionarily Conserved Transmembrane Protein That Is a Novel Downstream Target of Neurotrophin and Ephrin Receptors,” *J. Neurosci.*, vol. 21, no. 1, pp. 176–185, 2001.

[133] J. C. Arévalo, H. Yano, K. K. Teng, and M. V. Chao, “A unique pathway for sustained neurotrophin signaling through an ankyrin-rich membrane-spanning protein,” (eng), *The EMBO Journal*, vol. 23, no. 12, pp. 2358–2368, 2004.

[134] X. Yao, H.-Y. Kwan, and Y. Huang, “Regulation of TRP channels by phosphorylation,” (eng), *Neuro-Signals*, vol. 14, no. 6, pp. 273–280, 2005.

[135] D. A. Walsh, J. P. Perkins, and E. G. Krebs, “An adenosine 3',5'-monophosphate-dependant protein kinase from rabbit skeletal muscle,” (eng), *The Journal of biological chemistry*, vol. 243, no. 13, pp. 3763–3765, 1968.

[136] G. Manning, “Genomic overview of protein kinases,” (eng), *WormBook : the online review of C. elegans biology*, pp. 1–19, 2005.

[137] D. Fabbro, S. W. Cowan-Jacob, and H. Moebitz, “Ten things you should know about protein kinases: IUPHAR Review 14,” (eng), *British journal of pharmacology*, vol. 172, no. 11, pp. 2675–2700, 2015.

[138] J. A. Endicott, M. E. M. Noble, and L. N. Johnson, “The structural basis for control of eukaryotic protein kinases,” (eng), *Annual review of biochemistry*, vol. 81, pp. 587–613, 2012.

[139] Y. Shi, “Serine/threonine phosphatases: mechanism through structure,” (eng), *Cell*, vol. 139, no. 3, pp. 468–484, 2009.

[140] B. Zimmermann, J. A. Chiorini, Y. Ma, R. M. Kotin, and F. W. Herberg, “PrKX is a novel catalytic subunit of the cAMP-dependent protein kinase regulated by the regulatory subunit type I,” (eng), *The Journal of biological chemistry*, vol. 274, no. 9, pp. 5370–5378, 1999.

[141] S. J. Beebe, P. Salomonsky, T. Jahnsen, and Y. Li, “The C gamma subunit is a unique isozyme of the cAMP-dependent protein kinase,” (eng), *The Journal of biological chemistry*, vol. 267, no. 35, pp. 25505–25512, 1992.

[142] K. Søberg, L. V. Moen, B. S. Skålhegg, and J. K. Laerdahl, “Evolution of the cAMP-dependent protein kinase (PKA) catalytic subunit isoforms,” (eng), *PloS one*, vol. 12, no. 7, e0181091, 2017.

[143] S. S. Taylor *et al.,* “PKA Cβ: a forgotten catalytic subunit of cAMP-dependent protein kinase opens new windows for PKA signaling and disease pathologies,” (eng), *The Biochemical journal*, vol. 478, no. 11, pp. 2101–2119, 2021.

[144] J. Isensee *et al.,* “PKA-RII subunit phosphorylation precedes activation by cAMP and regulates activity termination,” (eng), *The Journal of cell biology*, vol. 217, no. 6, pp. 2167–2184, 2018.

[145] P. Sassone-Corsi, “The cyclic AMP pathway,” (eng), *Cold Spring Harbor perspectives in biology*, vol. 4, no. 12, 2012.

[146] F. D. SMITH, B. K. SAMELSON, and J. D. SCOTT, “Discovery of cellular substrates for protein kinase A using a peptide array screening protocol,” (eng), *Biochemical Journal*, vol. 438, no. 1, pp. 103–110, 2011.

[147] T. Chijiwa *et al.,* “Inhibition of forskolin-induced neurite outgrowth and protein phosphorylation by a newly synthesized selective inhibitor of cyclic AMP-dependent protein kinase, N-[2-(p-bromocinnamylamino)ethyl]-5-isoquinolinesulfonamide (H-89), of PC12D pheochromocytoma cells,” *Journal of Biological Chemistry*, vol. 265, no. 9, pp. 5267–5272, 1990.

[148] T. M. Jay, H. Gurden, and T. Yamaguchi, “Rapid increase in PKA activity during long-term potentiation in the hippocampal afferent fibre system to the prefrontal cortex in vivo,” (eng), *The European journal of neuroscience*, vol. 10, no. 10, pp. 3302–3306, 1998.

[149] Y. Deng *et al.,* “Protein Kinase A Is Involved in Neuropathic Pain by Activating the p38MAPK Pathway to Mediate Spinal Cord Cell Apoptosis,” (eng), *Mediators of inflammation*, vol. 2020, p. 6420425, 2020.

[150] S. Herrmann *et al.,* “Protein kinase A regulates inflammatory pain sensitization by modulating HCN2 channel activity in nociceptive sensory neurons,” (eng), *Pain*, vol. 158, no. 10, pp. 2012–2024, 2017.

[151] A. Caretta and C. Mucignat-Caretta, “Protein kinase a in cancer,” (eng), *Cancers*, vol. 3, no. 1, pp. 913–926, 2011.

[152] M. G. Gold *et al.,* “Architecture and dynamics of an A-kinase anchoring protein 79 (AKAP79) signaling complex,” (eng), *Proceedings of the National Academy of Sciences of the United States of America*, vol. 108, no. 16, pp. 6426–6431, 2011.

[153] M. G. Gold *et al.,* “Molecular basis of AKAP specificity for PKA regulatory subunits,” (eng), *Molecular cell*, vol. 24, no. 3, pp. 383–395, 2006.

[154] J. L. Sanderson *et al.,* “AKAP150-anchored calcineurin regulates synaptic plasticity by limiting synaptic incorporation of Ca2+-permeable AMPA receptors,” (eng), *J. Neurosci.*, vol. 32, no. 43, pp. 15036–15052, 2012.

[155] M. Dacher, S. Gouty, S. Dash, B. M. Cox, and F. S. Nugent, “A-kinase anchoring protein-calcineurin signaling in long-term depression of GABAergic synapses,” (eng), *J. Neurosci.*, vol. 33, no. 6, pp. 2650–2660, 2013.

[156] M. J. M. Fischer, J. Btesh, and P. A. McNaughton, “Disrupting sensitization of transient receptor potential vanilloid subtype 1 inhibits inflammatory hyperalgesia,” (eng), *J. Neurosci.*, vol. 33, no. 17, pp. 7407–7414, 2013.

[157] K. J. Reissner, “Proteomic analyses of PKA and AKAP signaling in cocaine addiction,” (eng), *Neuropsychopharmacology*, vol. 38, no. 1, pp. 251–252, 2013.

[158] B. J. Tunquist *et al.,* “Loss of AKAP150 perturbs distinct neuronal processes in mice,” (eng), *Proceedings of the National Academy of Sciences of the United States of America*, vol. 105, no. 34, pp. 12557–12562, 2008.

[159] A. R. Wild and M. L. Dell'Acqua, “Potential for therapeutic targeting of AKAP signaling complexes in nervous system disorders,” (eng), *Pharmacology & therapeutics*, vol. 185, pp. 99–121, 2018.

[160] D. W. Carr, Z. E. Hausken, I. D. Fraser, R. E. Stofko-Hahn, and J. D. Scott, “Association of the type II cAMP-dependent protein kinase with a human thyroid RII-anchoring protein. Cloning and characterization of the RII-binding domain,” (eng), *Journal of Biological Chemistry*, vol. 267, no. 19, pp. 13376–13382, 1992.

[161] L. L. Gomez, S. Alam, K. E. Smith, E. Horne, and M. L. Dell'Acqua, “Regulation of A-Kinase Anchoring Protein 79/150–cAMP-Dependent Protein Kinase Postsynaptic Targeting by NMDA Receptor Activation of Calcineurin and Remodeling of Dendritic Actin,” (eng), *J. Neurosci.*, vol. 22, no. 16, pp. 7027–7044, 2002.

[162] I. Delint-Ramirez *et al.,* “Palmitoylation targets AKAP79 protein to lipid rafts and promotes its regulation of calcium-sensitive adenylyl cyclase type 8,” (eng), *The Journal of biological chemistry*, vol. 286, no. 38, pp. 32962–32975, 2011.

[163] D. J. Keith *et al.,* “Palmitoylation of A-kinase anchoring protein 79/150 regulates dendritic endosomal targeting and synaptic plasticity mechanisms,” (eng), *J. Neurosci.*, vol. 32, no. 21, pp. 7119–7136, 2012.

[164] P. K. Rathee *et al.,* “PKA/AKAP/VR-1 Module: A Common Link of G s -Mediated Signaling to Thermal Hyperalgesia,” *J. Neurosci.*, vol. 22, no. 11, pp. 4740–4745, 2002.

[165] K. E. Brandao, M. L. Dell'Acqua, and S. R. Levinson, “A-kinase anchoring protein 150 expression in a specific subset of TRPV1- and CaV 1.2-positive nociceptive rat dorsal root ganglion neurons,” (eng), *The Journal of comparative neurology*, vol. 520, no. 1, pp. 81–99, 2012.

[166] K. Schnizler *et al.,* “Protein kinase A anchoring via AKAP150 is essential for TRPV1 modulation by forskolin and prostaglandin E2 in mouse sensory neurons,” (eng), *J. Neurosci.*, vol. 28, no. 19, pp. 4904–4917, 2008.

[167] R. Efendiev, A. Bavencoffe, H. Hu, M. X. Zhu, and C. W. Dessauer, “Scaffolding by A-kinase anchoring protein enhances functional coupling between adenylyl cyclase and TRPV1 channel,” (eng), *The Journal of biological chemistry*, vol. 288, no. 6, pp. 3929–3937, 2013.

[168] UniProtKB - Q9EQG6, *KDIS_RAT: Kinase D-interacting substrate of 220 kDa*. Isoform 2. [Online] Available: https://www.uniprot.org/uniprot/Q9EQG6#Q9EQG6-2. Accessed on: May 26 2022.

[169] UniProtKB - O35433, *TRPV1_RAT: Transient receptor potential cation channel subfamily V member 1*. Isoform 1. [Online] Available: https://www.uniprot.org/uniprot/O35433#O35433-1. Accessed on: May 26 2022.

[170] H.U. Gerbershagen, J. Korb, B. Nagel & P. Nilges, *Das Mainzer Stadienkonzept des Schmerzes: Eine Standortbestimmung*, 1996.

[171] H.U. Gerbershagen, J. Korb, B. Nagel & P. Nilges, “Das Mainzer Stadienmodell der Schmerz-Chronifizierung (MPSS): Auswertungsformular,” https://www.drk-schmerz-zentrum.de/mz-wAssets/docs/downloads/mpss_deu.pdf.

[172] QIAGEN, *miRNeasy Serum/ Plasma Advanced Kit Handbook: For purification of total RNA, including miRNA, from serum and plasma.* [Online] Available: https://www.qiagen.com/us/resources/download.aspx?id=20e0ddd1-ad97-43ef-9edf-eef6a6d02a1d&lang=en. Accessed on: May 30 2022.

[173] QIAGEN, *QIAseq™ miRNA Library QC PCR Handbook: For quality control of RNA isolation for small RNA next-generation sequencing.* [Online] Available: https://www.qiagen.com/us/resources/download.aspx?id=8f2523cc-3af8-4cbf-bdd7-b8f538462755&lang=en. Accessed on: May 30 2022.

[174] QIAGEN, *QIAseq® miRNA Library Kit Handbook: Precision small RNA library prep for Illumina® NGS systems.* [Online] Available:

https://www.qiagen.com/us/resources/download.aspx?id=f0b9d117-f8c6-4825-9069-3236ed65521d&lang=en. Accessed on: May 31 2022.

[175] Agilent, *High Sensitivity DNA Kit Guide.* [Online] Available: https://www.agilent.com/cs/library/usermanuals/public/HighSensitivity_DNA_KG.pdf.pdf. Accessed on: May 31 2022.

[176] Sage Science, *BluePippin Operations Manual: 460013-Rev-D.* [Online] Available: https://www.sagescience.com/wp-content/uploads/2016/09/BluePippin-Operations-Manual-460013-Rev-D.pdf. Accessed on: May 31 2022.

[177] Illumina, *Index Adapters Pooling Guide.* [Online] Available: https://support-docs.illumina.com/SHARE/IndexAdapterPooling/index-adapters-pooling.pdf. Accessed on: May 31 2022.

[178] Illumina, *NextSeq System Denature and Dilute Libraries Guide.* [Online] Available: https://support.illumina.com/content/dam/illumina-support/documents/documentation/system_documentation/nextseq/nextseq-denature-dilute-libraries-guide-15048776-09.pdf. Accessed on: May 31 2022.

[179] Illumina, *MiSeq™ system Denature and Dilute Libraries Guide.* [Online] Available: https://support.illumina.com/content/dam/illumina-support/documents/documentation/system_documentation/miseq/miseq-denature-dilute-libraries-guide-15039740-10.pdf. Accessed on: May 31 2022.

[180] Illumina, *MiSeq System Guide.* [Online] Available: https://support.illumina.com/content/dam/illumina-support/documents/documentation/system_documentation/miseq/miseq-system-guide-for-windows-7-1000000154717-00.pdf. Accessed on: May 31 2022.

[181] QIAGEN, *Biomedical Genomics Analysis plugin.* [Online] Available: https://digitalinsights.qiagen.com/plugins/biomedical-genomics-analysis/. Accessed on: May 31 2022.

[182] QIAGEN, *CLC Genomics Workbench 22.* [Online] Available: https://digitalinsights.qiagen.com/products-overview/discovery-insights-portfolio/analysis-and-visualization/qiagen-clc-genomics-workbench/. Accessed on: May 31 2022.

[183] Sam Griffiths-Jones, *miRBase: Release 22.1.* [Online] Available: https://www.mirbase.org/. Accessed on: May 31 2022.

[184] QIAGEN, *User manual for Biomedical Genomics Analysis 22.0.4.* [Online] Available: https://resources.qiagenbioinformatics.com/manuals/biomedicalgenomicsanalysis/current/User_Manual.pdf. Accessed on: May 31 2022.

[185] GraphPad, *Prism.* [Online] Available: https://www.graphpad.com/scientific-software/prism/. Accessed on: May 31 2022.

[186] Agilent, *QuikChange Lightning Site-Directed Mutagenesis Kit: Instruction Manual Revision F.0.* [Online] Available: https://www.agilent.com/cs/library/usermanuals/public/210518.pdf. Accessed on: May 26 2022.

[187] PEQLAB, *peqGOLD Plasmid Miniprep Kit I: Instruction Manual v0815_E.* [Online] Available: https://de.vwr.com/assetsvc/asset/de_DE/id/17035106/contents/12-6942_12-6943_plasmid-mini-i_d-e_v0815.pdf. Accessed on: May 26 2022.

[188] SnapGene, *SnapGene | Software for everyday molecular biology.* [Online] Available: https://www.snapgene.com/. Accessed on: May 26 2022.

[189] Thermo Scientific, *GeneJET Plasmid Maxiprep Kit: Instruction Manual.* [Online] Available: https://assets.thermofisher.com/TFS-Assets%2FLSG%2Fmanuals%2FMAN0012654_GeneJET_Plasmid_Maxiprep_UG.pdf. Accessed on: May 26 2022.

[190] Thermo Fisher Scientific, *Pierce BCA Protein Assay Kit User Guide (Pub.No. MAN0011430 B.0).* [Online] Available: https://assets.thermofisher.com/TFS-Assets%2FLSG%2Fmanuals%2FMAN0011430_Pierce_BCA_Protein_Asy_UG.pdf. Accessed on: May 26 2022.

[191] BMG LABTECH, *Calcium Signaling using a Plate Reader.* [Online] Available: https://www.bmglabtech.com/de/cellular-dopamine-and-intracellular-calcium-signaling-using-next-generation-hts-microplate-reader/. Accessed on: May 30 2022.

[192] Luminex Corporation, *xMAP® Cookbook: A collection of methods and protocols for developing multiplex assays with xMAP® Technology.* [Online] Available: https://f.hubspotusercontent30.net/hubfs/128032/Cookbook/BR402139.xMAPCookbook.Ed5.All.Sections.WR.pdf. Accessed on: May 30 2022.

[193] cytiva, *Protein A Mag Sepharose Protein G Mag Sepharose: MagPlex-TAG Microspheres*. 28953763 AC. [Online] Available: https://d3.cytivalifesciences.com/prod/IFU/28953763.pdf. Accessed on: May 30 2022.

[194] M. M. Mukaka, “Statistics corner: A guide to appropriate use of correlation coefficient in medical research,” (eng), *Malawi Medical Journal : The Journal of Medical Association of Malawi*, vol. 24, no. 3, pp. 69–71, 2012.

[195] GraphPad, *GraphPad Prism 9 Statistics Guide - Interpreting results: Correlation.* [Online] Available: https://www.graphpad.com/guides/prism/latest/statistics/stat_interpreting_results_correlati.htm. Accessed on: Aug. 11 2022.

[196] GraphPad, *GraphPad Prism 9 Statistics Guide - How to: Correlation.* [Online] Available: https://www.graphpad.com/guides/prism/latest/statistics/stat_how_to_correlation.htm. Accessed on: Aug. 11 2022.

[197] J. Cohen, *Statistical power analysis for the behavioral sciences,* 2nd ed. Hillsdale, NJ: Erlbaum, 1988.

[198] H. Akoglu, “User's guide to correlation coefficients,” (eng), *Turkish journal of emergency medicine*, vol. 18, no. 3, pp. 91–93, 2018.

[199] M. R. Dalman, A. Deeter, G. Nimishakavi, and Z.-H. Duan, “Fold change and p-value cutoffs significantly alter microarray interpretations,” (eng), *BMC Bioinformatics*, vol. 13 Suppl 2, no. Suppl 2, S11, 2012.

[200] B. Zhao, A. Erwin, and B. Xue, “How many differentially expressed genes: A perspective from the comparison of genotypic and phenotypic distances,” (eng), *Genomics*, vol. 110, no. 1, pp. 67–73, 2018.

[201] *Bonferroni Correction -- from Wolfram MathWorld.* [Online] Available: https://mathworld.wolfram.com/BonferroniCorrection.html. Accessed on: Aug. 01 2022.

[202] Y. Chen and X. Wang, “miRDB: an online database for prediction of functional microRNA targets,” (eng), *Nucleic Acids Research*, vol. 48, no. D1, D127-D131, 2020.

[203] L. G. N. de Almeida *et al.,* “Proteomics and Metabolomics Profiling of Platelets and Plasma Mediators of Thrombo-Inflammation in Gestational Hypertension and Preeclampsia,” (eng), *Cells*, vol. 11, no. 8, 2022.

[204] T. J. Gauvin, L. E. Young, and H. N. Higgs, “The formin FMNL3 assembles plasma membrane protrusions that participate in cell-cell adhesion,” (eng), *Molecular biology of the cell*, vol. 26, no. 3, pp. 467–477, 2015.

[205] C. Hetheridge *et al.,* “The formin FMNL3 is a cytoskeletal regulator of angiogenesis,” (eng), *Journal of cell science*, vol. 125, no. Pt 6, pp. 1420–1428, 2012.

[206] M. V. Rao and R. Zaidel-Bar, “Formin-mediated actin polymerization at cell-cell junctions stabilizes E-cadherin and maintains monolayer integrity during wound repair,” (eng), *Molecular biology of the cell*, vol. 27, no. 18, pp. 2844–2856, 2016.

[207] E. Olinger *et al.,* “Biallelic variants in TTC21B as a rare cause of early-onset arterial hypertension and tubuloglomerular kidney disease,” (eng), *American journal of medical genetics. Part C, Seminars in medical genetics*, vol. 190, no. 1, pp. 109–120, 2022.

[208] I.-C. Su *et al.,* “Ubiquitin-Specific Protease 6 n-Terminal-like Protein (USP6NL) and the Epidermal Growth Factor Receptor (EGFR) Signaling Axis Regulates Ubiquitin-Mediated DNA Repair and Temozolomide-Resistance in Glioblastoma,” (eng), *Biomedicines*, vol. 10, no. 7, 2022.

[209] L. Zhang, J. Liu, P. Cheng, and F. Lv, “Correlation between miRNA target site polymorphisms in the 3' UTR of AVPR1A and the risk of hypertension in the Chinese Han population,” (eng), *Bioscience reports*, vol. 39, no. 5, 2019.

[210] T. Nakagawa *et al.,* “The Autism-Related Protein SETD5 Controls Neural Cell Proliferation through Epigenetic Regulation of rDNA Expression,” (eng), *iScience*, vol. 23, no. 4, p. 101030, 2020.

[211] S. M. Moore *et al.,* “Setd5 haploinsufficiency alters neuronal network connectivity and leads to autistic-like behaviors in mice,” (eng), *Translational Psychiatry*, vol. 9, no. 1, p. 24, 2019.

[212] E. Deliu *et al.,* “Haploinsufficiency of the intellectual disability gene SETD5 disturbs developmental gene expression and cognition,” (eng), *Nature neuroscience*, vol. 21, no. 12, pp. 1717–1727, 2018.

[213] S. Jang *et al.,* “Synaptic adhesion molecule IgSF11 regulates synaptic transmission and plasticity,” (eng), *Nature neuroscience*, vol. 19, no. 1, pp. 84–93, 2016.

[214] Y. Hayano *et al.,* “IgSF11 homophilic adhesion proteins promote layer-specific synaptic assembly of the cortical interneuron subtype,” (eng), *Science advances*, vol. 7, no. 29, 2021.

[215] D. Wagh *et al.,* “Piccolo Directs Activity Dependent F-Actin Assembly from Presynaptic Active Zones via Daam1,” (eng), *PloS one*, vol. 10, no. 4, e0120093, 2015.

[216] W. Luo, Z. Z. Lieu, E. Manser, A. D. Bershadsky, and M. P. Sheetz, “Formin DAAM1 Organizes Actin Filaments in the Cytoplasmic Nodal Actin Network,” (eng), *PloS one*, vol. 11, no. 10, e0163915, 2016.

[217] Q. Zhu *et al.,* “Syntaxin-binding protein STXBP5 inhibits endothelial exocytosis and promotes platelet secretion,” (eng), *The Journal of Clinical Investigation*, vol. 124, no. 10, pp. 4503–4516, 2014.

[218] L. A. Ridge *et al.,* “Non-muscle myosin IIB (Myh10) is required for epicardial function and coronary vessel formation during mammalian development,” (eng), *PLoS genetics*, vol. 13, no. 10, e1007068, 2017.

[219] B. Dash, C. Han, S. G. Waxman, and S. D. Dib-Hajj, “Nonmuscle myosin II isoforms interact with sodium channel alpha subunits,” (eng), *Molecular Pain*, vol. 14, 1744806918788638, 2018.

[220] Q. Jia *et al.,* “Synaptotagmin-4 promotes dendrite extension and melanogenesis in alpaca melanocytes by regulating Ca2+ influx via TRPM1 channels,” (eng), *Cell Biochemistry and Function*, vol. 38, no. 3, pp. 275–282, 2020.

[221] F. Matsushita, T. Kameyama, Y. Kadokawa, and T. Marunouchi, “Spatiotemporal expression pattern of Myt/NZF family zinc finger transcription factors during mouse nervous system development,” (eng), *Developmental dynamics : an official publication of the American Association of Anatomists*, vol. 243, no. 4, pp. 588–600, 2014.

[222] Y. Shi *et al.,* “Myt1L Promotes Differentiation of Oligodendrocyte Precursor Cells and is Necessary for Remyelination After Lysolecithin-Induced Demyelination,” (eng), *Neuroscience bulletin*, vol. 34, no. 2, pp. 247–260, 2018.

[223] J. Chen, A. Yen, C. P. Florian, and J. D. Dougherty, “MYT1L in the making: emerging insights on functions of a neurodevelopmental disorder gene,” (eng), *Translational Psychiatry*, vol. 12, no. 1, p. 292, 2022.

[224] Illumina, *Best practices for library quantification.* [Online] Available: https://emea.support.illumina.com/bulletins/2020/11/best-practices-for-library-quantification.html. Accessed on: Aug. 11 2022.

[225] *Cluster density guidelines for Illumina sequencing platforms using non-patterned flow cells.* [Online] Available: https://emea.support.illumina.com/bulletins/2016/10/cluster-density-guidelines-for-illumina-sequencing-platforms-.html. Accessed on: Aug. 11 2022.

[226] Illumina, “Optimizing Cluster Density on Illumina Sequencing Systems,” https://www.illumina.com/content/dam/illumina-marketing/documents/products/other/miseq-overclustering-primer-770-2014-038.pdf.

[227] Illumina, *MiSeq Reagent Kit v3 | Longest read lengths on any Illumina sequencer.* [Online] Available: https://emea.illumina.com/products/by-type/sequencing-kits/cluster-gen-sequencing-reagents/miseq-reagent-kit-v3.html. Accessed on: Aug. 11 2022.

[228] *Sequencing Quality Scores.* [Online] Available: https://emea.illumina.com/science/technology/next-generation-sequencing/plan-experiments/quality-scores.html. Accessed on: Aug. 11 2022.

[229] Thermo Fisher Scientific, *NGS Data Analysis for Illumina Platform—Overview and Workflow.* [Online] Available: https://www.thermofisher.com/de/de/home/life-

science/cloning/cloning-learning-center/invitrogen-school-of-molecular-biology/next-generation-sequencing/ngs-data-analysis-illumina.html. Accessed on: Aug. 11 2022.

[230] N. G. Panayotova, “NGS-QC-Metrics,” https://biotech.ufl.edu/wp-content/uploads/2021/03/NGS-QC-Metrics.pdf.

[231] Illumina, *What is the PhiX Control v3 Library and what is its function in Illumina Next Generation Sequencing?* [Online] Available: https://support.illumina.com/bulletins/2017/02/what-is-the-phix-control-v3-library-and-what-is-its-function-in-.html. Accessed on: Aug. 11 2022.

[232] A. Kovanda *et al.,* “Differential expression of microRNAs and other small RNAs in muscle tissue of patients with ALS and healthy age-matched controls,” (eng), *Scientific reports*, vol. 8, no. 1, p. 5609, 2018.

[233] M. Grunert, S. Appelt, I. Dunkel, F. Berger, and S. R. Sperling, “Altered microRNA and target gene expression related to Tetralogy of Fallot,” (eng), *Scientific reports*, vol. 9, no. 1, p. 19063, 2019.

[234] L. Streese *et al.,* “Untargeted sequencing of circulating microRNAs in a healthy and diseased older population,” (eng), *Scientific reports*, vol. 12, no. 1, p. 2991, 2022.

[235] *PMC - NCBI.* [Online] Available: https://www.ncbi.nlm.nih.gov/pmc/. Accessed on: Sep. 21 2022.

[236] W. Liu *et al.,* “Circulating microRNAs correlated with the level of coronary artery calcification in symptomatic patients,” (eng), *Scientific reports*, vol. 5, p. 16099, 2015.

[237] F. Hu, H. Liu, C. Wang, H. Li, and L. Qiao, “Expression of the microRNA-30 family in pulmonary arterial hypertension and the role of microRNA-30d-5p in the regulation of pulmonary arterial smooth muscle cell toxicity and apoptosis,” (eng), *Experimental and Therapeutic Medicine*, vol. 23, no. 1, p. 108, 2022.

[238] Y. Chen *et al.,* “RA Fibroblast-Like Synoviocytes Derived Extracellular Vesicles Promote Angiogenesis by miRNA-1972 Targeting p53/mTOR Signaling in Vascular Endotheliocyte,” (eng), *Frontiers in immunology*, vol. 13, p. 793855, 2022.

[239] A. W. Robert *et al.,* “Selective Loading and Variations in the miRNA Profile of Extracellular Vesicles from Endothelial-like Cells Cultivated under Normoxia and Hypoxia,” (eng), *International journal of molecular sciences*, vol. 23, no. 17, 2022.

[240] S. Chen *et al.,* “MiR-550a-3p restores damaged vascular smooth muscle cells by inhibiting thrombomodulin in an <emin vitro</em atherosclerosis model,” (eng), *European Journal of Histochemistry : EJH*, vol. 66, no. 3, 2022.

[241] J. Shi, Y. Ren, Y. Liu, Y. Cheng, and Y. Liu, “Circulating miR-3135b and miR-107 are potential biomarkers for severe hypertension,” (eng), *Journal of human hypertension*, vol. 35, no. 4, pp. 343–350, 2021.

[242] M. Park *et al.,* “NF-κB-responsive miR-155 induces functional impairment of vascular smooth muscle cells by downregulating soluble guanylyl cyclase,” (eng), *Experimental & Molecular Medicine*, vol. 51, no. 2, pp. 1–12, 2019.

[243] J. Perez-Hernandez *et al.,* “Urinary exosome miR-146a is a potential marker of albuminuria in essential hypertension,” (eng), *Journal of translational medicine*, vol. 16, no. 1, p. 228, 2018.

[244] H. Gu *et al.,* “Hypoxia-responsive miR-124 and miR-144 reduce hypoxia-induced autophagy and enhance radiosensitivity of prostate cancer cells via suppressing PIM1,” (eng), *Cancer Medicine*, vol. 5, no. 6, pp. 1174–1182, 2016.

[245] Center for Advanced Cardiac and Vascular Interventions, *Diabetic Neuropathy - Center for Advanced Cardiac and Vascular Interventions.* [Online] Available: https://cacvi.org/conditions/vascular-conditions/diabetic-neuropathy/. Accessed on: Sep. 22 2022.

[246] N. E. Cameron, S. E. Eaton, M. A. Cotter, and S. Tesfaye, “Vascular factors and metabolic interactions in the pathogenesis of diabetic neuropathy,” (eng), *Diabetologia*, vol. 44, no. 11, pp. 1973–1988, 2001.

[247] W. R. Timperley, A. J. Boulton, G. A. Davies-Jones, J. A. Jarratt, and J. D. Ward, “Small vessel disease in progressive diabetic neuropathy associated with good metabolic control,” (eng), *Journal of clinical pathology*, vol. 38, no. 9, pp. 1030–1038, 1985.

[248] P. J. Dyck *et al.,* “Capillary number and percentage closed in human diabetic sural nerve,” (eng), *Proceedings of the National Academy of Sciences of the United States of America*, vol. 82, no. 8, pp. 2513–2517, 1985.

[249] R. A. Malik *et al.,* “Hypoxic neuropathy: relevance to human diabetic neuropathy,” (eng), *Diabetologia*, vol. 33, no. 5, pp. 311–318, 1990.

[250] L. L. Tan, J. Alfonso, H. Monyer, and R. Kuner, “Neurogenesis in the adult brain functionally contributes to the maintenance of chronic neuropathic pain,” (eng), *Scientific reports*, vol. 11, no. 1, p. 18549, 2021.

[251] A. V. Apkarian *et al.,* “Role of adult hippocampal neurogenesis in persistent pain,” (eng), *Pain*, vol. 157, no. 2, pp. 418–428, 2016.

[252] D. García-González *et al.,* “Neurogenesis of medium spiny neurons in the nucleus accumbens continues into adulthood and is enhanced by pathological pain,” (eng), *Molecular psychiatry*, vol. 26, no. 9, pp. 4616–4632, 2021.

[253] A. V. Apkarian, M. N. Baliki, and P. Y. Geha, “Towards a theory of chronic pain,” (eng), *Progress in neurobiology*, vol. 87, no. 2, pp. 81–97, 2009.

[254] A. Tyrtyshnaia, A. Bondar, S. Konovalova, and I. Manzhulo, “Synaptamide Improves Cognitive Functions and Neuronal Plasticity in Neuropathic Pain,” (eng), *International journal of molecular sciences*, vol. 22, no. 23, 2021.

[255] S.-I. Hiraga, T. Itokazu, M. Nishibe, and T. Yamashita, “Neuroplasticity related to chronic pain and its modulation by microglia,” (eng), *Inflammation and regeneration*, vol. 42, no. 1, p. 15, 2022.

[256] K. Ghosh and H.-L. Pan, “Epigenetic Mechanisms of Neural Plasticity in Chronic Neuropathic Pain,” (eng), *ACS chemical neuroscience*, vol. 13, no. 4, pp. 432–441, 2022.

[257] G. Hannig and C. Jany, “Co-transfection of Plasmid DNA,” *BioTechniques*, vol. 54, no. 1, p. 47, 2013.

[258] Cell Signaling Technology, *Phospho-PKA Substrate (RRXS*/T*) (100G7E) Rabbit mAb.* [Online] Available: https://www.cellsignal.com/products/primary-antibodies/phospho-pka-substrate-rrxs-t-100g7e-rabbit-mab/9624. Accessed on: Sep. 21 2022.

[259] Sandra Mükusch, *Identifizierung post-translationaler Modifikationen mittels Peptid Mikroarrays.* [Online] Available: https://refubium.fu-berlin.de/bitstream/handle/fub188/9713/Dissertation_SandraMuekusch.pdf. Accessed on: Sep. 21 2022.

[260] G. Bhave *et al.,* “cAMP-Dependent Protein Kinase Regulates Desensitization of the Capsaicin Receptor (VR1) by Direct Phosphorylation,” (eng), *Neuron*, vol. 35, no. 4, pp. 721–731, 2002.

[261] V. Spahn *et al.,* “Opioid withdrawal increases transient receptor potential vanilloid 1 activity in a protein kinase A-dependent manner,” (eng), *Pain*, vol. 154, no. 4, pp. 598–608, 2013.

[262] A. Lochner and J. A. Moolman, “The many faces of H89: a review,” (eng), *Cardiovascular drug reviews*, vol. 24, no. 3-4, pp. 261–274, 2006.

[263] M. Franz-Wachtel *et al.,* “Global detection of protein kinase D-dependent phosphorylation events in nocodazole-treated human cells,” (eng), *Molecular & cellular proteomics : MCP*, vol. 11, no. 5, pp. 160–170, 2012.

[264] D. P. Mohapatra and C. Nau, “Desensitization of capsaicin-activated currents in the vanilloid receptor TRPV1 is decreased by the cyclic AMP-dependent protein kinase pathway,” (eng), *Journal of Biological Chemistry*, vol. 278, no. 50, pp. 50080–50090, 2003.

[265] S. Kim *et al.,* “TRPV1 recapitulates native capsaicin receptor in sensory neurons in association with Fas-associated factor 1,” (eng), *J. Neurosci.*, vol. 26, no. 9, pp. 2403–2412, 2006.

[266] I. Vetter *et al.,* “Rapid, opioid-sensitive mechanisms involved in transient receptor potential vanilloid 1 sensitization,” (eng), *Journal of Biological Chemistry*, vol. 283, no. 28, pp. 19540–19550, 2008.

[267] J. Btesh, M. J. M. Fischer, K. Stott, and P. A. McNaughton, “Mapping the binding site of TRPV1 on AKAP79: implications for inflammatory hyperalgesia,” (eng), *J. Neurosci.*, vol. 33, no. 21, pp. 9184–9193, 2013.

[268] UniProtKB- P21578, *LUXY_ALIFS. Yellow fluorescent protein.* [Online] Available: https://www.uniprot.org/uniprotkb/P21578/entry#sequences. Accessed on: Aug. 15 2022.

[269] Cell Signaling Technology, *AKAP5 (D28G3) Rabbit mAb.* [Online] Available: https://www.cellsignal.com/products/primary-antibodies/akap5-d28g3-rabbit-mab/5671. Accessed on: Aug. 15 2022.

[270] Melanie Kaufholz, *Charakterisierung eines cAMP-abhängigen Signalmoduls zur Regulation von TRPV1: Dissertation zur Erlangung des akademischen Grades des Doktors der Naturwissenschaften*.

[271] V. Carnevale and T. Rohacs, “TRPV1: A Target for Rational Drug Design,” (eng), *Pharmaceuticals (Basel, Switzerland)*, vol. 9, no. 3, 2016.

[272] *Drug Approval Package: Onpattro (patisiran).* Accessed on: Aug. 15 2022.

[273] Sylentis - RNAi Biopharmaceuticals, *The World Health Organization selects tivanisiran as the International Nonproprietary Name for SYL1001 - Sylentis.* [Online] Available: https://sylentis.com/la-oms-selecciona-tivanisiran-como-denominacion-comun-internacional-dci-de-syl1001/. Accessed on: Aug. 15 2022.

[274] P. Wang, Y. Zhou, and A. M. Richards, “Effective tools for RNA-derived therapeutics: siRNA interference or miRNA mimicry,” (eng), *Theranostics*, vol. 11, no. 18, pp. 8771–8796, 2021.

[275] Y. Wang *et al.,* “MiR-4638-5p inhibits castration resistance of prostate cancer through repressing Kidins220 expression and PI3K/AKT pathway activity,” (eng), *Oncotarget*, vol. 7, no. 30, pp. 47444–47464, 2016.

Appendix

The whole appendix is also available via Box.UP from University of Potsdam:

https://boxup.uni-potsdam.de/s/aACi9iJkEE4LSXs

PW: polyneuropathy-miRNA

Pre library preparation quality control

SampleQC.xlsx

Pre sequencing quality control

2100 expert_High Sensitivity DNA Assay

2100 expert_High Sensitivity DNA Assay

2100 expert_High Sensitivity DNA Assay

2100 expert_High Sensitivity DNA Assay

2100 expert_High Sensitivity DNA Assay

Sequencing statistic

200701_M05871_0014_000000000-J7FC

200623_M05871_0013_000000000-J7PP

220426_M05871_0019_000000000-KCM

220425_M05871_0018_000000000-KBVH

200609_M05871_0010_000000000-J6RD

Sample-to-sample comparison

Correlation.xlsx

Correlation.pzfx

Sequencing FASTQ

Due to the size of the FASTQ files (~20 GB) they are only available via Box.UP:

https://boxup.uni-potsdam.de/s/oYCaXDm466WYT3E

PW: polyneuropathy-miRNA

miRNA analysis

Expression Browser.xlsx

Crawler-based literature research

pubmed.py

Polyneuropathy_miRNA.html

Mutation confirmation

pcDNA 3.1 ARMS inkl PKA Mutanten.dna

TRPV1/ARMS co-immunoprecipitation

220928_TRPV1ARMS co-immunoprecipitati

ARMS phosphorylation sites

220928_ARMS phosphorylation sites

ARMS/AKAP79 co-immunoprecipitation

220928_ARMSAKAP79 co-immunoprecipi

Calcium flux measurements

220928_Clacium flux measurements_Dose.

220928_Calcium flux measurements_EC50.

shRNA mediated ARMS silencing

220928_shRNA mediated ARMS silen

220928_shRNA mediated ARMS silen

220928_shRNA mediated ARMS silen